Investigation on Mechanical Properties, Geometric Accuracy and Surface Roughness Improvement for Fused Deposition Modeling

A Dissertation Submitted in partial fulfillment of the requirement for the award of the degree of

Master of Engineering

in

Production Engineering

Submitted by

Ashu Garg

Roll No. 801382005

Under the Supervision of

Dr. Anirban Bhattacharya

Assistant Professor

Mechanical Engineering Department

Thapar University, Patiala

MECHANICAL ENGINEERING DEPARTMENT

THAPAR UNIVERSITY, PATIALA

JULY-2015

Certificate

I hereby declare that the thesis entitled "**Investigation on Mechanical Properties, Geometric Accuracy and Surface Roughness Improvement for Fused Deposition Modeling**" is an authentic record of my study carried out as requirement for the award of the degree of **Master of Engineering** in **Production Engineering** at **Thapar University, Patiala,** under the supervision of **Dr. Anirban Bhattacharya**, Assistant Professor, Mechanical Engineering Department, Thapar University, Patiala during July 2014 to July 2015. The matter embodied in this thesis has not been submitted to any other University or Institute for the award of any degree.

Date: 13-7-2015

Ashu Garg

Ashu Garg

(Reg. No. 801382005)

This is to certify that above statement made by the student is correct to the best of my knowledge and belief.

Anirban Bhattacharya

Dr. Anirban Bhattacharya
Assistant Professor,
Mechanical Engineering Department,
Thapar University, Patiala-147004

Countersigned by:

Dr. S.K. Mohapatra
Senior Professor & Head,
Mechanical Engineering Department,
Thapar University, Patiala-147004

Dr. S.S. Bhatia
Dean of Academic Affairs
Thapar University, Patiala-147004

Dedicated to

Parents

Acknowledgements

In the first place, I would like to express my sincere and devoted gratitude to Dr. Anirban Bhattacharya, Assistant Professor, Mechanical Engineering Department, Thapar University, Patiala for his continuous encouragement, support, and guidance throughout this work, without which this wouldn't have been completed. He has always been behind in every step of this work and has always stood for any problems, difficult situations whatsoever.

I would also like to thanks Dr. S.K. Mohapatra, Senior Professor and Head, Mechanical Engineering Department, Thapar University, Patiala and Dr. Ajay Batish, Professor and Dean of Partnership and Accreditation, Thapar University, Patiala for their encouragement and inspiration for execution of the work.

I specially acknowledge All India Council for Technical Education (AICTE), New Delhi, India for providing the financial support to carry out the work. I am grateful to Dr. H. Bhunia, Associate Professor, Chemical Engineering Department, Thapar University, Patiala, for his generous support to use the testing facilities and Mr, Manjit Singh for his help.

The generous and intellectual support of all the staff members of Mechanical Engineering Department is greatly appreciated. Finally, I would like to express my heartful thanks to my parents and friends for their help and best wishes for the successful completion of this work.

Above all, I express my indebtedness to the 'ALMIGHTY' for all his blessing and kindness.

Ashu Garg

Ashu Garg

Abstract

Fused deposition modeling (FDM) process is one of rapid prototyping (RP) technology widely adopted by the industries for producing low cost complex geometrical parts. This prototype making process involves environmental friendly thermoplastic material in form of a filament to melt and deposit materials layer by layer with admirable accuracy and part strength. Materials are deposited through nozzles in a desired pattern onto a worktable that moves in Z direction (depth) whereas nozzle head moves on plane of worktable in X and Y direction. The bonding between the adjoining layers is caused due to thermally driven diffusion bonding. After one layer is deposited, the work table moves down by amount of layer thickness and next layer is added. Simplicity of operation together with the ability to fabricate complex parts resulted in its wide spread applications not only for prototyping but also for making functional parts. However, FDM process has its own demerits related with highly anisotropic mechanical properties, geometric accuracy, surface quality etc. Hence, it is absolutely necessary to investigate role of controllable factors for improvement of part quality.

In this direction, present study focuses on the improvement of part build methodology by properly controlling the process parameters. The thesis deals investigation of with various part quality such as mechanical properties (tensile and flexural strength), improvement in geometric accuracy, minimization of surface roughness and build cost of FDM processed ABS P430 parts. The understanding generated in this work not only explains the complex build mechanism but also present in detail the influence of process parameters such as part orientation and raster angle on responses with the help of experimental results, scanning electron microscopy and multi response optimization using analytical hierarchy process. For experimental investigation three different part orientation (along X, Y and Z axis) and four different raster angles (0°, 30°, 60°, 90°) are considered for building of components and tested for mechanical strength (tensile and flexural) and surface roughness. For geometric accuracy and surface quality measurement, parts with different primitives and doubly curved/ freeform surfaces are considered which are built at seven different part orientation (0°, 15°, 30°, 45°, 60°, 75°, 90°) about Y axis and part orientation along X, Y and Z axis are considered for freeform surfaces. Geometric error of the built part with respect to the CAD geometry is measured for all the parts. For FDM parts, model material, support material

consumption along with build time cumulatively represents the build cost. For each of the part orientation and raster angle, the volume of model and support material consumption, build time are measured and compared. Next, all the parts are chemically treated with cold vapor of dimethylketone and tensile strength, flexural strength, surface roughness and geometric accuracy are measured and compared with those without any post treatment. Rapture surfaces under tensile and flexural loading are also studied by SEM to understand the failure mode of the specimen under different loading conditions. Later, the FDM process parameters that affected the studied responses were identified and optimized by multi-response optimization using analytic hierarchy process for maximum achievable tensile and flexural strength, with improved geometric accuracy, surface finish and lower the build time.

The methods adopted in this study are quite general and can be used for other related or allied processes, and believed to be beneficial for industries like aerospace, automobile, home appliances, etc. for identifying the process capability and further improvement in FDM process.

Keywords: Fused deposition modeling; Part orientation; Raster angle; Tensile strength; Flexural strength; Geometric accuracy; Surface roughness; Model material; Support material; Build time; Cold-vapors; Analytic hierarchy process.

Table of Contents

List of Figures

List of Tables

Nomenclature

X = Part orientation along X axis (along the longitudinal direction of build platform)

X-0 = Part orientation along X axis, raster angle 0°

X-30 = Part orientation along X axis, raster angle 30°

X-60 = Part orientation along X axis, raster angle 60°

X-90 = Part orientation along X axis, raster angle 90°

Y = Part orientation along Y axis (along the transverse direction of build platform)

Y-0 = Part orientation along Y axis, raster angle 0°

Y-30 = Part orientation along Y axis, raster angle 30°

Y-60 = Part orientation along Y axis, raster angle 60°

Y-90 = Part orientation along Y axis, raster angle 90°

Z = Part orientation along Z axis (along the build/depth direction of specimen)

Z-0 = Part orientation along Z axis, raster angle 0°

Z-30 = Part orientation along Z axis, raster angle 30°

Z-60 = Part orientation along Z axis, raster angle 60°

Z-90 = Part orientation along Z axis, raster angle 90°

Greek Symbols

α = Part orientation, °

λ_m = Maximum Eigen value

Acronyms

3D	≡	Three Dimensional
ABS	≡	Acrylonitrile Butadiene Styrene
AHP	≡	Analytic Hierarchy Process
ANN	≡	Artificial Neural Network
ANOVA	≡	Analysis Of Variance
ASTM	≡	American Society for Testing and Materials
CAD	≡	Computer Aided Design
CAM	≡	Computer Aided Manufacturing
CCD	≡	Centered Composite Design
CI	≡	Consistency Index
CMM	≡	Coordinate Measuring Machine
CR	≡	Consistency Ratio
DOE	≡	Design Of Experiments
EDP	≡	Extruder Deposition Process
FDM	≡	Fused Deposition Modeling
LM	≡	Layered Manufacturing
LOM	≡	Laminated Object Manufacturing
LR	≡	Laboratory Reagent
LV	≡	Low Vacuum
NURBS	≡	Non-Uniform Rational B-Spline
QPSO	≡	Quantum Behaved Particle Swarm Optimization
R_a	≡	Average Surface Roughness (µm)
RI	≡	Random index
RP	≡	Rapid Prototyping
R_q	≡	Root Mean Square Surface Roughness (µm)
SEM	≡	Scanning Electron Microscope
SLA	≡	Stereolithography
SLS	≡	Selective Laser Sintering
STL	≡	Standard Tessellation Language
UTM	≡	Universal Tensile Testing
UV	≡	Ultraviolet

Chapter 1

Introduction

1.1 Introduction

Many exogenous factors lead to modify the way the products are being designed and manufactured for firms to sustain in a competitive environment. Among them the introduction of new materials, technologies for reducing design and manufacturing lead time, services and end user requirements are critical to gain edge over competitors [Tolio *et al.*, 2010]. The emphasis on reduction in product development cycle and time has a profound influence on the manufacturing processes and resulted in the birth of a new technology which manufactures parts directly from its computer aided design (CAD) models on layer by layer deposition principle without any use of dies, tools, fixtures and with minimum human intervention. The method of such additive part generation processes is known as 'Rapid Prototyping'. The rapid prototyping (RP) by layer forming process started early during 1980s with the advancement in computer aided design/computer aided manufacturing (CAD/CAM). Although RP process is cheap, flexible and fast way to create test models prior to production but material availability has traditionally limited the widespread application of this technology. But now, with ongoing research and advances in material sciences and RP technology, the opportunity has opened for more applications. So no longer this technology is just for prototyping but also for end products [Yan *et al.*, 2009]. Further, with advancement in the internet technologies, the future of manufacturing organizations will be information oriented, knowledge driven and much of their daily operations will be automated around the global information network that connects everyone together [Dong *et al.*, 2008].

1.2 Rapid Prototyping

In recent years rapid prototyping (RP) technology has become a focus for development of different products. This method can be used to fabricate any three dimensional (3D) shape from numerical data by quick, highly automated and flexible system. RP technology can reduce the manufacturing lead time of fabricated parts upto 30-50 percent even when complexity of part is relatively high [Kai and Fai, 2000]. Rapid manufacturing of parts and model can largely reduce the product development cycle and cost [Byun and Lee, 2005]. The RP processes available today are fused deposition modeling (FDM),

stereolithography (SLA), solid ground curing (SGC), laminated object manufacturing (LOM), three dimensional printing (3DP), selective laser sintering (SLS) etc. which can fabricate 3D models using CAD data without any use component specific dies and tooling. The surface finish and mechanical properties of components obtained by these RP processes is highly important, especially when these components are used in service as functional components.

The entire cycle of fabrication consists of creating a geometric model in solid modeler, determining a suitable part deposition orientation, slicing of the CAD model, generating the material deposition paths or laser scanning paths, part deposition and post processing task as shown in Fig. 1.1 [Pandey *et al.*, 2003a].

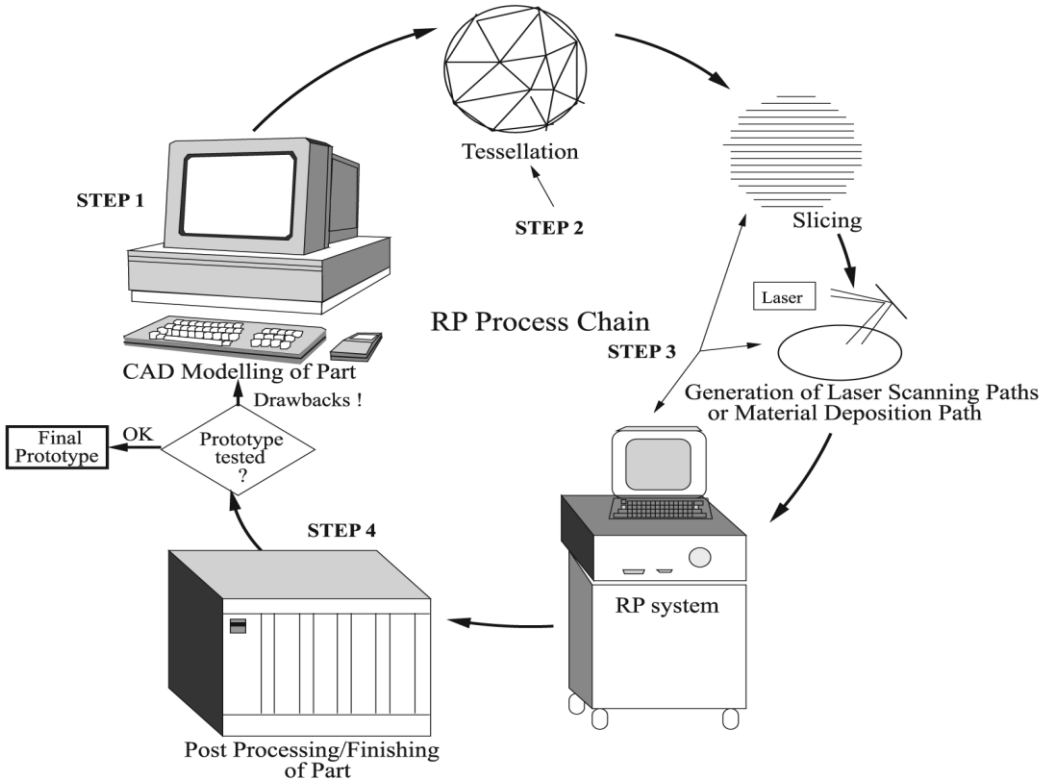

Figure 1.1: Fundamental process steps in RP process chain [Pandey *et al.*, 2003a]

In addition, different varieties of materials that can be used has been significantly increased, which has improved precisions and functionality of end products. Therefore, rapid manufacturing are now considered as alternative method of direct manufacturing of models, components or parts for use in manufacturing processes. The RP technique can easily produce complex geometrical structures that cannot be fabricated by any other conventional material removal processes and fabricated parts can be used as visualizing and verifications of design to check for forms and fit models, or to produce master patterns for casting

molding. Although there are advantages of using RP technology like it can reduce build time and cost for complex geometrical parts, but each RP process has their own demerits. Therefore, it is necessary that shortcoming of RP processes should be understood and proper remedial measures should be searched before it is recommended for industries. The surface quality, build time, part strength and accuracy are considered as key issues that should be addressed for successful implementing the RP technology [Rosochowski and Matuszak, 2000; Hopkinson *et al.*, 2006].

1.3 Different Rapid Prototyping Techniques

There are several RP techniques available today in the engineering industries. Few of them e.g. fused deposition modeling (FDM), stereolithography (SLA), laminated object manufacturing (LOM) and selective laser sintering (SLS) are described below.

1.3.1 Fused Deposition Modeling

The fused deposition modeling (FDM) process is a most widely used RP process that fabricates a 3D physical part directly from CAD model. It consist of very fine nozzle that moves in X and Y direction and fabricate a physical model by extruding semi liquid thermoplastic material in the form of layers. The nozzle position along the tool path is controlled by computer relative to the base which allows the enhanced geometric complexity of the part to be fabricated maintaining a tight tolerance [Sood *et al.*, 2012].

FDM uses two separate liquefier nozzles one for the model material and another for the support structure. Both model and support material are in the form of filaments melts at preselected temperature and get rapidly solidify in 0.1 second when adhered to the previous layer [Sood *et al.*, 2012]. The bonding between the neighboring fibers takes place through a thermally driven diffusion welding [Sood *et al.*, 2010]. The second nozzle creates a support structure and can be removed easily through a wash basin once the model is completed. The entire model is built on horizontal platform which is lowered in Z direction as each layer is added [Perez, 2002]. During the fabrication process, the velocity and temperature must be kept constant otherwise surface will be of poor quality.

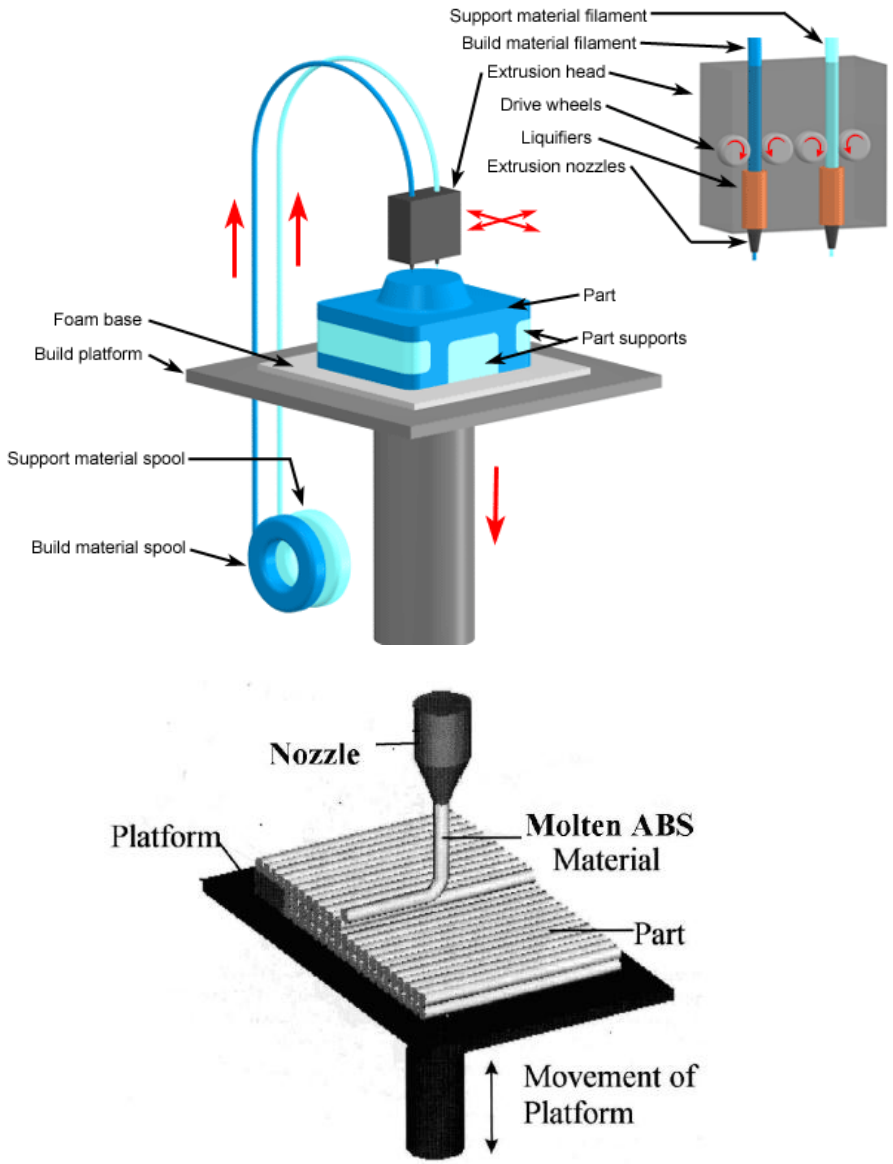

Figure 1.2: Fused deposition modeling process [Pham and Demov, 2001]

1.3.2 Stereolithography

The stereolithography (SLA) process uses a liquid resin, photosensitive liquid polymer that hardens when exposed to ultraviolet (UV) light. The SLA machine consists of a vat of this resin and a vertically moving platform on which the model is built. Argon ion laser or UV Helium-Cadmium laser are used as laser scanning system which scans a cross section from the CAD data onto the surface of liquid resin causing it to solidify and form a solid layer of the model [Bandyopadhyay *et al.*, 2011]. Platform is then lowered in downward direction equals to layer thickness and left for very short time interval known as dip-delay so that the liquid polymer settle down and leaves behind a very thin layer of liquid resin covering its surface. The new layer is then scanned over the previously formed layer and

complete model is formed by layer by layer building process. The fabricated model is then raised out from liquid resin and excess polymer is cleaned off from its surface. Figure 1.3 shows schematic diagram of a typical SLA process.

Nowadays in SLA systems, vacuum blade or leveling wiper is used which recoat the next layer of resin on the surface of previously formed layer to reduce the trapped volumes that occurs due to excessive polymerization at the layers end [Bandyopadhyay *et al.*, 2011].

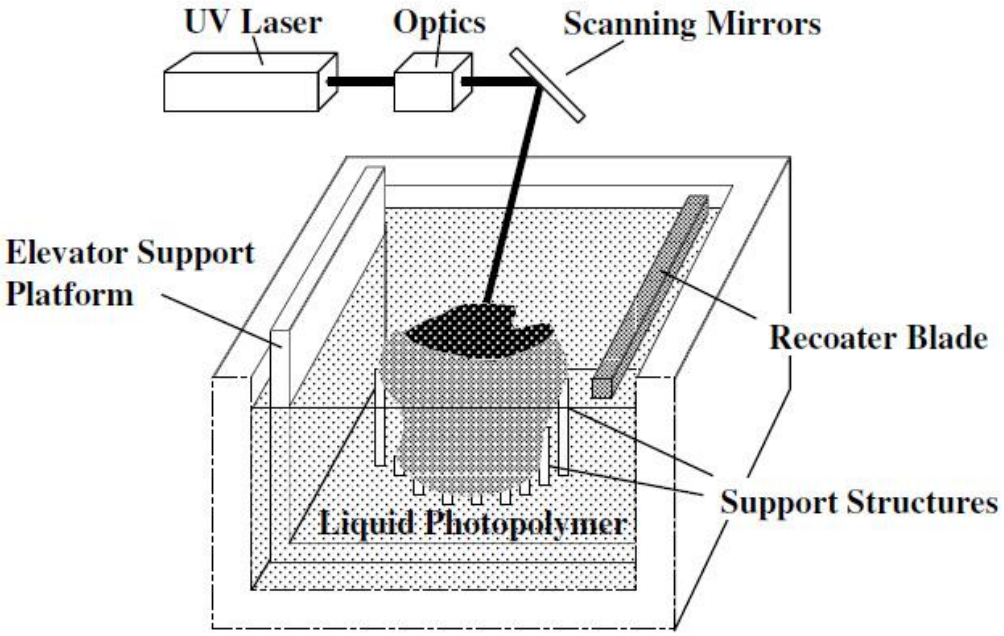

Figure 1.3: Stereolithography process [McMains, 1995]

1.3.3 Selective Laser Sintering

This process was originally developed and patented by the University of Texas at Austin in which parts are fabricated by focusing the laser beam which sinters (melts) the powder particles into a solid layer. The next solid layer is preciously built on top of the previously formed layer after the roller spreads out another fine layer of powder particles (shown in Fig. 1.4). The layers of the CAD model are precisely scanned on the unsintered powder by a finely focused laser beam under the guidance of an X–Y scanner system [Bandyopadhyay *et al.*, 2011]. The intensity of the laser beam is modulated to melt the powder only in areas defined by the part geometry whereas surrounding powder remains unsintered which serves as support structure. Therefore, there is no need to create a support structure within the CAD design prior to or during processing [Marcincinova *et al.*, 2013]. Once the laser scanning system completes the curing operation of a single layer, the bed

moves downward and the powder feeding chamber is raised so that an additional layer of powder can be deposited via a roller mechanism on top of the previously scanned layer. When the part is completed the unsintered powder can simply be brushed off and used again as build material.

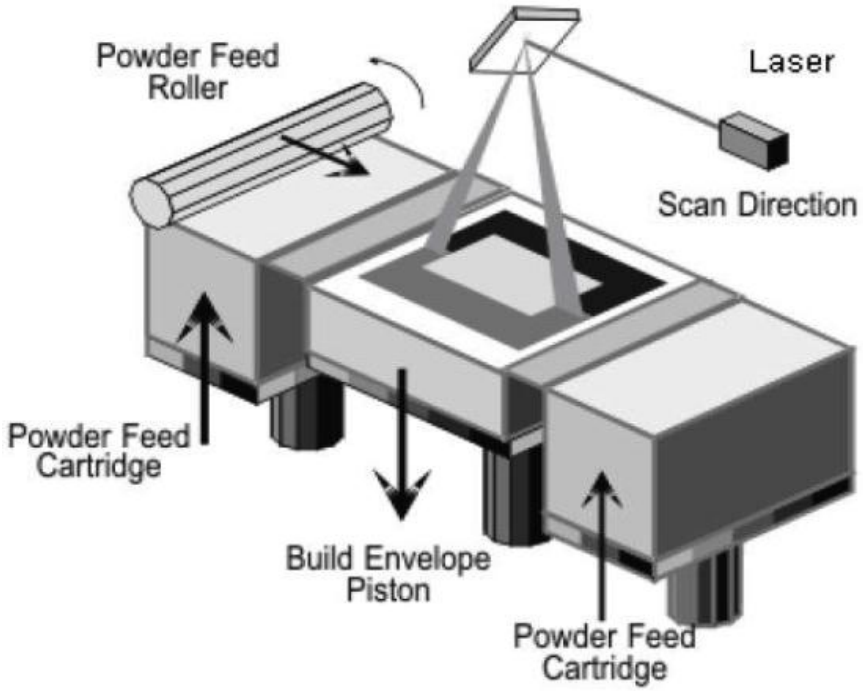

Figure 1.4: Selective laser sintering process [Pham and Demov, 2001]

1.3.4 Laminated Object Manufacturing

This process was original developed and introduced by Helisys, California, USA which fabricates the models using a unique additive/subtractive method. In this process, first layer of model is built on metallic platform which is coated with double sided adhesive. The supply roller feeds the sheet to the platform and bonded to the substrate/or to the previous layer, using a heated roller which passes over the material and melts the plastic adhesive on the bottom side of the build sheet to provide bonding between the laminates [Bandyopadhyay *et al.*, 2011]. The cross sectional outline of one slice of the part, the cross hatches, and the model perimeter are precisely generated by computer system and laser beam is used to cut to a depth equals to the sheet thickness. The remaining areas that are to be removed from the final model are crosshatch into small pieces, which act as support structure and can be removed easily during post processing [Bandyopadhyay *et al.*, 2011]. The platform is then lowered one layer thickness, another layer of material is stuck onto the previous layer and the

procedure is repeated with the next cross section slice of the part. These steps are repeated until all the layers are formed. The part which comes out of the machine is in form of an enclosed rectangular block of laminates. The post processing of LOM parts involves removing the crosshatched pieces, polishing, sanding, etc. Figure 1.5 shows detailed diagram of a typical LOM process.

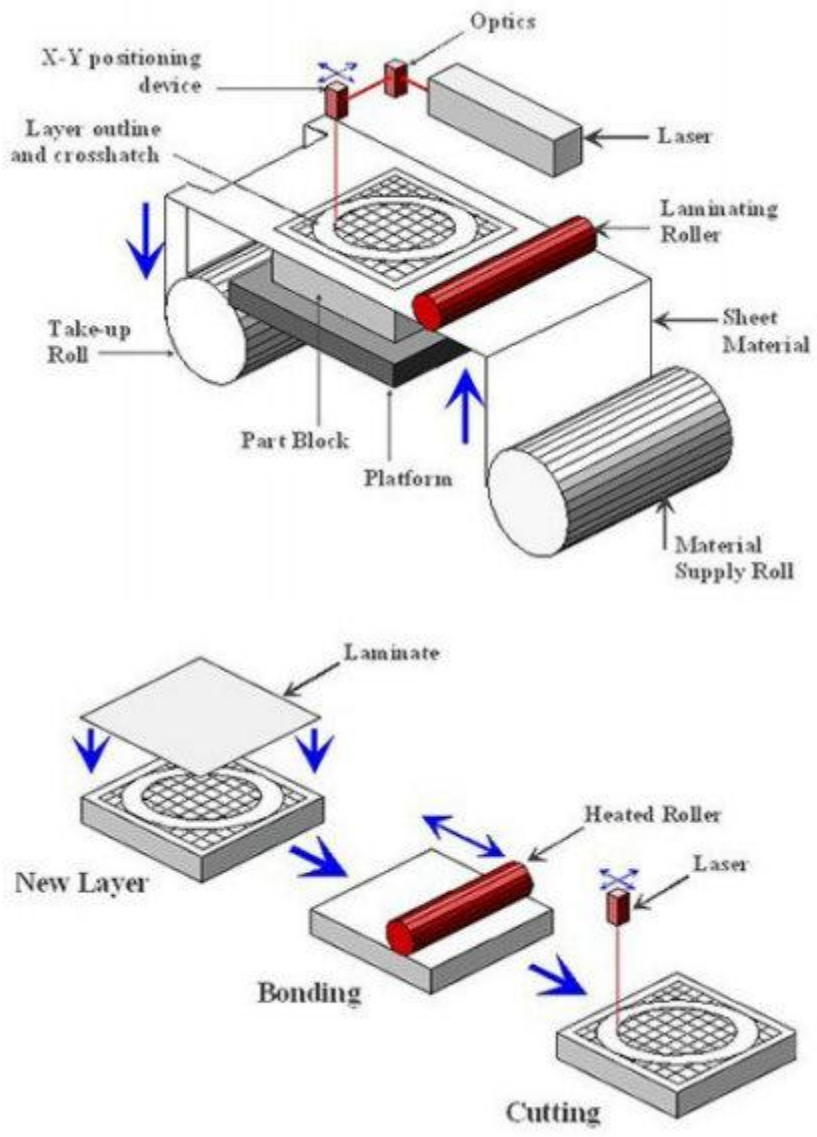

Figure 1.5: Laminated object manufacturing process [Pham and Demov, 2001]

1.4 Applications of Rapid Prototyping Process

RP technique has the potential to reduce time period from concept to physical model upto 30-50 %. It has ability to improve and enhance the product development cycle while at the same time reduces the build cost that may be considered as a major breakthrough in

manufacturing technology. But the final fabricated parts also suffer from desired surface quality, dimensional accuracy and mechanical strength which depend on various process parameters and machine settings. This technique can build a part with much geometric complexity. Therefore, RP techniques are widely adopted by different industries like aerospace, automotive, biomedical industries, coin making, home appliances, tableware, jewelry, etc. It is used for fabricating various functional parts, conceptual models, patterns for vacuum casting, investment castings, die casting and models for medical applications and for engineering analysis. Figure 1.6 represents the various applications of RP processes.

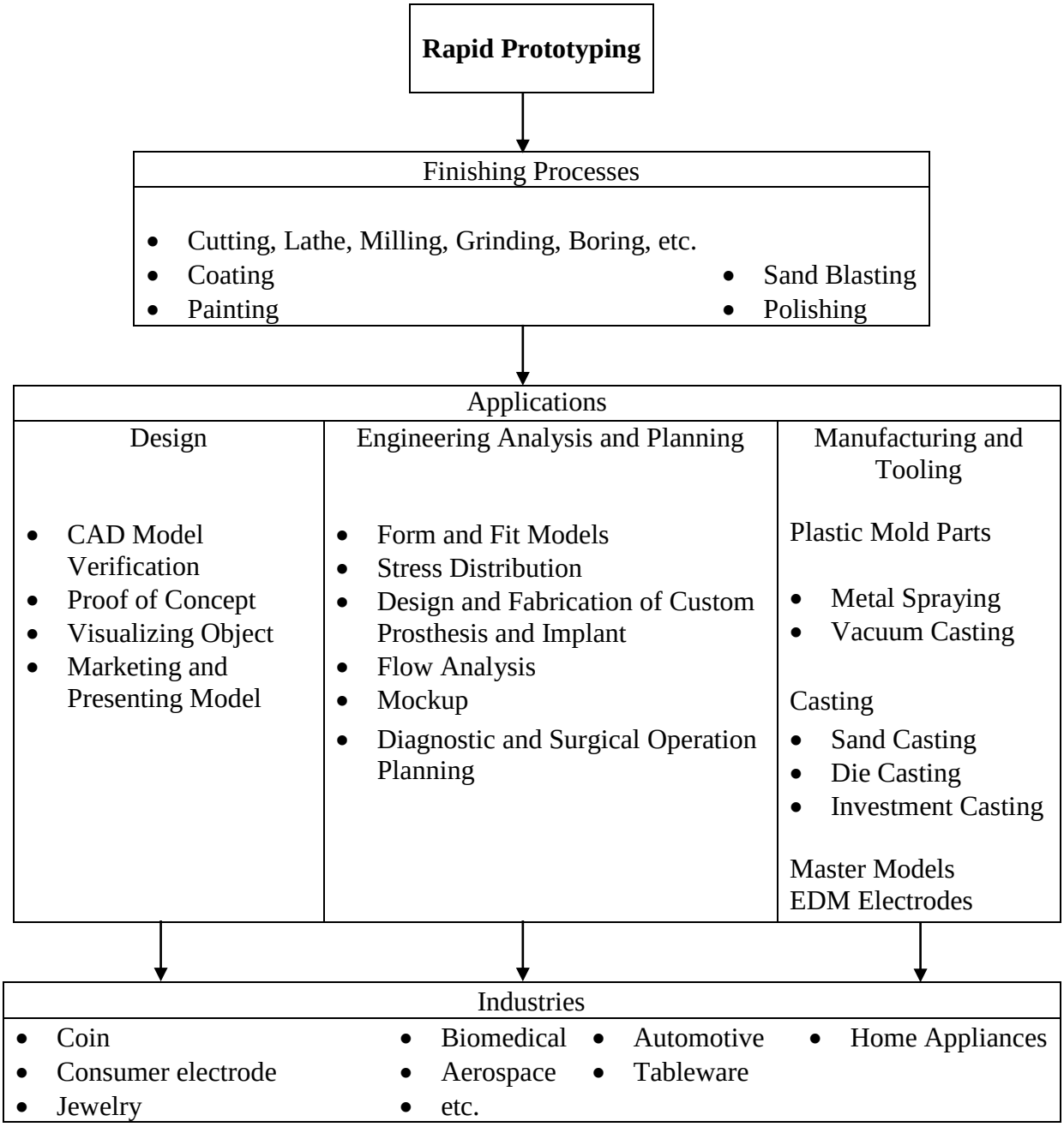

Figure 1.6: Applications of RP technologies [Chua and Leong, 2000]

1.5 Fused Deposition Modeling Process

Fused deposition modeling (FDM) process is one of RP technology widely adopted by the industries for producing low cost RP model having complex geometries. In this process, the model material is deposited layer-by-layer (additive manufacturing) through a very fine nozzle that moves in X and Y direction and fabricates a model by extruding semi-liquid thermoplastic material in the form of layers as shown in Fig. 1.7. After depositing one layer, the worktable moves down equals to one slice thickness so that the next layer can be deposited above the previously formed layer. The specific pattern of deposition and the nozzle movement i.e. the raster pattern decides the tool path, deposition time and controls many of the mechanical and physical property of the fabricated part. The nozzle position along the tool path is controlled by computer relative to the base which allows the enhanced geometric complexity of the part that can be fabricated maintaining a tight tolerance [Sood *et al.*, 2012b]. To fabricate the part without any geometric damage/distortion, the parts are fabricated with simultaneous deposition of support materials at the desired locations.

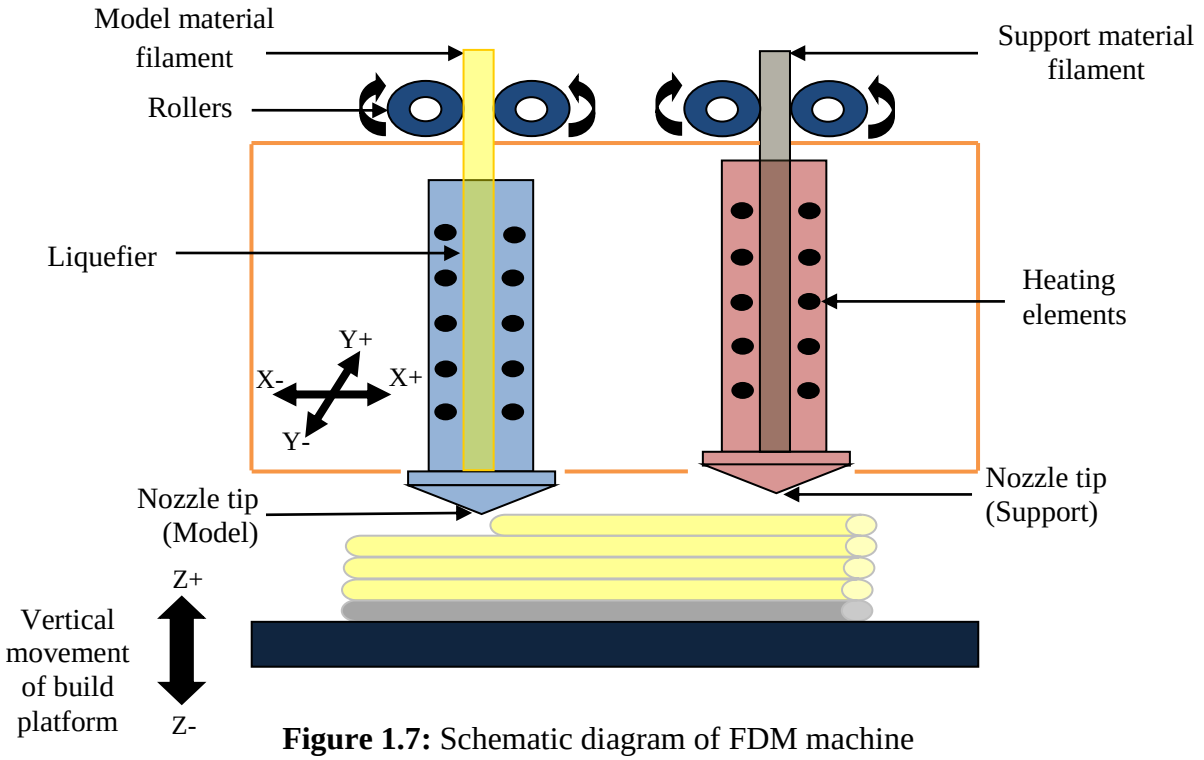

Figure 1.7: Schematic diagram of FDM machine

In FDM machine extrusion head consist of two separate liquefier nozzle, one for the part material (model material) and another for support structure. Both model and support materials are in the form of filaments which melts at preselected temperature and gets rapidly

solidify in 0.1 second when adhered to the previous layer [Gurrala and Regalla, 2014]. The bonding between the neighboring fibers can takes place through a thermally driven diffusion bonding [Sood *et al.*, 2010]. The second nozzle creates a support structure and can be removed easily once the model is completed. The entire part is built on a horizontal base table which is lowered in Z direction as each layer is added [Perez, 2002].

Figure 1.8 shows the basic steps in FDM process. The preliminary steps are the creation of 3D CAD model. Subsequently CAD data is converted into standard tessellation language (.stl) format that consists of not only coordinates of triangular facet but also their normal vectors altogether represents the outside skin of CAD model [Nagy and Matylsi, 2003]. Further the slicing of CAD model is done into horizontal layers and generations of deposition path for each layer. FDM machine studies each layer and fabricates the model in an additive manner layer by layer. After the generation of physical model it is separated from support structure and post processing is done. In this approach, fabricated part does not replicate the CAD model due to dimensional inaccuracy and poor surface quality caused by staircase effects and tessellation.

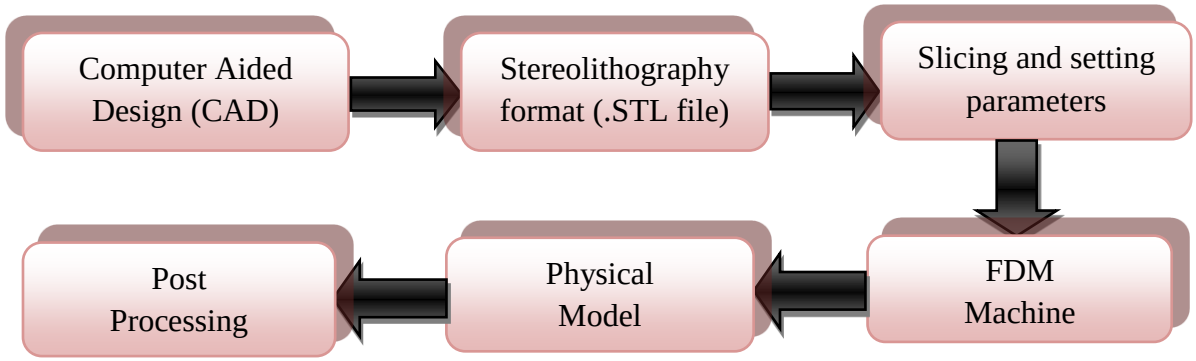

Figure 1.8: Basic steps in FDM process

1.5.1 Process Parameters

Important FDM process parameters (represented in Fig. 1.9) that directly impact the performance, part quality and accuracy are briefly described below.

a) **Slice thickness (height):** Creating contours of section of the geometry at various heights in the multiple of layer thickness. In RP, slicing of the CAD model is one of the important steps because slicing of the CAD model with a very small slice thickness leads to large build time. At the same time if large slice thickness is chosen, the surface quality is very poor due to staircase effect [Pandey *et al.*, 2007].

b) **Part orientations:** Part build orientation is refers to the inclination of part in build platform with respect to X, Y and Z axis. X and Y axis are parallel to build platform and Z axis is along the thickness i.e. height direction of a part [Sood *et al.*, 2012a].

c) **Raster angle:** It is the angle created between raster/deposited layer and X direction of build platform

d) **Raster width:** It is the thickness of raster that the FDM nozzle deposit to fill the interior region of part.

e) **Contour width:** It is the thickness of contour that the FDM nozzle deposits to create the perimeter and boundaries of given part [Agarwala *et al.*, 1996].

f) **Raster to raster air gap:** It is the gap between two adjacent beads (raster) which is zero by default, i.e. beads touch each other. It can be changed to positive gap, as a result adjacent beads do not touch each other and loosely packed structure is obtained and building time reduces. It can also be changed to negative gap, which causes adjacent beads to overlap partially the same space and dense structure is achieved however, building time increases.

g) **Model build temperature:** It is the temperature at which model material is heated by the system. This controls the extrusion of molten material through the nozzle.

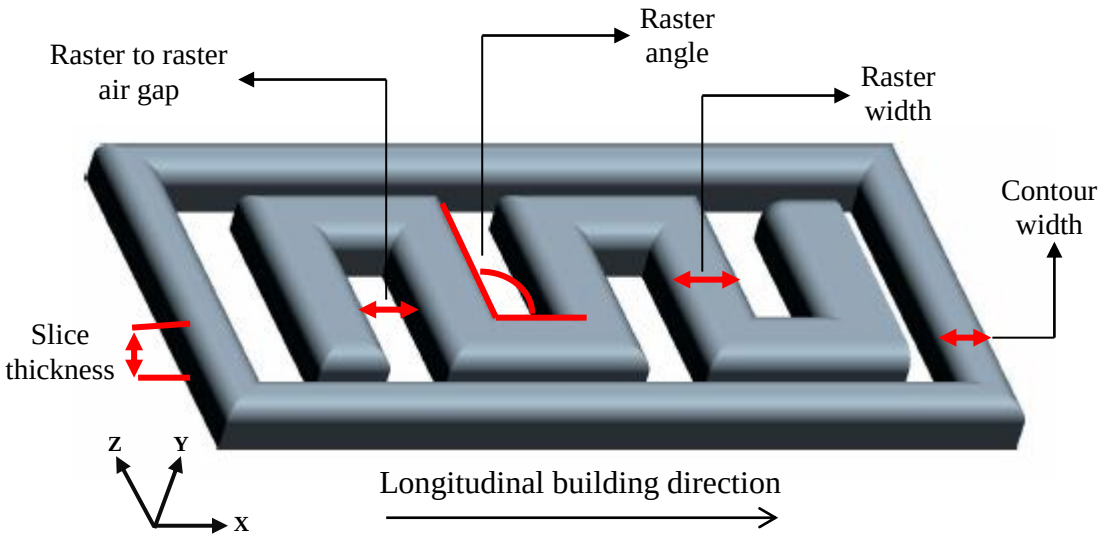

Figure 1.9: FDM process parameters

1.5.2 Issues in FDM Process

Different types of error that affects the surface quality, build time, part strength, geometric accuracy and repeatability of FDM fabricated parts are briefly described below.

a) **Part orientation:** Determining the optimal part deposition orientation is a fundamental problem in FDM process. Part orientation has significant effects on part quality and building aspects such as tensile strength, toughness, flexural strength, part surface quality, amount of support material required and build time. Therefore, the optimal build orientation can be determined by considering the various parameters which can meet the user requirements.

b) **Staircase effect:** It mainly appears along the inclined surface of the part as shown in Fig. 1.10 which becomes worse when inclination of part increases. This effect cannot be eliminating completely but can be minimized to some extent by polishing the surface during post processing operation. The staircase effect can also be reduced by selecting thinner slice thickness which also improves the surface finish but increases build time. However, layer thickness cannot be smaller than the minimum thickness that can be achievable by the given process. Therefore, if the requirement of layer to meet surface tolerance is beyond the limitations of the process, the surface accuracy is obviously not attainable and some additional post-treatment may be required.

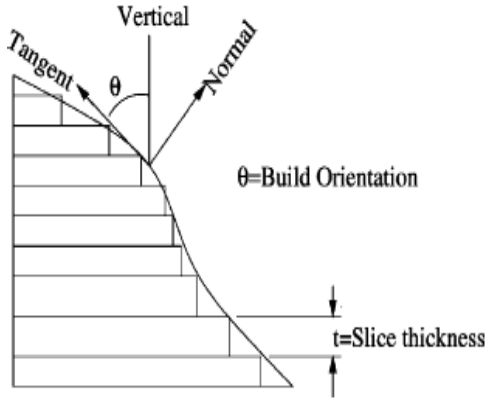

Figure 1.10: Staircase effect [Pandey *et al.*, 2003b]

c) **Tessellation error**: In tessellation procedure, surface of a CAD model is piecewise approximated by triangular facets with coordinates and surface normals of triangles listed by the system. The number of triangles and their size are controlled by the parameters such as facet deviation and chordal error. The deviation between the

original CAD geometry and tessellated model can be reduced by reducing the size of the triangles.

d) **Shrinkage and distortion**: As the FDM process extrudes the model material from its liquefier nozzle and cools them rapidly on deposition, stresses are induced by such rapid cooling in fabricated model. As such, shrinkages and distortions caused to the build model are a common occurrence and are usually difficult to predict, though with experience, users may able to compensate for these by adjusting the process parameters settings of the machine.

e) **Wavy surfaces**: This is result from the elliptical nature of molten filament extruded through a nozzle which causes poor surface finish. Therefore, good surface finish can be obtained by using thinner layers of material (slice thickness) and small size nozzles.

Different sources of error as commonly observed in FDM built parts are schematically represented in Fig. 1.11.

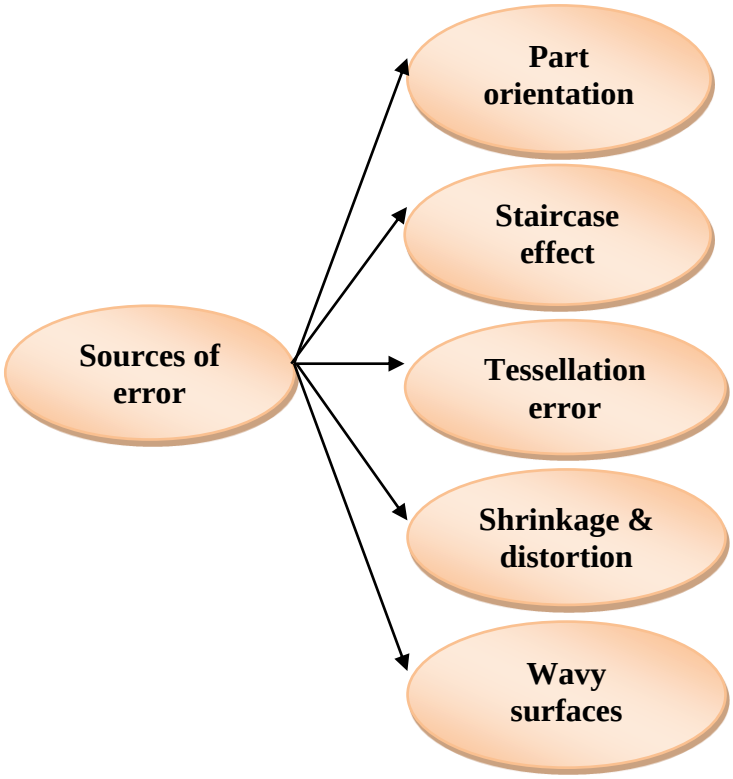

Figure 1.11: Sources of error in FDM process

1.5.3 Advantages, Disadvantages and Applications of FDM

Some salient advantages of FDM process are:

- Able to fabricates the models with material that are similar to actual molded product (functional parts)
- Only little need for cleaning up the prototype after fabrications (minimal wastage).
- Ease of support material removal by simply broken off or washed away.
- Cost/time effective.
- Relatively inexpensive materials.

Some salient disadvantages of FDM process are:

- Restricted accuracy because material used in this process is in form of filament.
- Unpredictable shrinkage due to rapid cooling of build materials which induces stresses in fabricated models.
- Very slow process as whole cross sectional area need to be filled with materials.

Applications

- FDM process is one of the widely adopted RP technology used for prototyping and rapid manufacturing. FDM process has also shown potential not only for prototyping but also for final part production due to simplicity in operation and durability of final parts.
- The extrusion-based process fabricates the functional parts or conceptual models for various industries, including automotive, aerospace, biomedical industries, architecture, consumer products, etc.
- By changing the deposition angle (raster angle) in each successive layer and by adjusting the road spacing, size and connectivity, any complex geometrical structures can be produced.
- FDM process is also used in tissue engineering for scaffold prototyping.

1.6 Thesis outline

The remaining of this thesis is organized as follows:

- Chapter 2: Literature Review

  Includes a literature review to provide a summary of the base of knowledge already available involving the issues of interest. Later, scope and objectives of present work are also discussed.

- Chapter 3: Methodology

  The description of the materials, equipment, test procedures, and experimentations methodology are discussed in this part of thesis.

- Chapter 4: Results and Discussions

  Effect of part orientations, raster angles and chemical treatment on part strength, geometric accuracy and surface roughness are studied in this part of thesis. Multi-response optimization technique namely analytic hierarchy process has been adopted to determine the optimum process parameter setting.

- Chapter 5: Conclusions and Scope for Future Work

  The conclusions and scope for future work are given in this part of thesis.

Chapter 2

Literature Review

2.1 Introduction

One of the current challenges faced by manufacturing industries is the reduction of product development time with good mechanical properties and surface finish through RP technologies. In this aspect, the current chapter provides an overview of previous research highlighting developments and problems associated with various aspects of RP with special relevance to FDM process. The available literatures are classified into an assortment of sections dealing with specific issues associated with RP as shown in Fig. 2.1.

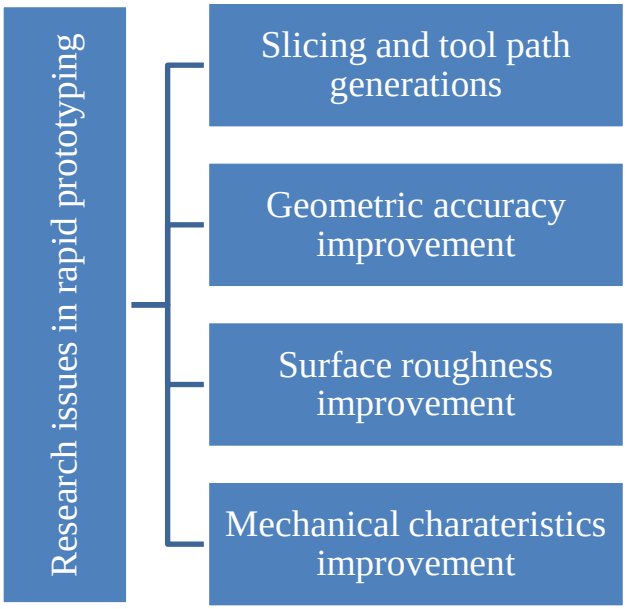

Figure 2.1: Research issues in RP

Sections 2.2 provide the brief discussion on available literatures focusing slicing and tool-path generation, geometric accuracy, surface roughness and mechanical properties. Section 2.3 summarizes the literature survey highlighting pioneers work and focuses on the scope of work. Thereafter, the scope and objectives of the present work are listed.

2.2 Literature Review

Although RP techniques offer advantages in terms of reduction in product build time for complex geometrical shapes and fabrication of parts without any use of tools, it has its own relative merits and demerits as far as part quality requirement is concerned. Therefore, it is necessary that shortcoming of RP processes should be understood and proper remedial measures should be searched before it is recommended for industries. Kim and Oh [2008] compared various RP process based on tensile strength, impact and compressive strength, heat resistance, hardness, surface roughness, geometrical and dimensional accuracy, material cost and manufacturing speed. It was verified that SLA process is advantageous in hardness, accuracy and surface roughness and poly jet process in tensile strength. The SLS process was advantageous in manufacturing speed and compressive strength, the 3D printing process in material costs and speed, and LOM process in heat resistance. The LOM and FDM process are superior in tensile strength and impact strength but the change of part building direction significantly reduces the tensile strength and impact strength. It has also been proposed that improvement of part strength, surface roughness, geometrical and dimensional accuracy, build time, and repeatability are key issues to be addressed for successful implementation of RP technology. Following sections will illustrate the past studies employed in this direction.

2.2.1 Slicing and Tool Path Generation

In RP or layered manufacturing (LM) processes parts are fabricated in layers. In RP slicing of the 3D CAD model is one of the important steps in prototype fabrications. Slicing of the model with a very small slice thickness leads to very large fabrication time whereas if large slice thickness is chosen, the surface quality is very poor due to staircase effect. This contradiction (small build time and good surface finish) leads to development of number of slicing procedure.

Jamieson and Hacker [1995] presented a methodology for direct and adaptive slicing of a CAD model using parasolid software developed at Cranfield University which converts the parasolid slices directly into CLI, HPGL or SLC format. Parasolid software is a solid modeling kernel of uni-graphics and underlying program can be directly accessed in C language. From results they had seen that direct slicing of CAD model is beneficial as it reduced the file size and cuts down the need to slice the tessellated model. Moreover, processing time is also reduced due to accuracy of direct slice CAD model having rounded and tubular design.

Kulkarni and Dutta [1995] studied the effect of staircase and containment problem on part accuracy and surface quality. They concluded that staircase effect and containment problem can be reduced by performing the adaptive slicing method in which maximum allowable cusp height can be specified for the object. The layer thickness are calculated based on the prescribed cusp height and surface geometry of the object which minimized the cusp height variation and gives good surface quality and reduced the build time of the object.

Sabourin *et al.* [1996] studied a new adaptive slicing method for layered manufactured parts using stepwise uniform refinement technique based on concept of limiting cusp height [Dolenc and Markela, 1994] as shown in Fig. 2.2. Here, a 3D CAD model is sliced into uniform horizontal slabs of thickness equal to maximum fabrication thickness (t_{max}). Those slabs which do not satisfy cusp height concept ($c < C_{max}$) are further subdivided individually into fine slabs of uniform thickness. Bidirectional interpolation is used to determine the optimal layer thickness. From result, they concluded that fabrication time (build time) is reduced upto 50 % when parts are built with adaptive slicing method without compromising the surface quality.

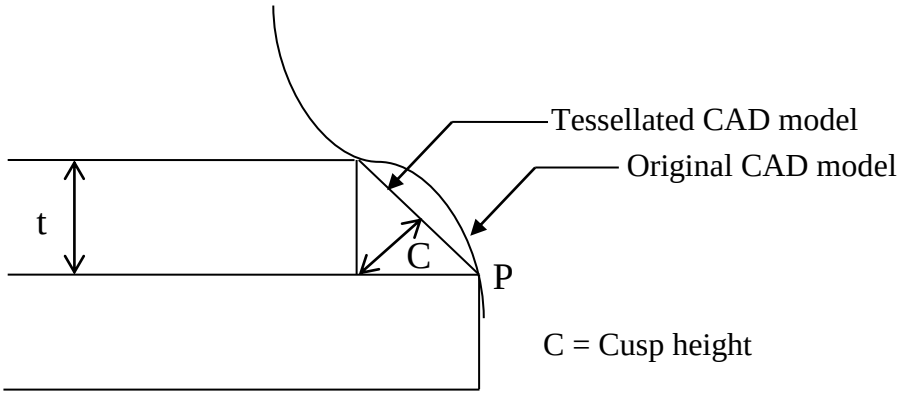

Figure 2.2: Cusp height [Dolenc and Markela, 1994]

Sabourin *et al.* [1997] presented a new approach in which part exterior is built precisely with thin layers using adaptive slicing method whereas the interior regions is built with thick and wide layers to complete the fabrication of LM parts. They concluded that accurate exterior and fast interior layered manufacturing method is important as it as potential to reduce the fabrication time upto 50-80 % without affecting the part integrity or surface quality. Further saving in built time can be achieved by increasing the fill rate of interior region or by adding voids to the interior region.

Xu *et al.* [1997] presented an approach for direct slicing of 3D CAD model for RP fabrication by using an adaptive slicing method and converted the slice data into the layer data format understood by the RP machines (without using STL file). The optimal build orientation is determined for SLA process based on variable slicing thickness technique considering accuracy, build time and stability of part as response variables. From results, they concluded that adaptive slicing method improved the part accuracy and reduced the build time. Results also showed that fabrication of parts with curved surfaces by adaptive slicing approach gives an effective and practical solution.

Hope *et al.* [1997] presented a new approach of adaptive slicing with sloping boundary surfaces that reduces the staircase effect which otherwise is characteristic for LM parts with square boundaries. They considered cusp height and maximum difference in plane layers as two types of error as shown in Fig. 2.3 and outlined a method for predicting these errors for sloping boundary surfaces. They concluded that main advantage achieved by this method is improvement in surface quality and decreased in fabrication time as thick layers can be used by this method.

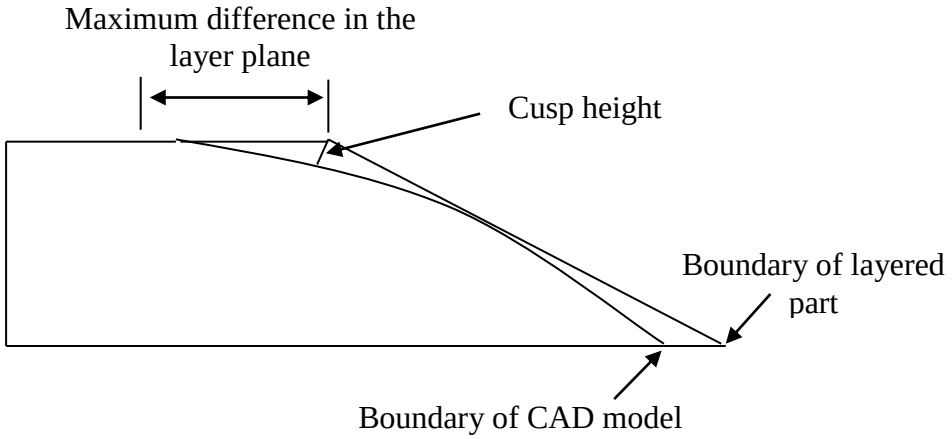

Figure 2.3: Cusp height and maximum difference in the layer plane, for layers with a sloping boundary surface [Hope *et al.*, 1997]

Tyberg and Bohn [1998] presented a new local adaptive slicing method based on cusp height concept to determine the slice thickness. In this method first individual parts and features are identified and then slicing of each part and features is carried out independently of one another. It is more often the case when several parts and features coexist at the same height but having different geometries such that each geometry require different slice thickness to meet the required tolerance. This approach improves over conventional adaptive slicing algorithms by reducing the most of the slices that do not improve the overall surface quality of the part. Moreover an unnecessary layer also increases the fabrication time. From

results they concluded that local adaptive slicing method reduces the fabrication time upto 17-37 % as compared to the conventional adaptive slicing methods.

Tata *et al.* [1998] demonstrated that the productivity of LM processes can significantly be improved by upgrading the slicing software. They proposed new slicing algorithm in which layer thickness can vary according to the surface complexity. They considered cusp height, chordal length, maximum deviation and volumetric error per unit length as four different criteria to vary the layer thickness whereas horizontal surfaces, vertical surfaces, pointed edges and pointed ends were considered as key characteristics of the object based on surface complexity. Finally, they developed the concept in which facets are grouped together based on their vertex coordinates so that number of searches for possible interaction of facets with slice planes can be minimized. They concluded that fabrication of parts with new slicing algorithm produced superior part quality in a short build time.

Ma and He [1999] proposed the adaptive slicing method with selective hatching strategies for slicing the non-uniform rational B-spline (NURBS) surfaces. From result they concluded that selective hatching method is very useful for RP parts having free form part geometries or part with slope surfaces. But in case of parts with thin walls or parts with slope surface, the selective hatching method may not be much help useful. Integration of adaptive slicing method with selective hatching strategy is an effective approach for obtaining smooth and accurate surface quality and fast building speed.

Mani *et al.* [1999] proposed different cusp heights for different surfaces of fabricated model rather than fixed cusp height on entire part. The difference between regions based adaptive slicing and traditional adaptive slicing method was shown in Fig. 2.4. The region based slicing method was implemented in four steps. Firstly critical surfaces are identified according to cusp height concept; secondly the model is decomposed into adaptive slice thickness (region A, refer Fig. 2.4) which was sliced and built, based on cusp height and geometry requirement and common interface layers (region C, refer Fig. 2.4) which was built with maximum possible layer thickness. The method of decomposition of the part into different regions is almost similar to the work proposed by [Sabourin *et al.*, 1997] as described earlier. They concluded that region based adaptive slicing method not only reduces the built time but also improves the surface quality especially for parts with complex geometries.

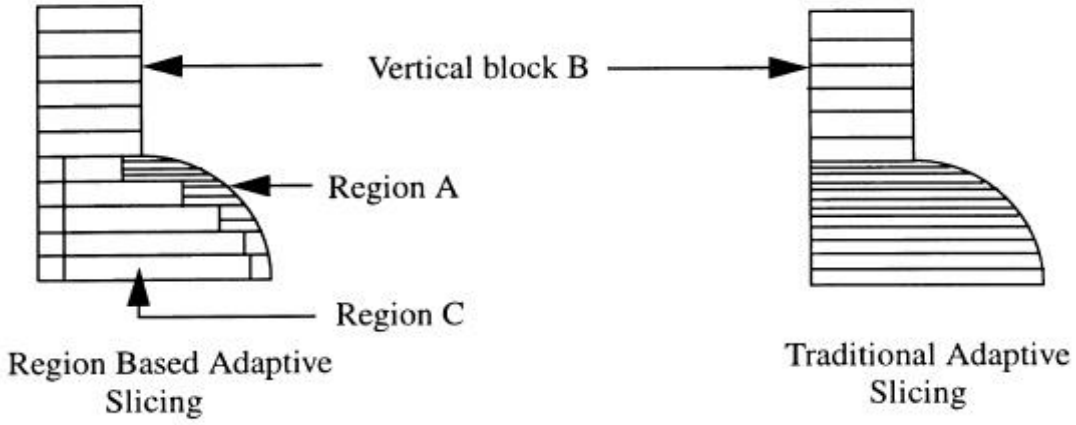

Figure 2.4: Slicing of a model by region based adaptive slicing and traditional based adaptive slicing [Mani *et al.*, 1999]

Lee and Choi [2000] presented a new methodology that drastically improved the computational (execution) time with better accuracy for LM parts using contour line intervals. The computational time is reduced by introducing the concept of sampling point in which perpendicular distance in calculated between two consecutive slices i.e. contour line intervals rather than calculating the slice thickness. They minimized the contour line intervals between two consecutive slices on the same *x-y* plane instead of minimizing the slice thickness. They were able to improve the efficiency further by introducing the vertical character line concept i.e. the curve that narrow down the area for optimum sampling points. They concluded that time spent in calculating the slice thickness for LM parts is significantly reduced by this new concept and accuracy of part is improved. This method gives better results when applied to bigger models having complex geometrical surfaces.

Zhao and Laperriere [2000] also carried out adaptive slicing method based on limited area deviation concept and implemented the concept using AutoCAD Run Time Extension and Microsoft Visual C++. This method directly slices the solid model based on area deviation ratio and avoids any intermediate representation. This method also minimizes the staircase effect and reduces the number of layers because it modifies the slice thickness to take the surface curvature into account along the vertical direction. Therefore, they concluded that adaptive direct slicing has potential to fabricate the parts with higher accuracy and efficiency.

Han *et al.* [2003] proposed the adaptive slicing method based on build time analysis so that fabrication speed can be increased for FDM process in order to increase the productivity. They considered that part is made up of many divisions, and for each division the slice thickness is the same as shown in Fig. 2.5. They concluded that build time will decrease with increase in slice thickness, working and ideal speed and reducing the number of repositioning distances.

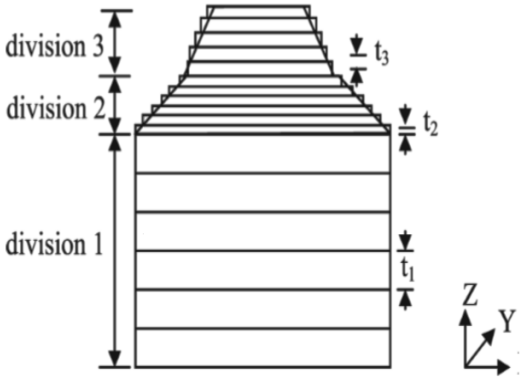

Figure 2.5: A part of 3 divisions ($t_1 > t_3 > t_2$) [Han *et al.*, 2003]

Zhau *et al.* [2004] presented an approach of direct and adaptive slicing of the CAD model using non uniform cusp height concept and avoid the intermediate representation (.stl file). In this approach 3D model is imported to adaptive slicing system from CAD system using .stp format where solid model is displayed and user has to specify the allowable cusp height for every highlighted features. Thus model is sliced with different cusp height for different surfaces. They concluded that adaptive slicing with non-uniform cusp height increases the efficiency and decreases the number of layers and build time of fabricated parts than common adaptive slicing procedure.

Hayasi and Asiabanpour [2014] presented a curved form adaptive slicing method for tessellated CAD model having diverse types of surfaces (convex, concave and flat). The resulting surface will closely fit its original CAD model boundary with much less geometry deviation error which will pave the way for fabricating the functional parts and tooling accurately that are made by layer building process. From result they concluded that this approach significantly reduces the staircase effect on either convex or concave edges, increases the part accuracy and reduces the fabrication time significantly.

2.2.2 Geometric Accuracy Improvement

The geometric accuracy of fabricated parts by various RP processes is highly important, because it represents the degree of agreement between fabricated part and designed part. The RP processes produce parts in low volume and need to be robust and fit to designed functionality otherwise fabricating new prototype will be expensive and time consuming. These make it essential that geometric accuracy of fabricated parts meet the required standards. Regarding these issues some studied are reviewed and summarized below.

Frank and Fadel [1995] studied the effect of part build orientation on accuracy, build time and support structure required to fabricate an object. They observed that the part inaccuracy is mainly due to staircase effect which cannot be avoided completely but can be reduced to some extent by orientation of parts in suitable direction. The build time was considered second important parameter as LM processes can manufacture model rapidly than any other conventional methods. Support structure was considered least important as it is intrinsic part of LM techniques.

Alexander *et al.* [1998] measured the effect of part orientation on part accuracy and build cost of LM parts. Dimensional inaccuracy is due to staircase effect which was measured in term of weighted cusp height concept and calculated by multiplying facet area with cusp height. The average weighted cusp height is calculated in which sum of weighted cusp height is divided by total facet area. The optimal part deposition orientation was selected from preselected orientation on the basis of minimum average weighted cusp height which gives maximum part accuracy and minimum build cost of LM parts.

Dao *et al.* [1999] calculated shrinkage compensation factors for FDM parts with varying lengths. They observed that mean error after shrinkage compensation follows a linear trend i.e. error increases as nominal dimensions increases. Also, the residual errors are found to be scattered due to lack of process stability. They attributed this trend to the noise shrinkage which is not compensated by the scaling factors used.

Xu *et al.* [1999] determined the optimal part deposition orientation for various RP techniques considering part inaccuracy, build time and build cost as response variables. They considered part inaccuracy as the sum of oversize volume, staircase volume and trapped volume, whereas build cost was considered as the sum of amount of model material and support material required. The optimal orientation is selected for which weighted sum of three response variables is minimum.

Xu *et al.* [2000] measured the dimensional accuracy of complex parts fabricated by various RP techniques. From results they concluded the SLA process gives the best dimensional accuracy for the majority of the dimensions measured followed by LOM, FDM, and SLS processes. In terms of the roundness of cylindrical features, SLA and LOM produce the best results whereas SLS gives intermediate results, while FDM performs worst.

Zhou *et al.* [2000] proposed parameter tuning approach using Taguchi experimental design to improve the dimensional accuracy of SLA parts. A standard sample was developed to act as a benchmark for comparison of the total of twenty different dimensional, geometrical, and surface features. Analysis suggests that the best setting of control factors for each individual feature is different. For example, blade gap has the largest effect for horizontal dimension whereas overcure is more influencing in vertical direction for dimensional accuracy improvement.

Masood *et al.* [2000] presented a new method to study the effect of build orientation on volumetric error of FDM parts. They considered different part shapes (cube, sphere, cylinder and pyramids) each build at different build orientation (0°, 15°, 30°, 45°, 60°, 75°, 90°) to calculate the volumetric error and optimal orientation is selected based on minimum volumetric error. They concluded that for cube and cylindrical shapes volumetric error is minimize at 90° and 0° part orientation whereas in case of sphere the volumetric error is constant for all angles of orientation. For pyramid shapes volumetric error is minimized at 64° build orientation.

Rattanawong *et al.* [2001] presented a methodology to study the effect of part depositions orientation on volumetric error of LM parts. They considered primitive volume approach in which complex part was divided into different primitive volumes such as cubes, cylinder, cones, hemispheres and pyramids. Volumetric error was calculated in each primitive volume after which error was calculated in part made from the combination of these primitives. The system graphically displays volumetric error for different orientation and best orientation is selected based on minimum volumetric error in complete part.

Masood and Rattanawong [2002] calculated the volumetric error in FDM parts for different part orientation using generic algorithm method. They considered both simple and complex geometrical parts and calculate the volumetric error which is mainly due to staircase effect. An algorithm slices the CAD model and volumetric error is calculated for each layers. The system than calculate the volumetric error in each parts having different orientation and optimal orientation is selected based on minimum amount of volumetric error in FDM parts.

Perez [2002] studied the effect of slope variation on dimensional accuracy of FDM manufactured parts. The dimensional parameters were studied with the help of coordinate measuring machine (CMM) to determine the capability of FDM machine for manufacturing the parts. From results they concluded that uncertainties in dimensional accuracy are more or less the same for different slope variations. They also concluded that better dimensional accuracy can be obtained by reducing the layer height due to reduce in staircase effect and manufacturing time, build cost is also reduced by reducing the layer height.

Pennington *et al.* [2003] studied the effect of different process parameters on dimensional accuracy of parts fabricated by FDM process. Dimensions are measured with the help of CMM and digital micrometers. From analysis of twelve different dimensions, it was reported that the part size, envelope temperature and location in the work envelope had a significant effect on dimensional accuracy of FDM parts.

Wang *et al.* [2007] investigated the effect of process parameters (scanning speed, layer thickness, hatch pattern, delay time, laser power and bed temperature) on shrinkage characteristics in SLS process. From results, they found that percentage shrinkage increases with increase in the hatch spacing and scanning speed, but decreases with increasing layer thickness, bed temperature, laser power and delay time.

Sood *et al.* [2009] studied the effect of raster angle, layer thickness, air gap, part orientation and raster width on dimensional accuracy of FDM manufactured parts. For their experimental work, they considered Taguchi method and optimum process parameters settings were selected so that three dimensions (length, thickness and width) show minimum deviation from their actual value. Using analysis of variance (ANOVA) they concluded that 0.178 mm layer thickness, 0° part ordination, 0.4564 mm road width, 0° raster angle and 0.008 mm air gap are optimal settings for achieving overall dimensional accuracy.

Nancharaiah *et al.* [2010] studied the effect of four process parameters such as air gap, raster angle, road width and layer thickness on dimensional accuracy of FDM processed parts. They conducted an experiment using Taguchi method with 3 levels for each factors. From results they concluded that layer thickness, air gap and road width are most significant factors that affect the dimensional accuracy of FDM parts. However, the effect of raster angle is least significant. They also conducted a correlation analysis which indicates that layer thickness and dimensional accuracy are moderately correlated.

Bakar *et al.* [2010] studied the effect of layer thickness, contour width and internal rasters on dimensional accuracy of FDM fabricated parts. They measured the dimensional accuracy for different features (slot, ring, cube and cylinder) in test model. Results showed that contour width and layer thickness are significant factors that affect the dimensional accuracy of FDM parts. Dimensional accuracy increases for smaller layer thickness. The larger internal rasters and wide contour produce good bonding quality between adjacent layers which increases the dimensional accuracy of parts.

Paul and Anand [2011] investigated the relation between cylindricity tolerance and part orientation in LM parts. The effect of part orientation on cylindricity error was analyzed by three methods: using simple analytic method, simulating the manufactured surface and by using STL files of the part. From results, they found that cylindricity error obtained from simulating the CAD model and analytical method were the same but cylindricity error was more when using STL file of the part. They also demonstrated the same method for determining the optimal part deposition orientation for test parts with multiple cylindrical features.

Phatak and Pande [2012] studied the effect of part build orientation on dimensional accuracy, build time and build cost using genetic algorithm method. In their approach the CAD model was converted into STL file and orientated model is sliced and hollowed with required thickness. They converted the objective functions into single objective function after assigning some suitable weights. The optimal part deposition orientation is selected for minimum weighted average sum of objective functions.

Gurrala and Regalla [2014] studied the effect of build interior, vertical build direction and horizontal build direction on volumetric shrinkage of FDM parts. For their experimental work they considered centered composite design (CCD) method. From results, they showed that for better dimensional accuracy or lower volumetric shrinkage; lower angle of material deposition in horizontal direction with optimal settings in vertical build direction and maximum build interior should be selected.

2.2.3 Surface Roughness Improvement

Surface finish of parts fabricated by various RP processes is highly important, especially in cases where the parts come in contact with other elements or materials in their service life. The surface finish can affect the ability of parts to resist fatigue and wear, to increase or decrease abrasion between mating surfaces. As these characteristics become

critical under various loading/operating condition. Surface finish can dictate the integrity, performance and service life of components fabricated by RP processes.

Seth and Dutta [1994] determined the optimal part orientation by reducing the contact area of model with support structure, which also reduces the build time, improves surface finish and ensures better stability of fabricated model. In their approach best orientation is selected from pre-selected orientation and when two orientations had same area of contact with support structure, the orientation with lower center of mass is selected.

Kattethota and Henderson [1998] considered part orientation and layer thickness as process parameters to study the effect on surface roughness of FDM parts. They considered three type of surface i.e. quadric, planar and freeform and concluded that 10°-40° angle of part orientation was a critical range for which surface roughness deteriorate to maximum therefore these range should be avoided for obtaining better surface quality.

Bharath *et al.* [2000] carried out experiment considering fractional factorial design to determine the effect of air gap, layer thickness, part orientation, raster width and model temperature on surface finish of FDM parts. Using ANOVA they concluded that part orientation and layer thickness and their interactions are significant parameters that effect the surface quality of the specimen whereas air gap, raster width and model temperature does not have much influence on surface quality FDM parts.

Anitha *et al.* [2001] performed experiment using Taguchi method to assess the influence of three process parameters such as layer thickness, road width and deposition speed on surface roughness of FDM processed parts. It has been observed that quality of parts is significantly affected by layer thickness as compared to road width and deposition speed and contribution of interactions are also found negligible. They also conducted a correlation analysis which demonstrated that there exists a strong inverse relation between layer thickness and surface roughness.

Perez [2002] studied the effect of slope variation on surface roughness of FDM manufactured parts. Perez considered average surface roughness (*Ra*) and root mean square surface roughness (*Rq*) to evaluate the surface quality of FDM parts for different slope variations. From results they concluded that R_q value is greater than R_a value because rms value is more affected by isolated errors thus detects error better than average value. They also concluded that better surface quality can be obtained by reducing the layer height due to reduced staircase effect. Manufacturing time, build cost is also reduced by reducing the layer height.

Campbell *et al.* [2002] compared the surface roughness visualization of test samples made by several RP processes like SLA, Thermo Jet, LOM, 3D printers and FDM with surface roughness prediction model proposed by Reeves and Cobb [1995] given by Eqn. 2.1.

$$R_a = \alpha \frac{a \sin\theta}{4 \tan\theta} \tag{2.1}$$

where R_a is average surface roughness, θ is the angle between the surface normal and vertical direction and α is layer thickness. It has also shown that surface quality can be well predicted in wide range of angles for majority of systems. However, equation estimates higher value of roughness for upward facing surface in parts built by FDM, 3D printers and Thermo Jet processes. The study also indicates that apart from layer thickness, other parameters also influence the surface roughness of RP parts.

Pandey *et al.* [2003b] proposed a hybrid FDM system in which materials deposition in a layer-by-layer fashion and machining of edges by hot cutter machining simultaneously. They carried out experiment considering rake angle, cutting speed, build orientation and direction of cuts as process parameters and machining is performed along both the direction i.e. along and across the length of the specimen and average surface roughness is measured along both directions. From results they concluded that proposed machining method reduces the staircase effect and enhance the surface quality of the specimen upto R_a = 0.5μm with 87% of confidence level.

Pandey *et al.* [2004] conducted an experiment using non-dominated sorting genetic algorithm II to determine optimal deposition orientation considering average surface roughness (R_a) and build time as objective functions. From results they concluded that surface roughness and build time are two contradicting objective functions. Therefore, optimal orientation is selected which minimized the weighted sum of average surface roughness and build time. In evaluating the build time and surface roughness the effect of support structure is also considered in their work.

Thrimurthulu *et al.* [2004] conducted an experiment using real time genetic algorithm to study the effect of part orientation on surface quality and build time of FDM parts. They converted the two objective functions (build time and surface quality) into single objective function after assigning some suitable weights. The surface roughness and build time are two contradicting objective functions which are minimized by minimizing their total weighted sum. The optimal part deposition orientation is selected for minimum build time and surface roughness.

Byun and Lee [2005] considered genetic algorithm to determine the optimal part deposition orientation considering surface roughness as objective function. They considered average weighted surface roughness instead of cusp height concept in order to determine the optimal orientation. In evaluating the surface roughness, build time and support structure is also minimized in fabricating freeform parts. In their next work, Byun and Lee [2006] determined the optimal part deposition orientation from pre-selected candidate orientation using multi-criteria decision making method. The part inaccuracy was estimated in term of surface roughness (R_a) due to staircase effect. The optimal part orientation is again selected based on minimizing the weighted sum of build time, surface roughness and support structure.

Reddy *et al.* [2007] conducted an experiment to study the effect of chamber temperature, nozzle temperature and road gap on surface finish of extruder deposition process (EDP) manufactured parts. Extruder deposition process is new method based on polymer extrusion principle. They concluded that with increase in road gap surface roughness increases whereas surface roughness decreases with increase in nozzle or chamber temperature. They also concluded that good surface finish for EDP parts is obtained for lower road gap and higher nozzle temperature.

Ahn *et al.* [2009] presented a new approach to model surface roughness of FDM samples. They considered surface angle, layer thickness, and overlap interval and cross sectional shape of the filament as process parameters that affects the surface quality of FDM parts. From experimental results they concluded surface quality of parts is significantly affected by layer thickness as compared to other parameters. The thinner layer thickness would generate high surface quality of FDM specimen. They also proved that, surface quality of specimen also depends upon different angles (part orientation) of FDM parts. Therefore, for maximizing the surface quality and reducing the post processing work, thinner layer thickness must be applied along with other parameters.

Galantucci *et al.* [2009] analyzed the surface roughness of FDM parts considering nozzle tip diameter, raster width and slice height as process parameters. Using ANOVA they concluded that tip diameter has very little effect on surface roughness of build specimen whereas slice height and raster width are significant factors that affect the surface roughness. A chemical post treatment by dimethyl-ketone and water solution had also been analyzed which showed that chemical treatment significantly improved the surface finish of FDM parts.

Galantucci *et al.* [2010] presented a method for improving the surface roughness of FDM fabricated parts by chemical post treatment with 90% dimethyl-ketone and 10% water solution and compared the surface roughness of chemical finished specimens with untreated specimen. They conducted experiments considering raster angle, raster width and immersion time as process parameter each varied at 3 levels. From results they concluded that chemical treatment cuts away material but the subtracted ABS is balanced by the absorption of the solution and the surface roughness of the specimens significantly improved. Roughness can further be improved by increasing the immersion time of specimen in chemical solution.

Nancharaiah *et al.* [2010] studied the effect of four process parameters such as air gap, road width, layer thickness, and raster angle on surface quality of FDM processed parts. They conducted experiments using Taguchi method and concluded that layer thickness and road width are most significant factors that affect the surface finish of FDM parts. However, the effect of raster angle and air gap is least significant factor for surface roughness. They also conducted a correlation analysis and observed that layer thickness and surface roughness are strongly correlated.

Bakar *et al.* [2010] studied the effect of contour width, internal rasters and layer thickness on surface roughness on FDM fabricated parts. They measured the surface roughness along both the directions i.e. vertical and horizontal directions and proved that horizontal direction surface is always better then vertical surface because elliptical curves are formed along vertical direction during bonding of layers. Results also showed that internal rasters and contour width are significant factors that influence the surface quality. The larger internal rasters and wide contour produce good surface finish due to good bonding quality between adjacent layers.

Phatak and Pande [2012] studied the effect of part orientation on part quality, build time and build cost using genetic algorithm method. In their approach the CAD model was converted into STL file and orientated model is sliced and hollowed with required thickness. They converted the objective functions into single objective function after assigning some suitable weights. The optimal part deposition orientation is selected for minimum weighted average of objective functions.

Boschetto *et al.* [2013a] conducted an experiment using artificial neural network (ANN) technique to determine the surface roughness of FDM processed functional parts. They measured the surface roughness as the function of layer thickness and part deposition angle. From results, they concluded that ANN predicts the surface roughness accurately as compared to other traditional surface roughness measuring methods. In another work,

Boschetto *et al.* [2013b] measured the surface roughness of FDM model using profilometric analysis. The considered all surface roughness parameters rather than average surface roughness parameter to measured surface roughness of FDM parts. The proposed profile model is very effective in describing surface roughness of micro geometrical surface of FDM specimen.

Ali *et al.* [2014] performed an experiment using Taguchi method to study the effect seven process parameters such as road width, slice height, raster angle, air gap, number of contours, STL angle and STL deviation on surface roughness of FDM processed parts. From results it has been observed that surface quality of the specimen is significantly affected by the raster angle, road width and air gap whereas the effects of other parameters and contribution of the interactions are found to have negligible effect on surface quality.

Durgun and Ertan [2014] investigated the effect of part orientation and raster angle on the surface roughness of FDM parts. They manufactured the specimens considering three different part orientations (horizontal, vertical and perpendicular direction) and five different raster angles (0°, 30°, 45°, 60° and 90°). From results they concluded that part orientation affects surface roughness more significantly than raster angles. They also concluded that part build with 0° raster angle along horizontal direction exhibit good surface quality.

2.2.4 Mechanical Characteristic Improvement

The various RP techniques have shown huge potential not only for fabricating 3D models but also for fabricating the final functional parts due to simplicity of operation and durability of parts in term of mechanical strength and accuracy. In RP processes, the generation of error in manufactured parts depends mainly on process parameters setting during fabrication of specimens. These process parameters namely part orientation, layer thickness, raster angle, raster width, air gap, etc. directly impact the final mechanical properties like stiffness, tensile and flexural strength, impact strength, toughness, etc. both individually as well as combination with other parameters. Regarding these issues:

Cheah *et al.* [1997] studied the mechanical properties of parts fabricated by SLA process using acrylic based polymer and post cured the specimen under UV light. It was observed that post curing the specimen yield higher values of tensile strength, elastic modulus and elongation of fracture. They also observed that these properties are function of laser exposure density and layer pitch. Mechanical properties of specimen can be increased by decreasing the layer pitch and increasing the laser exposure density.

Said *et al.* [2000] studied the effect of layer orientation on mechanical properties (tensile, flexural and impact strength) of ABS P400 FDM parts. For their experimental work they considered five different raster angles (0°, 45°/0°, 45°/-45°, 45° and 90°) to fabricate specimens. Results showed that 0° raster angle displayed highest strength than all other layer orientation due to strong interlayer bonding and maximum interlayer porosity between adjacent rasters.

Rodriguez *et al.* [2001] studied the mechanical behavior of ABS monofilaments and ABS plastic materials with three mesostructure. They determined the strength and elastic modulus for FDM ABS materials and ABS monofilament feedstock. From results they concluded that elastic modulus reduced to 11-37 % whereas strength reduces to 22-57 % for ABS materials as compared to ABS monofilaments which was mainly due to the presence of voids and loss of molecular orientation during extrusion process.

Ahn *et al.* [2002] investigated the effect of air gap, raster orientation, color, model temperature and bead width on compressive and tensile strength of FDM processed parts using design of experiments (DOE) approach. They concluded that air gap and raster orientation are the significant factors that affects the tensile strength whereas the effects of model temperature, color and bead width are negligible. Results also showed that measured compressive strength is higher than tensile strength and build direction has no effect on it. They also concluded that mechanical properties are anisotropic in nature.

Bellini and Guceri [2003] presented a methodology to determine the mechanical characteristics of parts fabricated by FDM process. They considered road shape and road-to-road interactions and path are important parameter that affects the performance of finished product. From results they concluded that mechanical characteristics of final part depend upon two important modeling phases i.e. the chosen path (the way each layer is filled by beads) and chosen building direction (orientation of parts with respect to substrate).

Lee *et al.* [2005] studied the effect of raster width, layer thickness, air gap and raster angle on elastic performance of FDM manufactured parts. They considered experimental deign technique to study the effect of process parameters each varies at three levels. The experiments are conducted at 10°, 15° and 20° angle of displacement and concluded that air gap, raster angle and layer thickness are significant factors that affects the flexibility of FDM parts where the effect of raster width is found to be negligible.

Jain *et al.* [2008] studied the effect of various process parameters namely refresh rate, layer thickness, hatch pattern and bed temperature on parts fabricated be SLS process. They conducted the experiments based on taguchi methods. ANOVA was used to obtain the

significant factors that affect the part strength and optimal strength condition was obtained by maximizing the signal\noise ratio.

Chockalingam *et al.* [2008] studied the effect of three process parameters such as post curing time, layer thickness and part orientation on tensile, flexural and impact strength of parts fabricated by SLA process. Using ANOVA they concluded that layer thickness, post curing time and orientation are significant factors that affect the strength of SLA parts. Moreover from the three process parameters the layer thickness had major contribution factor on part strength.

Bellehumeur *et al.* [2008] experimentally demonstrated that bond quality between adjacent filaments depends on envelope temperature and variations in the convective conditions within the building part while testing flexural strength specimen. Temperature profiles reveal that temperature at bottom layers rises above the glass transition temperature and rapidly decreases in the direction of extrusion head movement. The minimum temperature increases with the number of layers. Microphotographs indicate that diffusion phenomenon is more prominent for adjacent filaments in bottom layers as compared to upper layers.

Panda *et al.* [2009] studied the effect of part orientation, layer thickness, air gap, raster angle and raster width on three response variables such as tensile, flexural and impact strength of test model fabricated by FDM technique using bacterial forging method with each response variables varies at three levels. They concluded that part orientation and raster angle should be maintained at lower level for improving the tensile and flexural strength whereas when they are kept at higher level for impact strength improved. On the other hand if raster width and raster angle was maintained at higher level than all the three response variables increased whereas when it was kept at medium and higher level than flexural strength and tensile strength increases. The effect of air gap on impact strength was found to be negligible

Sood *et al.* [2010] studied the effect of raster angle, raster width, part orientation, layer thickness and air gap on three responses variables i.e. flexural strength, impact strength and tensile strength of specimen fabricated by FDM process. They considered ANOVA and central composite design (CCD) methods to drive the relationship between process parameters and response variables. Results showed that the effect of individual process parameters is not much significant but their interaction with other parameters significantly affects the response variables.

Galantucci *et al.* [2010] presented a new methodology in which fabricated FDM parts are post treated with 90% dimethyl-ketone and 10% water solution and compared the tensile strength and flexural strength of chemical finished specimens and untreated specimens. They conducted an experiment considering raster angle, raster width and immersion time as process parameter each varies at 3 levels. From results they concluded that tensile strength of treated specimen significantly reduced as compared to untreated specimen which further reduces as immersion time increases as shown in Fig. 2.6. On the other hand flexural strength of specimen increased after post treatment with chemical solution.

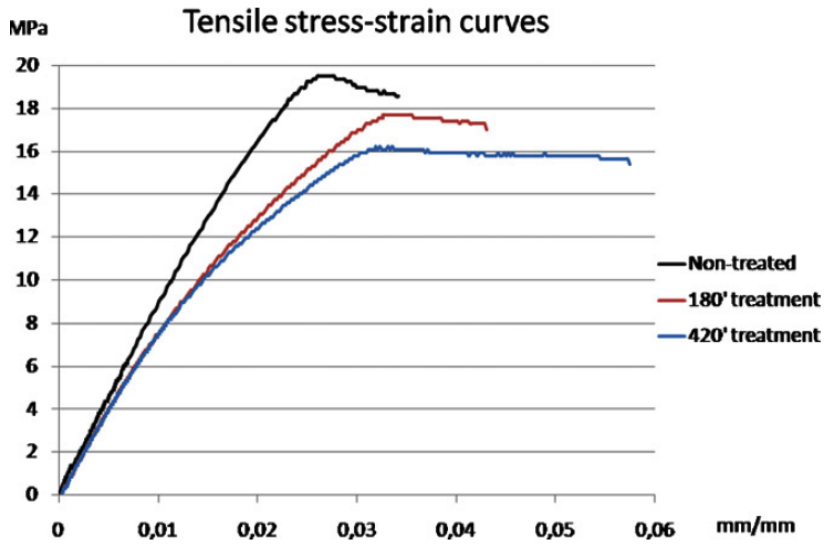

Figure 2.6: Tensile stress strain curves for treated specimen and untreated specimens [Galantucci *et al.*, 2010]

Percoco *et al.* [2012] compared the compressive strength of chemical finished specimens with dimethyl-ketone and water solution and untreated specimen. They considered raster angle, raster width and immersion time as process parameter each varies at 3 levels. From results they concluded that chemical treatment cuts away material but the subtracted ABS is balanced by the absorption of the solution. They also showed that compressive strength of the specimen increases after chemical treatment as compared to untreated specimen.

Sood *et al.* [2012a] studied the effect of raster angle, raster width, part orientation, layer thickness and air gap on sliding wear of test model fabricated by FDM process. They considered response surface methodology to drive the relationship between the process parameters and sliding wear of test model. The equations are derived to determine optimal process parameters settings through quantum behaved particle swarm optimization (QPSO)

methods and artificial neural network are employed to validate the results obtained by QPSO method. In their next work Sood *et al.* [2012b] studied the effect of raster angle, raster width, part orientation, layer thickness and air gap on compressive strength of test model. The equations are derived to determine optimal process parameters settings through QPSO methods and compressive strength is predicted through ANN and compared with predictive equations. The experimental results also established brittle and anisotropic nature of FDM processed parts.

Tymrak *et al.* [2014] studied the tensile strength, elastic modulus and strain at maximum strength for parts fabricated by 3D printer using ABS and polylactic acid (PLA) materials. Results showed that tensile strength and elastic modulus of parts fabricated by PLA material was comparatively higher than that of parts fabricated by ABS material.

Durgun and Ertan [2014] investigate the effect of part orientation and raster angle on the tensile and flexural strength of FDM parts. They manufactured the specimen considering three different part orientations (horizontal, vertical and perpendicular) and five different raster angles (0°, 30°, 45°, 60° and 90°). From results they concluded that part orientation affects the mechanical properties more significantly than raster angles. They also concluded that part build with 0° raster angle along horizontal direction exhibit maximum tensile and flexural strength.

Gurrala and Regalla [2014a] investigated by both mathematical modeling and experimentation the effect of bonding between the filaments on tensile strength of the parts fabricated by FDM process. The considered two different build orientations for conducting tensile load testing. Agreement between mathematical modeling and experimental tensile load and scanning electron microscope (SEM) images of fracture surfaces they concluded that strength of the specimen is mainly due to inter-layer bonding, intra-layer bonding and neck growth between the filaments of FDM specimen.

Gurrala and Regalla [2014b] studied the effect of build interior, vertical build direction and horizontal build direction on tensile strength of FDM parts. For their experimental work they considered centered composite design (CCD) method. From results, they showed that for better tensile strength the recommended FDM settings are maximum angle of material deposition in vertical direction with optimal settings in horizontal build direction and maximum model interior.

2.3 Scope and Objectives of Present work

The RP process offers distinct advantage of the ability to fabricate in virtually tool free environment and geometrically insensitive parts in comparison to conventional metal forming or subtractive manufacturing processes. The present applications not only limited to form, fit and functional testing but it is coming into increasingly widespread use in specialized technological applications where limited quantities of durable precision components are needed. Further, integrating these technologies with other secondary processes not only reduce the time to market but also give the cost benefit to the practitioners [Chua *et al.*, 1999; Shan *et al.*, 2003]. Among the different RP technologies available today, FDM process is one of the widely adopted process by the industries due to low maintenance cost, large variety of materials available, low fabrication cost even with complex geometries, environmental friendly and easy operation with very little or no supervision required. But in this process the performance of final fabricated part is influenced by many process parameters and machine settings which directly impact the final mechanical properties, surface roughness, geometrical and dimensional accuracy, build time etc. of the parts thus posing challenge in obtaining the optimal values with desired attributes.

Regarding these issues number of studies has been carried out to study the effect of process parameters: layer thickness, air gap, raster angle, raster width, model build temperature, contour width, tool path generation, etc. on performance of fabricated parts. Adaptive slicing of CAD model based on cusp height concept was first introduced by [Dolenc and Makela, 1994] for enhancement of surface finish and reduced the build time. Many attempts based on same concept like stepwise uniform refinement technique [Sabourin *et al.*, 1996], fast interior and accurate exterior [Sabourin *et al.*, 1997], local adaptive slicing [Tyberg and Bohn, 1998], region based adaptive slicing [Mani *et al.*, 1999] of a solid model having different cusp heights for different surfaces rather than fixed cusp height. The adaptive slicing method with selective hatching strategies for slicing the NURBS surfaces was implemented by Ma and He [1999]. Many attempts [Jamieson and Hacker, 1995; Xu *et al.*, 1997; Zhao and Laperriere, 2000; Zhau *et al.*, 2004] have been made for direct adaptive slicing of 3D CAD model to achieve higher accuracy and reduced build time. The concept of adaptive slicing with sloping (curved) boundary surfaces [Hope *et al.*, 1997; Lee and Choi, 2000; Hayasi and Asiabanpour, 2014] can lead better result by reducing staircase effects and build time. Adaptive slicing method based on build time analysis was reported by [Han *et al.*, 2003] which reduces the build time, increases part surface quality and increases the

fabrication time. Algorithm to calculate layer thickness according to surface complexity is also presented, which produced superior part quality in a short build time [Tata *et al.*, 1998].

Benchmark studies have been performed on geometrical and dimensional accuracy improvement of RP fabricated parts [Frankel and Fadel, 1995; Alexander *et al.*, 1998; Xu *et al.*, 1999; Xu *et al.*, 2000] shows that part quality differs not only with different rapid prototyping technologies, but also for different geometrical features and part orientation. The variation in properties is also noted. For a stable manufacturing process, the random errors should be small and evenly distributed. The systematic errors common in the RP processes may come from the shrinkage effect, positioning error, laser overcuring or overheating effect, distortion in the post processing stage, improper setting of process parameters [Dao *et al.*, 1999; Zhou *et al.*, 2000; Wang *et al.*, 2007]. Many attempts [Masood *et al.*, 2000; Rattanawong *et al.*, 2001; Masood and Rattanawong, 2002; Gurala and Regalla, 2014] have been made to investigate the effect of part build orientation and build interior on volumetric shrinkage of FDM parts. They calculated volumetric error due to staircase effect for both simple and complex geometrical part shapes and volumetric error is calculated which is mainly due to staircase effect. The effect of layer thickness, part orientation, raster width, air gap, raster angle, contour width were investigated on dimensional accuracy of FDM parts using Taguchi method approach [Perez, 2002; Pennington *et al.*, 2003; Sood *et al.*, 2009; Nancharaiah *et al.*, 2010; Bakar *et al.*, 2010]. Genetic algorithm method to calculate the optimal part build orientation based on dimensional accuracy of RP parts is also presented, which produced superior part quality in a short build time and build cost [Paul and Anand, 2011; Phatak and Pande, 2012].

Poor surface quality is sometimes overcome by performing finishing operations such as grinding or polishing after an object is built. These post-processing operations are however unfavorable to the original geometry of the component and are time consuming [Kim *et al.*, 2005; Ahn *et al.*, 2007]. Earlier attempts to improve this are related with slicing accuracy and part build orientation determination using empirical models. Later on, many attempts were made to understand the functional relationship between process parameters (layer thickness, part orientation, chamber temperature, nozzle temperature, air gap, raster angle, raster angle and contour width) and surface roughness using experimental analysis technique [Bharath *et al.*, 2000; Anitha *et al.*, 2001; Reddy *et al.*, 2007; Ahn *et al.*, 2009; Bakar *et al.*, 2010; Nancharaiah *et al.*, 2010; Durgun *et al.*, 2014; Ali *et al.*, 2014]. Most of the surface roughness models consider layer thickness and build orientation as most influencing factors neglecting many other parameters involved during actual part building stage [Seth and Dutta, 1994,

Kattethota and Henderson, 1998, Perez, 2002, Armillotta, 2006; Boschetto *et al.*, 2013a; Boschetto *et al.*, 2013b]. The correlation analysis is also conducted by [Anitha *et al.*, 2001] which indicates that there is strong inverse relationship between layer thickness and surface roughness. In very few attempts [Pandey *et al.*, 2003b; Byun and Lee, 2005; Byun and Lee, 2006] has consider part inaccuracy is mainly due to staircase effect which is estimated in terms of R_a value which is widely accepted in engineering design and manufacturing practice. Many attempts [Pandey *et al.*, 2004; Thrimurthulu *et al.*, 2004; Byun and Lee, 2005; Byun and Lee, 2006; Phatak and Pande, 2012] considered Genetic algorithm method to determine optimal part deposition orientation considering surface roughness and build time as response variables. The development of new method [Galantucci *et al.*, 2009; Galantucci *et al.*, 2010] which improve the surface finish of FDM parts by chemical dipping in dimethylketone and water solution considering raster angle, raster width and immersion time as process parameters

One of the major issues concerning with RP is the mechanical strength of processed part. The mechanical strength of RP processed parts are usually less compared to conventional manufacturing process or to original material. Part of this drawback is due to process able material related constraints but major limitation is due to their own part building principles and process parameters settings. Many attempts [Said *et al.*, 2000; Ahn *et al.*, 2002; Bellini and Guceri, 2003; Lee *et al.*, 2005; Panda *et al.*, 2009; Sood *et al.*, 2010; Sood *et al.*, 2012b, Durgun and Ertan, 2014; Gurrala and Regalla, 2014b] made to understand the effect of process parameters (layer thickness, part orientation, chamber temperature, nozzle temperature, air gap, raster angle, raster angle and contour width) on tensile strength, flexural strength, impact strength and compressive strength of FDM parts using experimental analysis method. They also concluded that mechanical properties also exhibit anisotropic behavior [Ahn *et al.*, 2002]. Influence of laser exposure density, layer thickness, part orientation, curing time on mechanical properties of SLA parts were investigated by Cheah *et al.* [1997]; and Chockalingam *et al.* [2008]. In very few attempts [Rodriguez *et al.*, 2001; Bellehumeur *et al.*, 2008; Gurrlla and Regalla, 2014a], was measured strength in terms of inter-layer bonding, intra-layer bonding and neck growth phenomenon. They considered diffusion phenomenon is more prominent for adjacent filaments in bottom layers as compared to upper layers and bond quality depends on envelope temperature. The influence of raster width, raster angle, air gap, layer thickness and part orientation were investigated on sliding wear of FDM parts [Sood *et al.*, 2012a]. The development of new method improves the flexural and compressive strength

of FDM parts but slightly decreases tensile strength where parts are post treated by chemical dipping in dimethylketone-water solution [Galantucci *et al.*, 2010; Percoco *et al.*, 2012].

The trend of current literature suggests that all RP technologies have some generic and exclusive common features, which convey a number of synergies among them. The main appeal is towards the novel possibilities and applications offered by these technologies. However, these technologies still differ greatly in terms of physical process, geometry, performance and materials that can be processed. Studies carried out worldwide have shown the significant variation in the part properties took place with changing process parameter conditions. This highlights the scope of improvement in them. Though much work has been reported on various RP technologies but the possibility of improvement in FDM process can further be explored. Therefore, there is a need to develop a systematic approach to understand the influence of various process parameters in FDM and develop empirical model so that users can easily predict and control the functional requirement of the part. A methodology for computing the volumetric error for part built with different orientations holds a very bright scope. Part orientation and raster angle are important process parameters which can be studied along with their interactions and effect of such parameters on mechanical properties, surface roughness, and geometric accuracy of FDM parts. Very limited literature has been available on the effect of process parameters on surface finish, accuracy of complex or freeform part shapes. It is also observed that very little work has been performed to understand the wear nature of FDM built parts. Adaptive slice thickness method where slicing of each part and features is carried out independently of one another approach which reduces the surface roughness, build time, build cost of FDM processed parts holds a large potential. Very little work has been reported on direct slicing of CAD model i.e. without generating any STL file which not only reduce the build time and cost but also increases the productivity. No work has been reported on the effect of cold vapor treatment with dimethylketone solution on mechanical properties, geometric accuracy and surface finish of FDM parts and this method holds a large potential in future. Study of part distortions and mechanical behavior in FDM process using finite element analysis will reflect the insight of failure of parts. The effect of chamber temperature on volumetric shrinkage, mechanical properties inter-layer bonding between adjacent rasters and study of parts distortion and mechanical behavior using finite element analysis holds a very bright scope. No work has been reported on the effect of interstitial voids (air gap) between adjacent rasters formed during fabrication on mechanical strength, surface roughness and geometric accuracy of FDM parts which also holds scope of future work.

Based on the scope mentioned above, the objectives of present research are as follows:

- ❖ Study the effect of part orientation and raster angles on tensile and flexural strength, surface roughness of the parts built by FDM process.
- ❖ Study of failure behavior under tensile and bending for different FDM parts built with different part orientation and raster angle.
- ❖ Optimal part deposition orientation for FDM parts to improve the geometric accuracy and surface roughness.
- ❖ Quantitative analysis of post-built treatment by cold vapors of dimethylketone to study of mechanical characteristics of FDM parts.
- ❖ Post-built chemical treatment to reduce inter-road voids and study of surface finish and geometric accuracy.
- ❖ Multi-response optimization using Analytic Hierarchy Process to predict optimal process settings for fabricating FDM parts.

Methodology adopted for achieving these objectives are quite general and can provide common methods for measuring the benefits and limitations of various RP processes.

Chapter 3

Methodology

3.1 Introduction

FDM process is one of the widely adopted RP processes by the industries due to low maintenance cost, large variety of materials available, low fabrication cost of RP models even with complex geometries, environmental friendly and easy to operate with very little or no supervision required. FDM process offers time and cost advantages over the other conventional manufacturing technologies. One of the present challenges faced by the FDM users is the quality of parts produced and mechanical properties which is allied with the accurate application for the specified performance. This makes it essential to understand the effect of process variables in the performance of parts fabricated by FDM process to make them reliable for industrial applications. To achieve this, the present chapter describes the materials and methods used for the fabrication and testing of FDM processed part. It presents the details of the part fabrication methodology and various tests performed on the samples built at different process parameter settings. Geometrical and dimensional accuracy, surface roughness, mechanical characteristics (tensile and flexural strength) and build cost are considered as response variables of part in accordance to industrial requirements. Tensile and flexural samples are built according to the ASTM standards and all tests are performed at room temperature.

3.2 Material

The material used for fabrication is acrylonitrile butadiene styrene ABS P430^{TM} model material (make: Stratasys, USA). ABS (chemical formula $(C_8H_8.C_4H_{6.}C_3H_3N)_n$) is a carbon chain copolymer and belongs to styrene ter-polymer chemical family (n = degree of polymerization). ABS is derived from acrylonitrile, butadiene, and styrene (refer Fig. 3.1). It contains 90-100% acrylonitrile/butadiene/styrene resin and may also contain mineral oil (0-2%), tallow (0-2%) and wax (0-2%). Acrylonitrile is a synthetic monomer produced from propylene and ammonia; butadiene is a petroleum hydrocarbon obtained from the C_4 fraction of steam cracking; styrene monomer is made by dehydrogenation of ethyl benzene (hydrocarbon obtained in the reaction of ethylene and benzene).

ABS is made by polymerization process i.e. by polymerizing styrene and acrylonitrile in the presence of poly-butadiene. The result is a long chain of poly-butadiene crisscrossed with shorter chains of poly-styrene-co-acrylonitrile. The nitrile groups from neighboring chains, being polar, attract each other and bind the chains together, making ABS stronger than pure polystyrene. Its three structural units provide a balance of properties with the acrylonitrile providing heat resistance, butadiene imparting good impact strength and the styrene gives the copolymer rigidity.

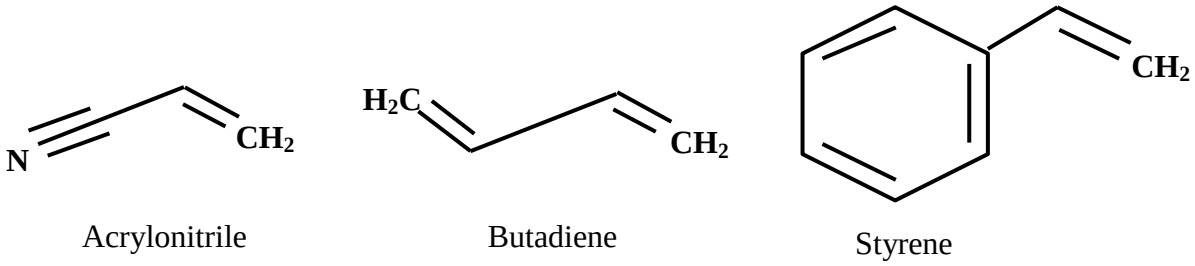

Acrylonitrile Butadiene Styrene

Figure 3.1: Monomers in ABS plastic

Varying the proportion of constituents in the material or the conditions under which the material is being processed may vary the material properties. Tables 3.1 list the mechanical properties of commercially available extruded and molded ABS P430. In the present study, the material supplied by the original equipment manufacturer is used.

Table 3.1: Mechanical properties of ABS P430 [Durgun and Ertan, 2014]

Mechanical properties	**Value**
Tensile strength (MPa)	37
Tensile modulus (MPa)	2320
Tensile elongation (%)	3
Flexural delamination (MPa)	31
Flexural strength (MPa)	53
Flexural modulus (MPa)	2250
Izod impact, notched (J/m)	106

3.3 Specimen Fabrication

Specimens are fabricated using FDM® Mojo™ machine for respective characteristic measurement (refer Fig. 3.2). This machine is developed and marketed by Stratasys, Eden Prairie, MN, USA having a maximum build size 5″×5″×5″. All specimens are built using ABS P430™ model material (color: Ivory) (make: Stratasys, USA), a common variant of ABS and SR30™ support material (make: Stratasys, USA). Support material use can be easily breakaway by hands or can be removed by dissolving in wash tank.

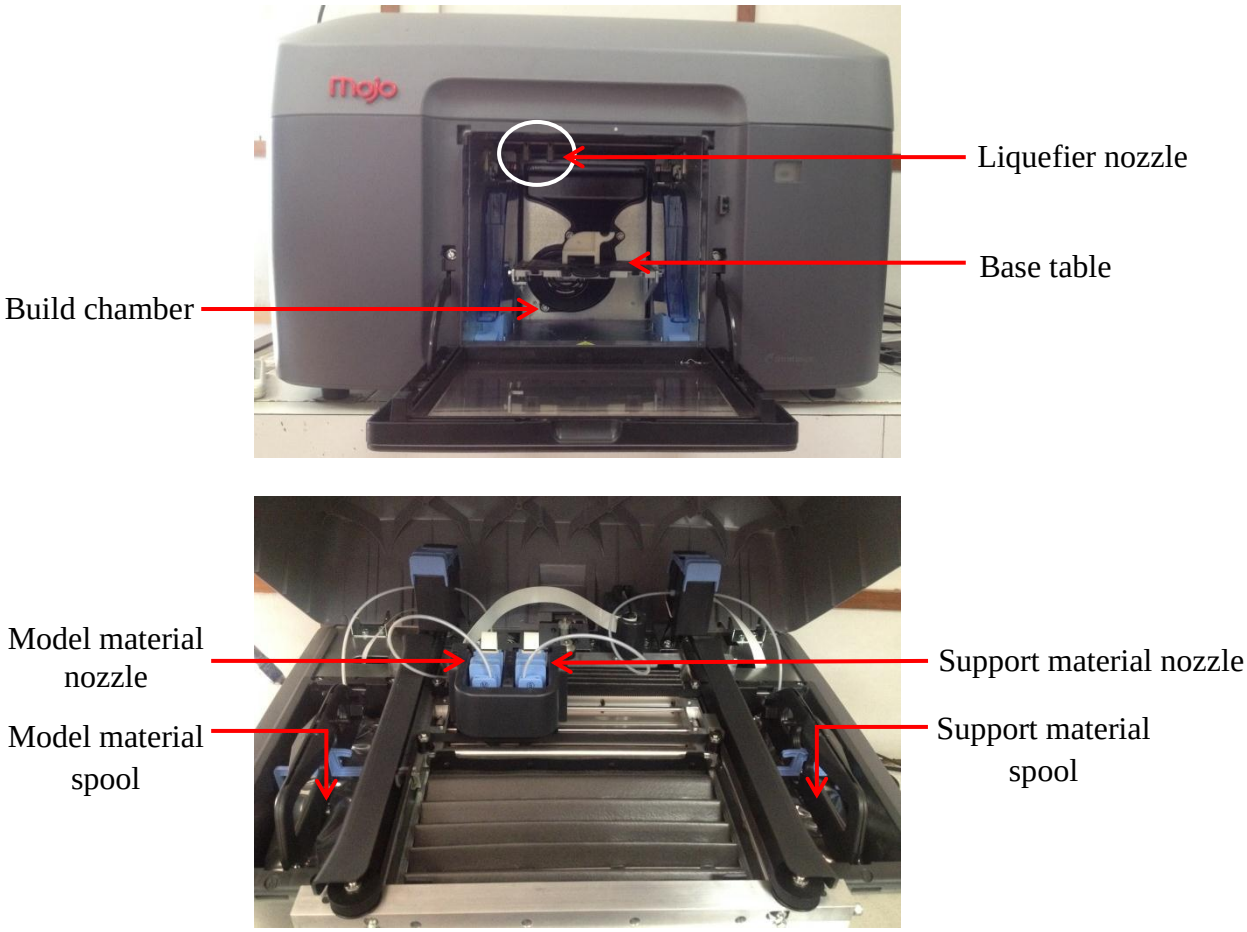

Figure 3.2: FDM machine and head assembly

Parts are built by layers building process by depositing the material in semi-liquid state with 0.178 mm constant layer thickness. It has one loaded model material and one loaded support material spools of plastic filaments with 80 cubic inch modeling material per filament spools. The 3D models of specimens are generated using Pro\Engineer 5.0 solid modeling software and exported as standard tessellation language (.STL) format (a neutral format) for input to the FDM machine software (Mojo Print Wizard 1.1) for generation of

material deposition path. The forming material (ABS P430), in the form of a flexible strand of solid material is supplied from a supply source spool to the head of the machine. The machine extrusion head consists of two separate liquefier nozzles one for the model material and another for the support material. The position of this liquefier nozzle is computer controlled with respect to the base, which allows the fabrication of geometrically complex model with precise dimensions and geometry. Schematic of FDM machining process is shown in Fig. 3.3.

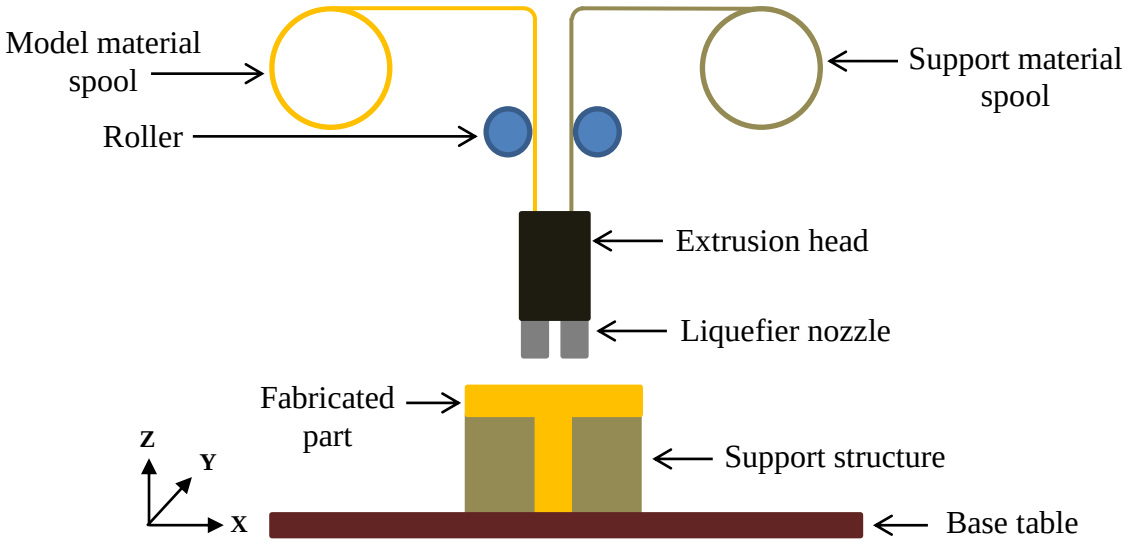

Figure 3.3: Schematic of fused deposition modeling

The parts are fabricated by depositing the molten filament being extruded through a nozzle in a desired pattern onto a base table (platform) which rapidly solidifies and adheres to the adjoining layers. The bonding between the adjoining fibers is caused due to thermally driven diffusion welding. When one complete layer is deposited, the work table moves down (Z axis) by layer thickness and next layer is added. For each layer generation process, contour is laid down first to generate boundary of the layer and then interior is filed through vector filling (known as raster), the raster angle is alternated between consecutive layers to obtain adequate interlocking between layers through efficient bonding of rasters. The fabricated part takes the form of a laminate composite with vertically stacked layers, each of which consists of continuous material fibers or raster with interstitial voids. After building is over, the components are placed inside wash tank for support material removal. The FDM technique has also shown its potential not only for fabricating 3D models but also for fabricating the final functional parts due to simplicity of operation and durability of parts in term of strength and part accuracy.

3.4 Measurements

To study the effect of part orientation, raster angle and post treatment process on mechanical properties, surface roughness, geometric accuracy and fracture examination of FDM specimens the following measurements and equipment's are required:

3.4.1 Geometric Accuracy Measurement

The dimensions of fabricated models are measured with the help of Nikon V-10A profile projector (make: Nikon, Japan) having least count of 0.001 mm asshown in Fig. 3.4. This inspection instrument projects an enlarge image of an area or feature of a specimen onto a screen with accurate and magnified using diascopic illumination technique. Required dimensions can be measured directly onto a screen or can be compared with standard reference at correct magnifications. The display screen consist an inbuilt grid and this grid can be rotated through 360° to align with required edge as displayed on a screen. Point position, measurements, calculation, etc. can be performed with the help of digital readout device. Dimensions are measured twice on each surface and average value is considered for analysis and comparing with actual dimensions of CAD model.

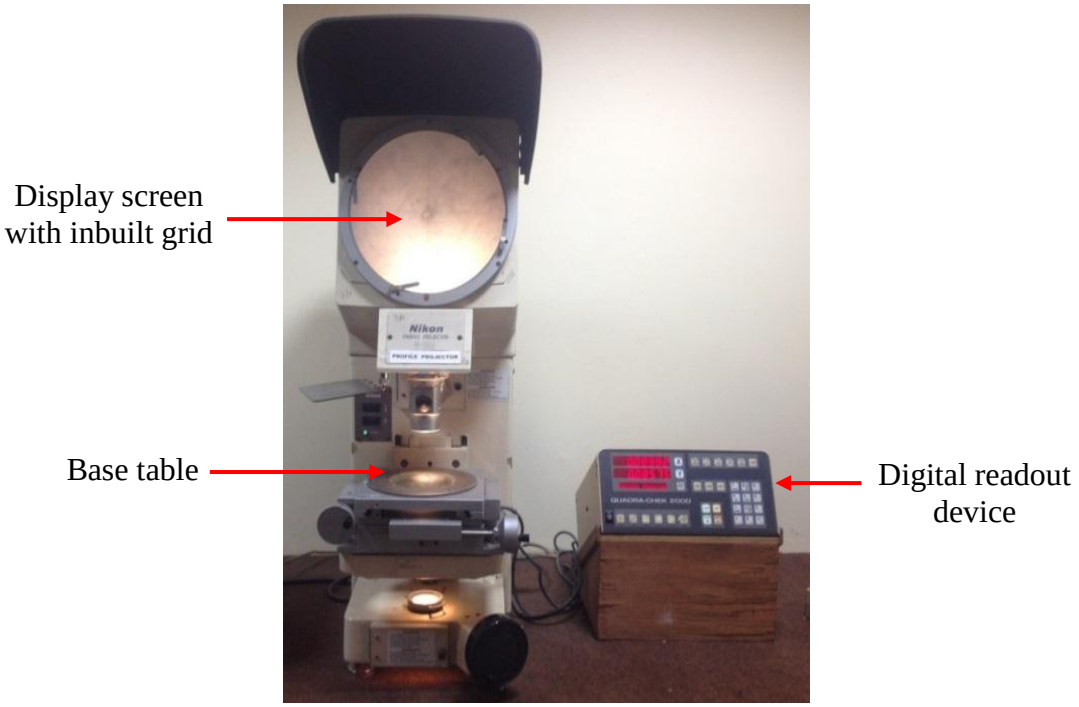

Figure 3.4: Nikon V-10A profile projector

3.4.2 Surface Roughness Measurement

The surface roughness of the parts are measured with the help of Mitutoyo SJ400 contact type surface roughness tester (make: Mitutoyo, Japan) using 0.8 mm cut-off length as shown in Fig. 3.5.

Figure 3.5: Mitutoyo SJ400 Surface Roughness Tester Machine

The tester uses the stylus method of measurement with profile resolution of 12 nm and measure surface roughness upto 100 µm. The stylus mounted on a probe arm, which pivots perpendicular to the tracing level and moves over the surface to be measured. Roughness is measured twice and the average values are considered for analysis. Average surface roughness (R_a) is measured in two orthogonal directions i.e. along and across the length of the specimen for each part on its top surface as shown in Fig. 3.6.

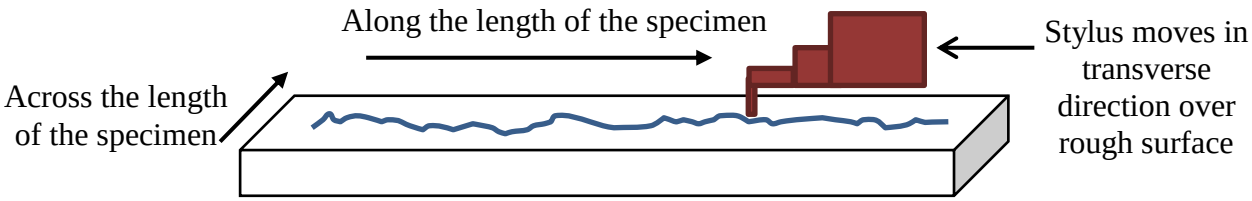

Figure 3.6: Direction of R_a value measured on test specimen

3.4.3 Tensile Strength Measurement

Tensile specimens are fabricated according to ASTM D638 (Standard test method for tensile properties of Plastics). Figure 3.7 (a) shows the shape and dimensions of the test sample. Tensile testing of the samples are conducted on Universal Tensile Testing (UTM) machine of Zwick/Roell Z010 (Zwick-Roell, Germany) having 10 kN load capacity as shown in Fig. 3.7(b). A gripper arrangement on the machine for tensile testing is shown in Fig. 3.7(c) respectively. Tensile testing are conducted at crosshead speed (strain rate) of 5 mm/min.

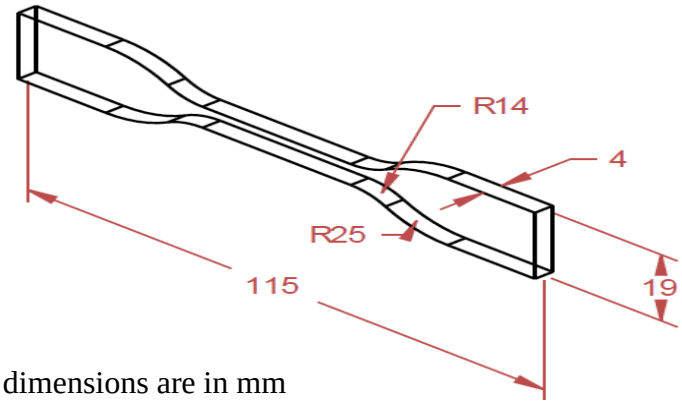

All dimensions are in mm

(a)

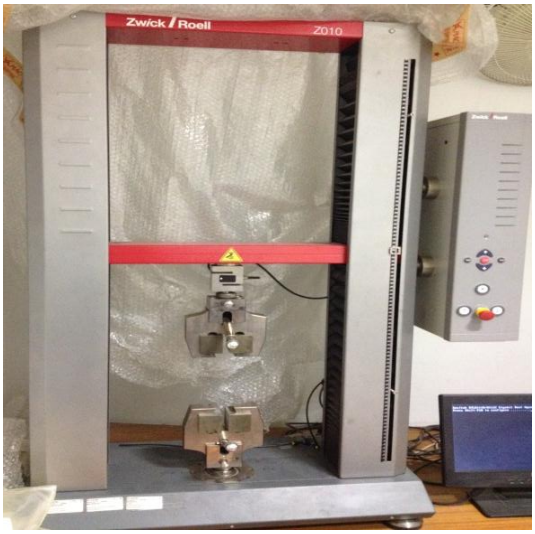

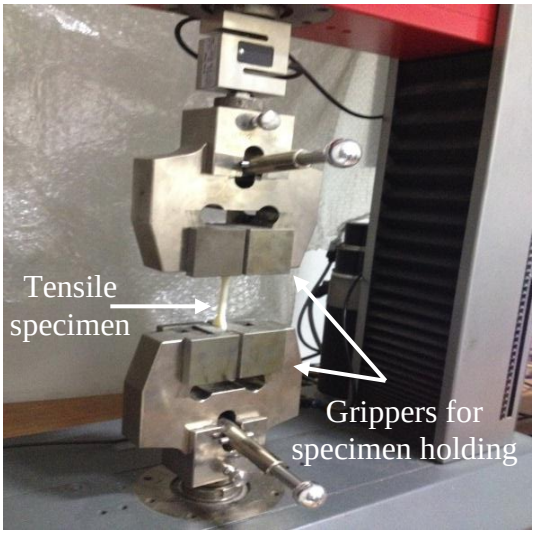

(b) (c)

Figure 3.7: Tensile testing specimen (as per ASTM D638) and their testing arrangement

3.4.4 Flexural Strength Measurement

Flexural specimens are fabricated according to ASTM D790 (Standard test method for flexural properties of Plastics). Figure 3.8 (a) shows the shape and dimensions of the test sample. Flexural testing (three point bending) of the specimen are conducted on UTM machine of Zwick/Roell Z010 (Zwick-Roell, Germany) having 10 kN load capacity as shown in Fig. 3.8(b). Gripper arrangement on the machine for flexural testing is shown in Fig. 3.8(c) respectively.

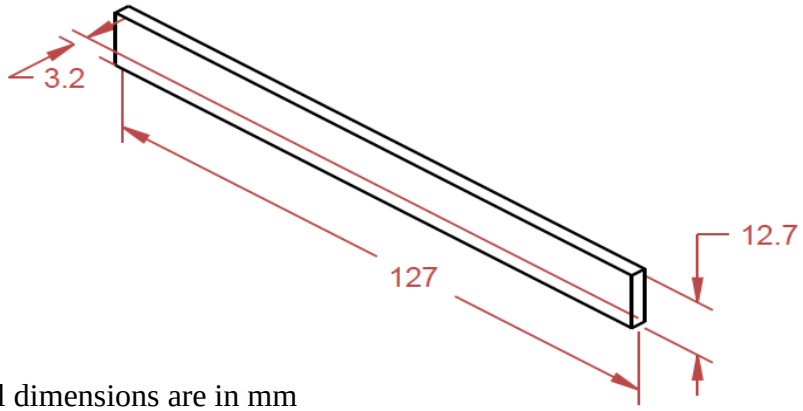

All dimensions are in mm

(a)

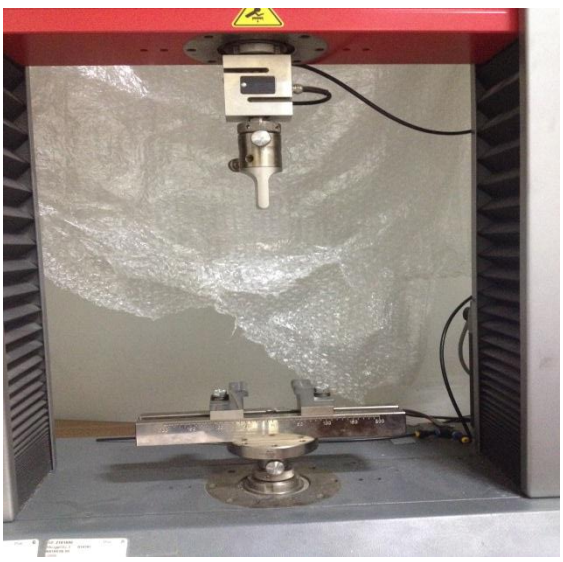

(b)

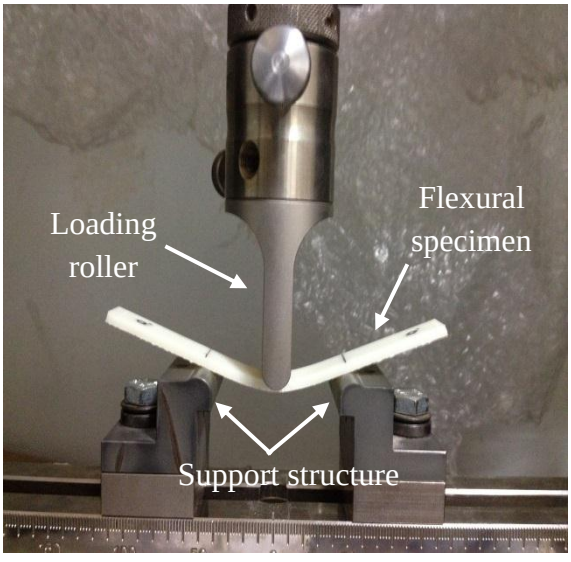

(c)

Figure 3.8: Flexural testing specimen (as per ASTM D790) and their testing arrangement

For flexural testing specimens are placed on two supports structure (maintaining support span to depth ratio = 16) and load is applied in the middle until the specimen gets fractured. From the results maximum load at fracture, the modulus of rupture are calculated

for different samples. The flexural strength or modulus of rapture (MOR) is calculated by Eqn. (3.1).

$$\text{Modulus of rupture} = \frac{3FL}{2bt^2} \qquad (3.1)$$

Where, F is maximum load applied (N), L = length between rollers (mm), b = width of specimen (mm) and t = thickness of specimen (mm).

3.5 Optical Measuring Microscope

The sample surfaces for surface defects (air voids, cracks, etc.) and raster pattern are examined with the help of optical measuring microscope (model: Axio Scope A1, make: Carl Zeiss, Germany) having least count of 0.001 mm as shown in Fig. 3.9. The Axio Scope A1 is a high performance optical measuring microscope. The transmitted light beam path provides sharp image contrast and minimizes any scatter light; an advantage especially for low light and low contrast samples. The eyepiece lens also consist an inbuilt grid which can be rotated through 360° to align with required edge to measure linear dimensions with the help of digital readout device.

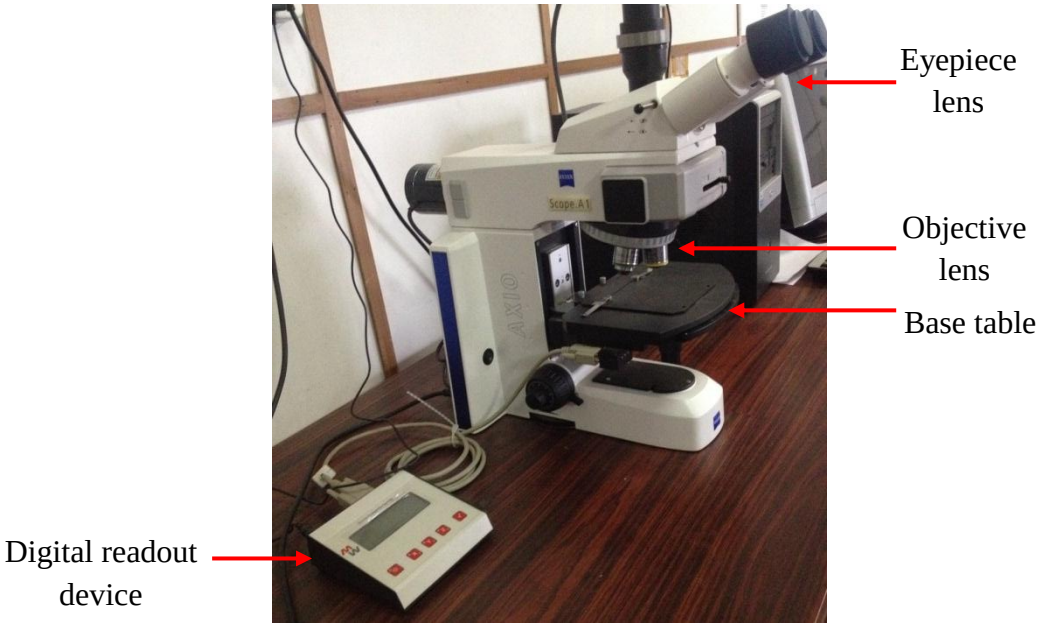

Figure 3.9: Optical measuring microscope

3.6 Scanning Electron Microscope (SEM)

The fracture surfaces are subsequently prepared by gold plating and analyzed by scanning electron microscope (SEM), (make: JEOL, JSM-6510LV, Tokyo, Japan) to study the fracture behavior of the FDM samples when built at different part orientation and raster angles. The JEOL, JSM-6510LV (Fig. 3.10) is a high-performance, SEM with a high resolution. The low vacuum (LV) mode allows for observation of specimens which cannot be observed at high vacuum due to the excessive water content or due to a non-conductive surface. Its asynchronous five-axis stage can accommodate a specimen of up to 8 inches in diameter.

Figure 3.10: Scanning electron microscope (SAI Lab, Thapar University, Patiala)

3.7 Post-built Treatment

The built specimens are subjected to post treatment process by exposing the parts to cold vapors of dimethylketone (acetone) laboratory reagent (LR) ≥ 99 % concentration. Acetone is chosen due to its very low toxicity, low cost and very high evaporation rate. Instead of pure acetone, acetone hot vapors or cold vapors could be used for treatment. But acetone cold vapors are considered for chemical treatment because with pure acetone or hot vapors it becomes difficult to control the chemical reaction with ABS material. Moreover immersion of ABS parts in pure acetone produces very aggressive reaction which damages

the surface completely as shown in Fig. 3.11(a). In such cases, the concentration of acetone and time of immersion should be optimized to prevent damage of surface. For treatment with hot vapor, the part is kept inside an airtight container filled with 20 ml acetone and the part is hanged from top. The total arrangement is heated for 30 s and the component is exposed to the vapor for additional 30 s without supplying any heat. After treatment with hot vapors, uneven surface due to non-uniform vapors exposure is observed. The surfaces close to liquid level are exposed to hot vapors first (as vapors generates and rises up) and the surfaces at the back comes in contact of the vapors late, thus an uneven smoothness in surfaces are noticed (refer Fig. 3.11(b)).

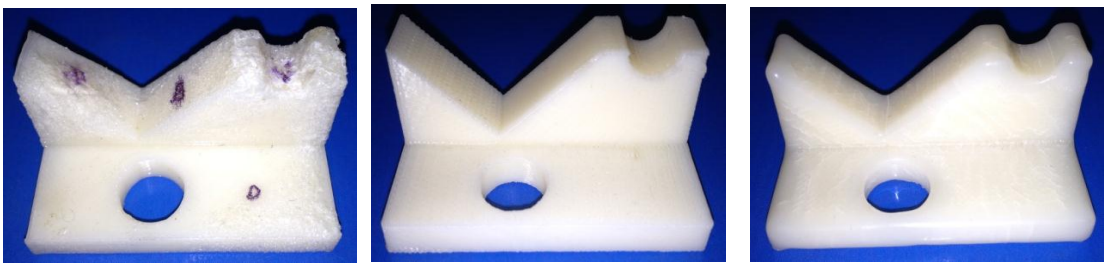

Figure 3.11: Surface quality of specimen after: (a) Immersion in pure acetone, (b) Hot vapor treatment and (c) Cold vapor treatment with long duration

Use of acetone cold vapors (exposure time 40 min) over pure acetone and hot vapors ensures consistent surfaces are achieved. However, a very long exposure duration under cold vapors also leads to geometrical change and loss in feature as shown in Fig. 3.11(c) where parts are exposed for 90 min and edges, sharp corners are get rounded off. For chemical treatment with cold vapor, the part is kept inside an airtight container having 1.3 L capacity. All walls of the container are lined with tissue paper soaked in liquid acetone. The container is kept at 18 to 20 °C for 40 min so that liquid acetone gets vaporize to form the cloud of cold acetone vapors inside the container. Mechanical properties (tensile and flexural strength), geometric accuracy and surface roughness are measured after chemical treatment so that change in mechanical properties, surface roughness and geometric accuracy can be evaluated.

Chapter 4

Results and Discussions

4.1 Introduction

This chapter presents experimental investigations on the influence of important process parameters such as part orientation and raster angle along with their interactions on tensile strength, flexural strength, geometrical and dimensional accuracy, surface roughness and build cost of FDM processed ABS P430 parts. Three different part orientation along the X, Y and Z axis and four different raster angles (0°, 30°, 60°, 90°) are considered for building of components and tested for surface roughness (along and across the length direction), tensile and flexural strength. Seven different part orientation (0°, 15°, 30°, 45°, 60°, 75°, 90°) along Y axis and part orientation along the X, Y and Z axis are considered to analyze the effect on geometric accuracy and surface roughnes of different primitive surfaces of a FDM model. Geometric error of the built part with respect to the CAD geometry is measured for all the parts. Model, support material consumption along with build time cumulatively represents the build cost. For each of the part orientation and raster angle, the volume of model and support material consumption, build time are measured and compared. Further, all the parts are chemically treated with cold vapors of dimethylketone and tensile strength, flexural strength, surface roughness and geometric accuracy are measured. Results so obtained after the treatment are compared with those obtained for the parts without any post treatment to study the change in tensile and flexural strength, improvement in surface roughness, geometric accuracy. Rapture surfaces under tensile and flexural loading are also studied by SEM to understand the failure mode of the specimen under different loading conditions. Later, the FDM process parameters that affect the studied responses were identified and optimized by multi-response optimization using analytic hierarchy process that will give maximum tensile and flexural strength, improved the geometric accuracy, surface finish and lower the build time.

4.2 Measurement of Mechanical Properties

The tensile strength and flexural strength for all the components built at three different part orientations and at four different raster angles (refer Fig. 4.1 and Fig. 4.2) are measured and analyzed to study the effect of process parameters on these responses.

Microscopic observations by SEM of tensile and flexural samples are carried out to analyze the fracture behavior of the specimen built by FDM. Later, all tensile and flexural specimens are chemically treated with cold vapors of dimethylketone. Tensile and flexural strength are measured after the treatment and compared with those obtained for the parts without any post treatment. For specimen fabrication, procedures of tensile and flexural testing are explained in Chapter 3 (section 3.4).

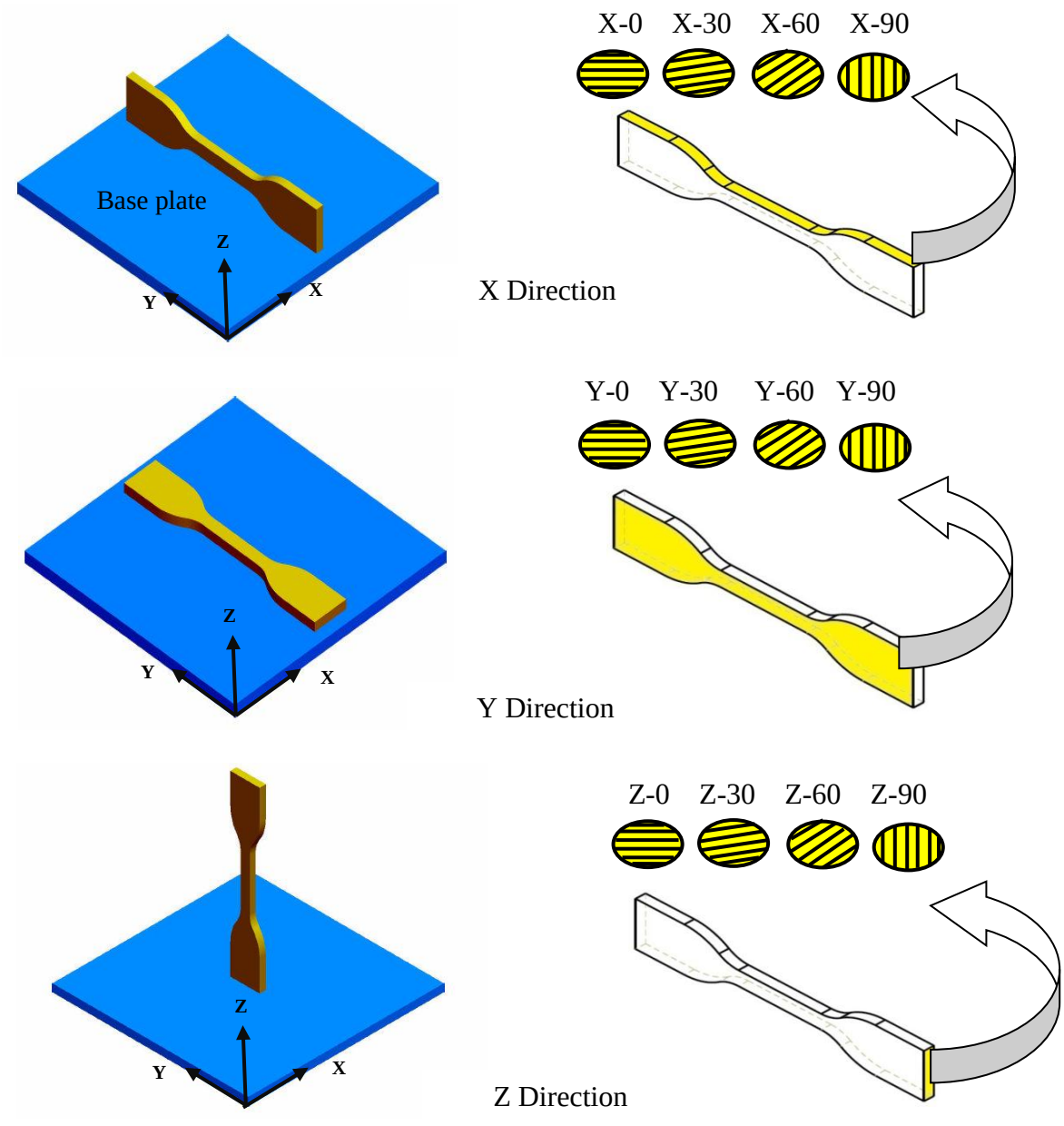

Figure 4.1: Schematic representation of different part orientations

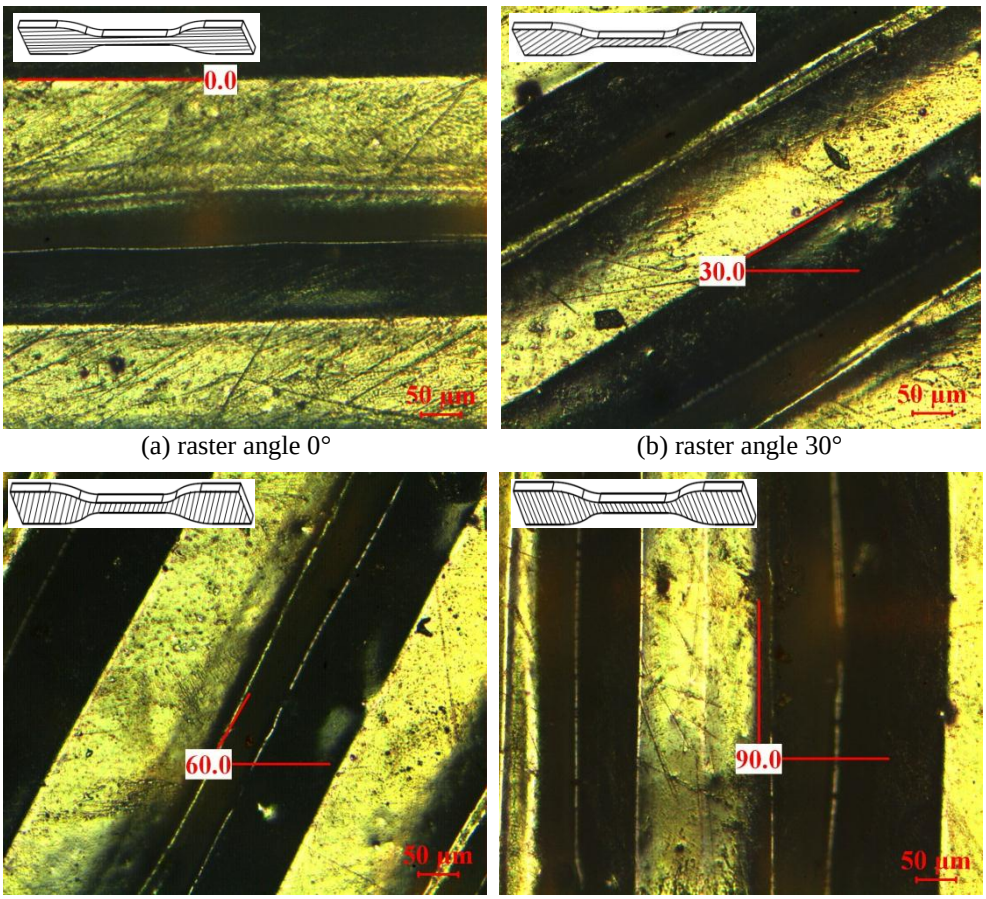

(a) raster angle 0° (b) raster angle 30°

(c) raster angle 60° (d) raster angle 90°

Figure 4.2: Optical microscopic images of build specimens with different raster angles

4.2.1 Tensile Strength

The tensile strength of all specimens built at different part orientation and raster angles are shown in Fig. 4.3. Figure 4.3(a), (b) and (c) shows the tensile strength of samples for part orientations along X, Y and Z axis respectively. From Fig. 4.3 it can be seen that the maximum tensile strength are achieved for the X and Y part orientation as compared to orientation about Z axis. Also, for X and Y orientation, minimum strength is achieved for 90° raster angle as compared to other raster orientations. This is due to the fact that in X and Y orientation for 90° raster angle, layers are aligned in a perpendicular direction (across the length of the specimens) to the applied load thus produces raster of smaller length. As a result, number of rasters of smaller length increases which increases the number of heating and cooling cycle which results in interlayer cracking, delamination and fabrication failure. However, 0° raster angle, rasters are laid along the length of the specimen and are aligned in the direction parallel to the applied load thus produces a strongest direction for raster layers. For sample built at 0° raster angle, tearing and brittle fracture of the deposited layers takes

place (as can be seen from SEM image in Fig. 4.6(a)) whereas for 30° and 60° raster angle along with tearing of layers shear failure is also involved. Figure 4.3(c) shows that significantly low tensile strength is obtained for the samples built with Z orientation because number of layers is significantly high with this orientation.

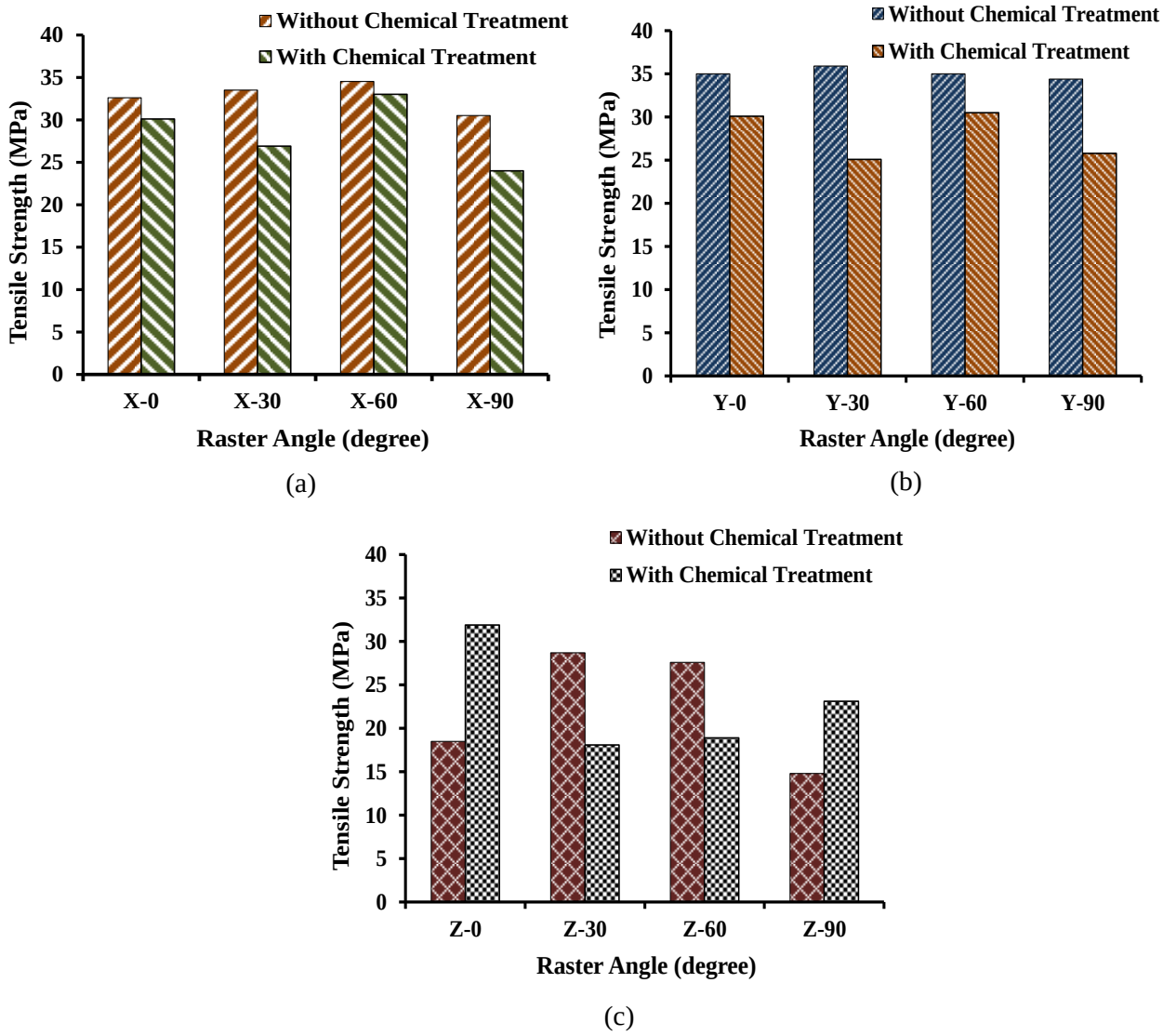

Figure 4.3: Tensile strength measurement for specimen built at different part orientations and raster angles with and without chemical treatment

Due to large number of layers, the inter-layer bonding strength varies along the specimen and all this layers are across the loading direction. Separation of layers for 0° and 90° raster orientation becomes easier as compared to 30° or 60° raster orientation due to smaller length of interlayer bonding. Thus, the above results showed that FDM specimens manufactured at different raster angles exhibit anisotropic properties and this is majorly dependent upon part built orientation rather than raster angle. The maximum tensile strength

(34.5 MPa) comparable to original strength of ABS material (37 MPa) is obtained when part orientation is along X axis and raster angle is 60° (X-60) whereas minimum tensile strength (14.8 MPa) is obtained when part orientation is along Z axis and raster angle is 90° (Z-90).

From Fig. 4.3 it can also be seen that with cold vapor chemical treatment the tensile strength of the specimen get reduces for different part orientation and raster angles (except Z-0 and Z-90) because the chemical treatment with acetone weakens the outer layer due to softening it thus reduces the tensile strength of the specimen. The maximum tensile strength after chemical treatment is again noted for the X and Y part orientation as compared to orientation about Z axis. Also, for X and Y orientation, minimum strength is achieved for 90° raster angle as compared to other raster orientations. This is due to the same fact that in X and Y orientation for 90° raster angle, layers are aligned in a perpendicular direction (across the length of the specimens) to the applied load thus produces raster of smaller length. As a result, number of rasters of smaller length increases which increases the number of heating and cooling cycle which results in interlayer cracking, delamination and fabrication failure. However, for samples built at 0° and 90° raster angles along Z axis the tensile strength of the specimen increases by 72.43 % and 56.08 % after chemical treatment because before the chemical treatment both Z-0 and Z-90 specimen consist of maximum number of layers each having smaller rasters thus crack propagates along weak inter-layer bonding between rasters as a result tensile strength is minimum than any other part orientation and raster angles whereas when chemical (cold vapors of dimethylketone) attacks the specimen the outer surface of the chemically treated specimen has bonded together into a continuous piece thus diminishes the crack propagation line across the surfaces thus reduces the stress concentration of the parts. The maximum tensile strength (33 MPa) is obtained when part orientation is along X axis and raster angle is 60° (X-60) which is also true in case of specimen without treatment whereas minimum tensile strength (18.1 MPa) is obtained when part orientation is along Z axis and raster angle is 30° (Z-30) which is more than the minimum tensile strength of 14.8 MPa (Z-90) for specimen without chemical treatment. In all specimens, (with and without chemical treatment) the failure mode is a result of the material separation in a plane approximately normal to the tensile stress as shown in Fig. 4.4.

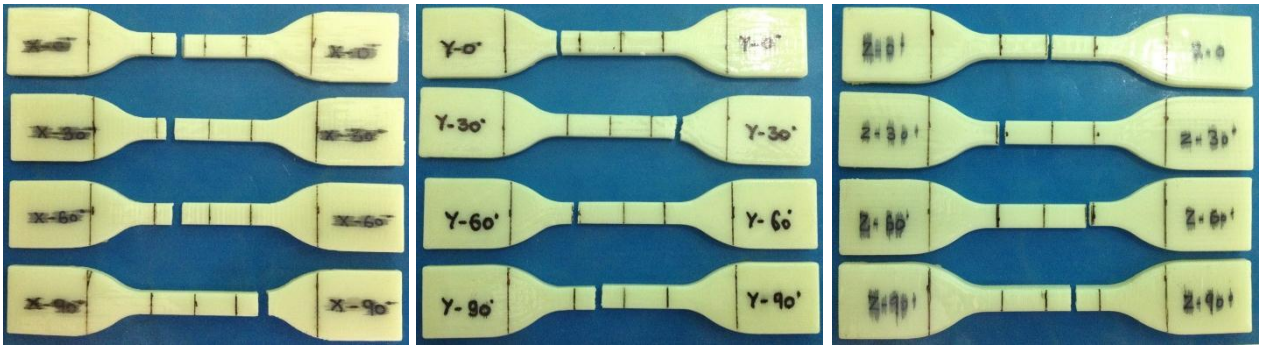

(a) (b) (c)

Figure 4.4: Fracture specimens under tensile loading with different part orientation

The physical inspections of FDM specimens are done both at macroscopic and microscopic levels. The fracture patterns are examined macroscopically to understand the weakest path for crack propagations. The specimen with 0° raster angle failed in transverse direction with some fiber pull-out and delamination occur at weak points and tearing of individual fibers took place. For, 90° specimens, crack propagates in the transverse direction (perpendicular to loading axis). Specimens with 30° and 60° raster angle failed along the 30° and 60° line mostly following the line of the deposited layers along the raster direction. These tendencies and patterns of fractures are schematically represented in Fig. 4.5(a) to (d).

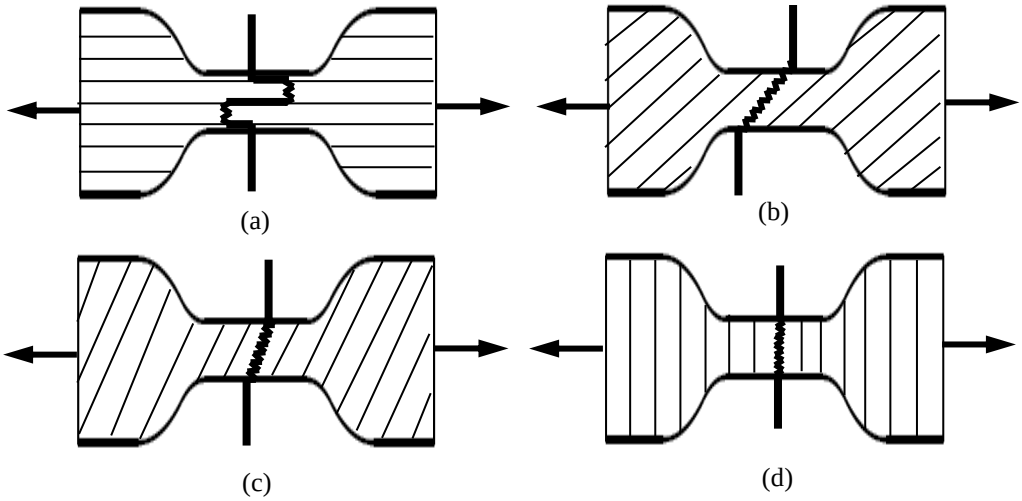

Figure 4.5: Schematic illustration of fracture type under uniaxial tensile loading of FDM built specimens at different raster angles (a) Y-0, (b) Y-30, (c) Y-60 and (d) Y-90

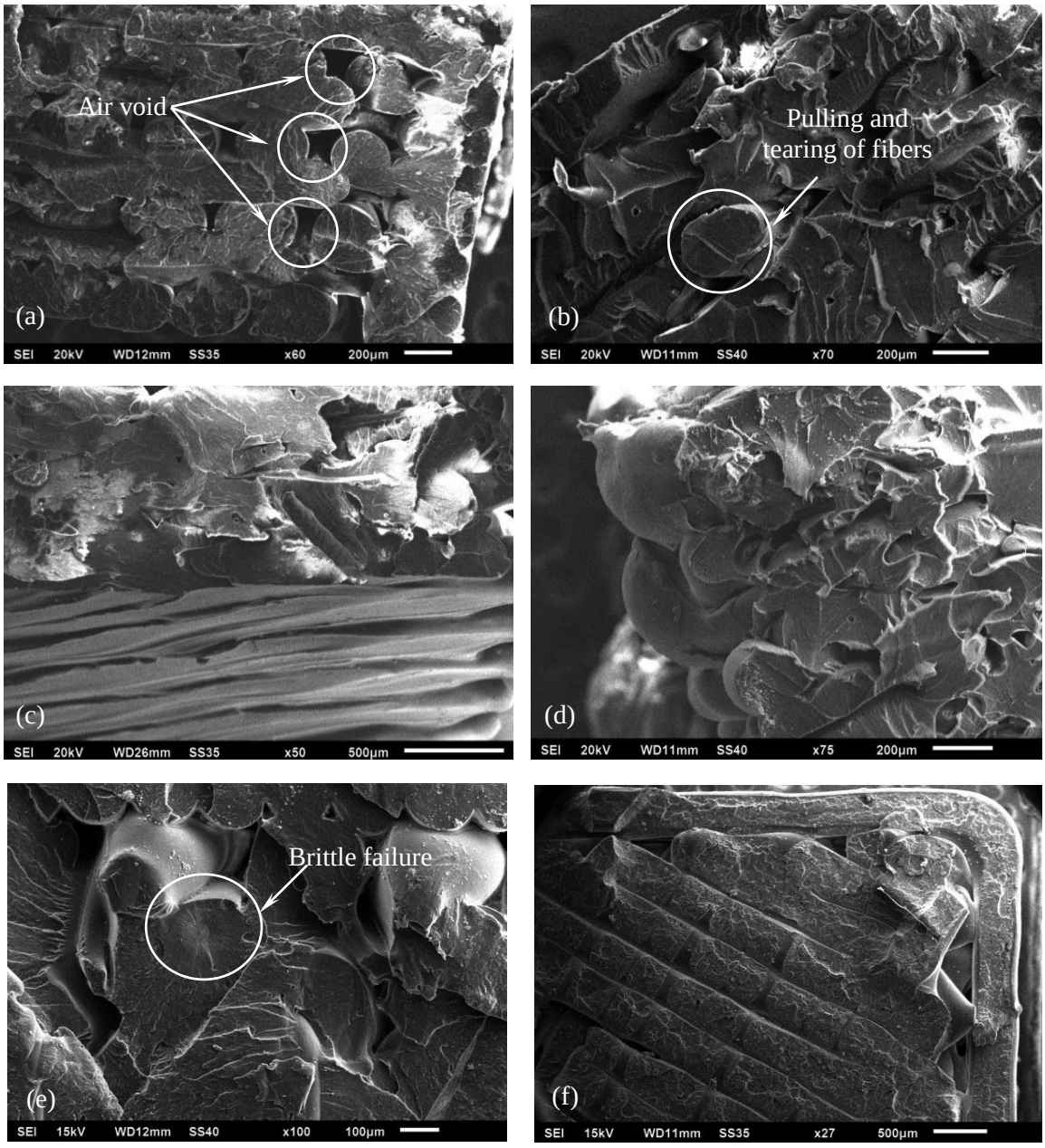

Figure 4.6: SEM fractograph of samples after tensile testing (a) Y-0, (b) Y-30, (c) Y-60, (d) Y-90, (e) X-60 and (f) Z-30

Microscopically, fracture surfaces are inspected with the help of SEM and results showed that the failures are mainly because of the pulling and rupturing of the raster fibers. It can be seen from Fig. 4.6(a) that that failure under tensile loading are mainly caused due to pulling and rupturing of the raster fibers and separation of materials occur in a normal direction to the tensile stress for 0° raster angle. Some air voids between the layers are more prominent for sample with 0° raster angle. In 30° and 60° raster angle, failure of the specimen is due to brittle shear, as each raster is pulled and raptured under tensile loading and failed at

30° and 60° relative to tensile loading as seen in Fig. 4.6(b) and Fig. 4.6(c) and relatively more amount of share take place in 30° sample, thereby increasing the tensile strength of the samples. Figure 4.6(d) for 90° raster, although shear takes during solidification of higher interlayer road path, the weak interlayer bonding reduces the tensile strength and layer separation of rasters provides easier failure. Figure 4.6(e) shows that specimen fails under brittle shears as each raster is pulled and rapture under tensile loading due to strong inter-layer bonding between rasters thus increases the tensile strength of the specimen. In 30° raster specimen along *Z* axis failure occurred between the layers and fracture path propagates along weak inter-layer bonding between rasters, thereby decreases the tensile strength of the sample and fracture surface exhibit smooth and flat pattern as shown in Fig. 4.6(f).

4.2.2 Flexural Strength

Flexural (three point bending) testing is carried out for all specimens built at different part orientations and raster angles and their comparison is shown in Fig. 4.7. From Fig. 4.7 it can be seen that flexural strength is higher than the tensile strength of the FDM specimens because flexural strength is measured at the outer most fiber of the part. Specimen with raster angle 90° exhibit lower flexural strength for different part orientation as compared to other raster angles (Fig. 4.7(a), (b)) because in 90° specimen rasters are deposited perpendicular to the bending plane thus produces rasters of smaller length under bending load thus produces opening of layer from adjoining boundaries and leads quick failure. For example, part orientation along the X axis and raster angle 30° (X-30) exhibit highest flexural strength as compared to other specimens with same orientation whereas for part orientation along the Y axis 0° raster angle exhibit higher flexural strength then specimen with 90° raster angle because rasters are laid parallel to the bending plane therefore exhibit higher resistance to bending. For part orientation along the Z axis (Fig. 4.7(c)), lowest flexural strength is obtained as compared to the other two part orientation direction due to the easier tendency of interlayer separation. Parts with 30° and 60° raster angle exhibit higher flexural strength as compared to other two raster angles due to relatively larger length of interlayer contact.

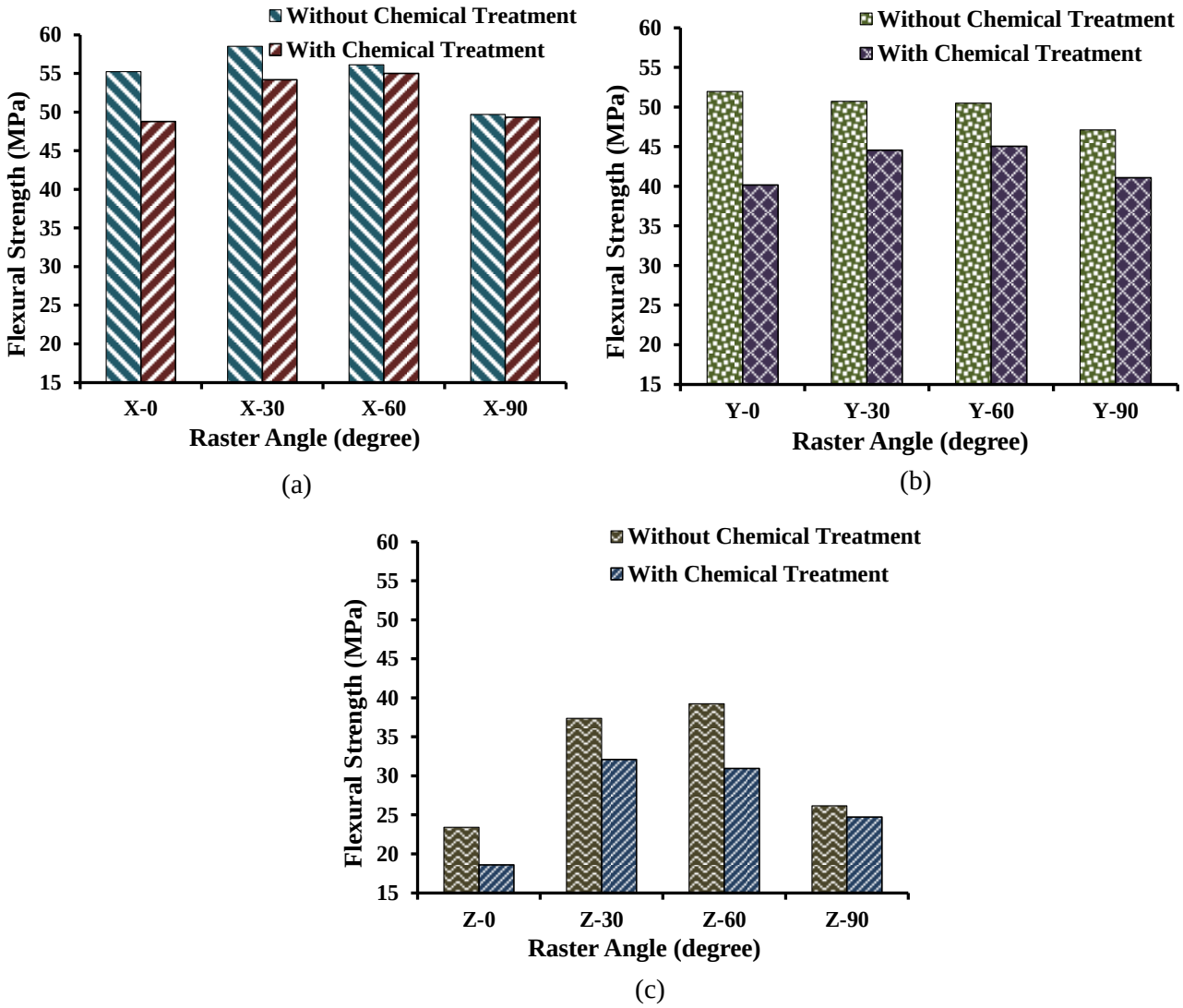

Figure 4.7: Flexural strength measurement for specimen built at different part orientations and raster angles with and without chemical treatment

From Fig. 4.7 it can also be seen that with cold vapor chemical treatment of the specimens the flexural strength of the specimen get reduces for different part orientation and raster angles because the chemical treatment with acetone weakens the outer layer due to softening it thus reduces the flexural strength of the specimen. Moreover specimen built by layer building process exhibit rasters with different orientation under bending plane which exhibit higher resistance to bending as compared to single solid layer due to diffusion of rasters into continuous layer after chemical treatment. The maximum flexural strength after chemical treatment is noted for the X and Y part orientation as compared to orientation about Z axis. But, for X and Y orientation, minimum strength is achieved for 0° raster angle as compared to 90° raster orientations which is contrary to previous results. This is mainly

because 90° raster specimen consist more rasters of smaller length per layer as compared due to 0° raster orientation thus when chemical attacks the specimen the outer surface of specimen with small rasters bonded together into a continuous piece, whereas in 0° raster orientation with long rasters are not diffuse together into a continuous piece leaving behind some air voids and small crater between rasters thus increases the stress concentration of the parts which reduces the flexural strength of the specimen.

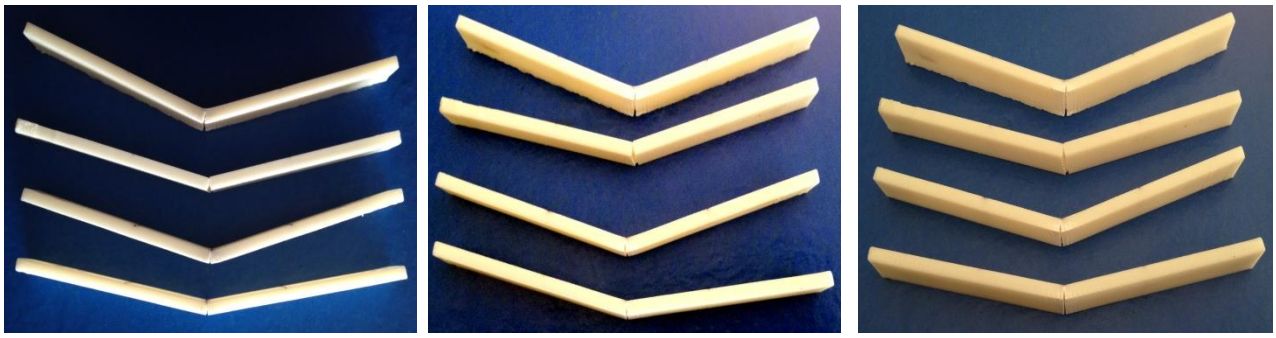

(a) (b) (c)

Figure 4.8: Fracture specimens under flexural loading with different part orientation

Examination of the surfaces also revealed that failure is initiated at the tensile side of the specimen but pieces stays together by unbroken fibers of the compression side as shown in Fig. 4.8. SEM images of some selected samples under flexural failure are shown in Fig. 4.9. The fracture tendency of specimen with 0° raster angle is shown in Fig. 4.9(a). Moreover, as raster angle changes from 30° to 90°, their inclination with respect to bending plane changes, thus producing raster of smaller length under flexural loading wherein resistance to bending decreases. This effect is shown in Fig. 4.9(d) where 90° raster orientation specimen shows little resistance to bending and catastrophic failure is noticed. Moreover, for part built with 0° raster angle along Z axis (Z-0) the cracks propagate along the weak interlayer bonding due to easier tendency of interlayer separation, thereby the crack surface of the sample exhibit flat and easy tear as shown in Fig. 4.9(e). However, for part built with 30° raster angle along X direction (X-30) exhibit strong interlayer bonding due to relatively larger length of interlayer contact. Fracture under flexural load for this sample leads to complete damage and higher flexural strength of the sample. Therefore the cracked surface of the sample exhibit erratic and rough pattern as shown in Fig. 4.9(f).

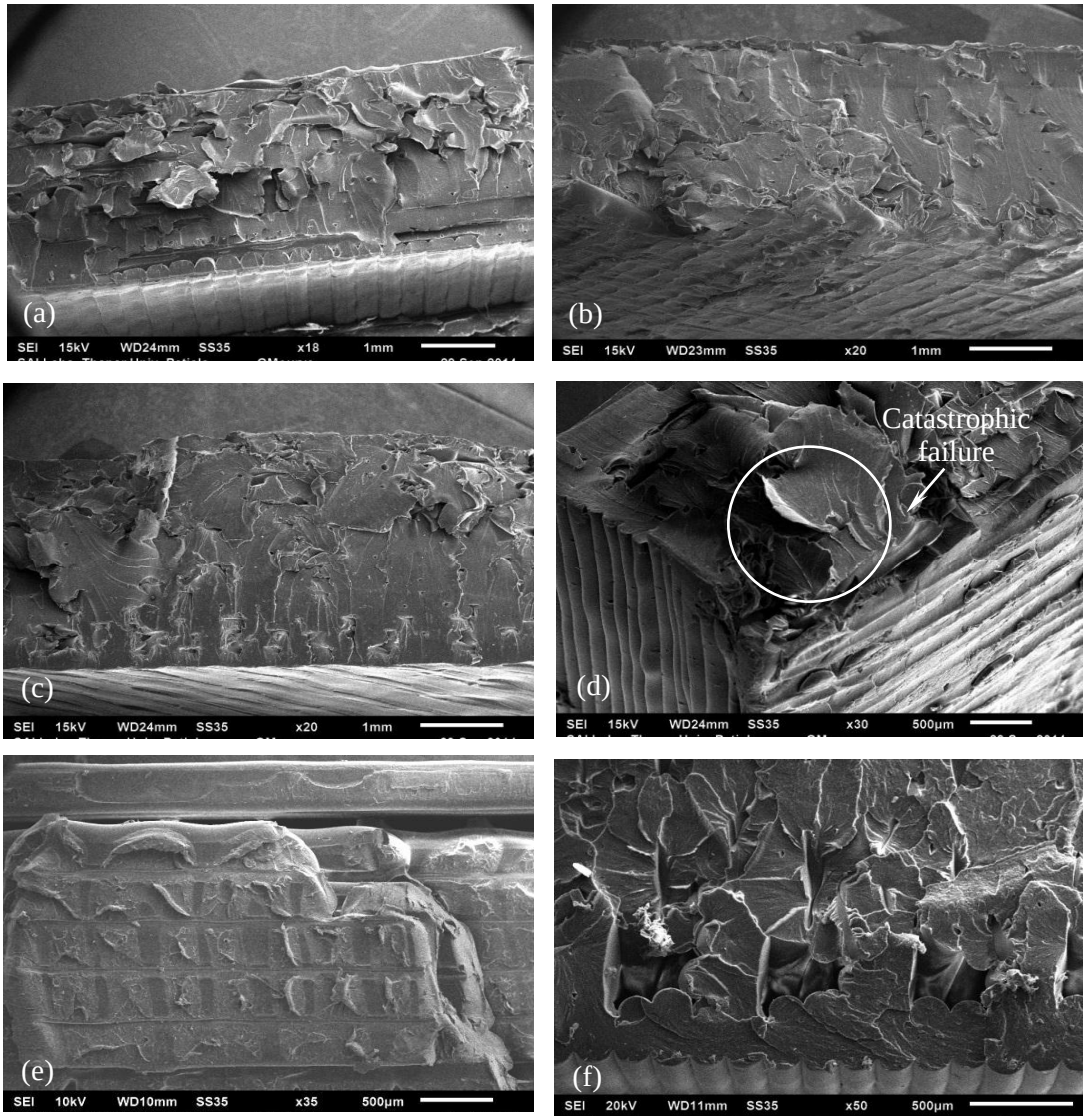

Figure 4.9: SEM fractograph of samples after flexural testing (a) Y-0, (b) Y-30, (c) Y-60, (d) Y-90, (e) Z-0 and (f) X-30

4.3 Geometric Accuracy

The geometric accuracy for all the components built at different part orientations (α) are measured and analyzed to study the effect of part orientation on geometrical and dimensional accuracy of FDM processed ABS P430 parts. Later all the parts are subjected to chemical treatment process exposing the parts to cold vapors of dimethylketone (acetone) laboratory reagent (LR) ≥ 99 % concentration and geometric accuracy are measured after the treatment and are compared with those obtained for the parts without any post treatment. For geometric accuracy different part geometries with different primitive surfaces and freeform part surfaces are considered for analyze and measurements.

4.3.1 Part with Primitive Surfaces

Parts are built at the seven different part orientation (0°, 15°, 30°, 45°, 60°, 75°, 90° about *Y* axis) and the geometric accuracy are measured for different primitive surfaces of FDM model. Figure 4.10 shows the schematic detailed geometry and dimensions of individual features of FDM model.

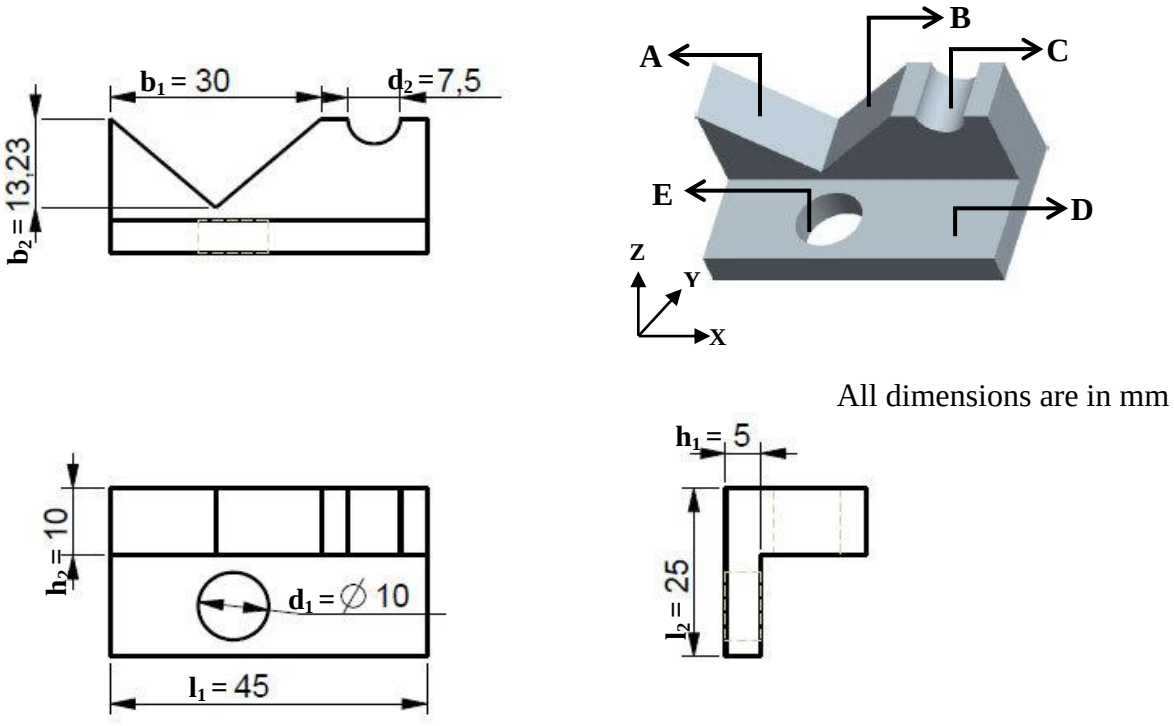

Figure 4.10: Part model with primitive surfaces

The primitive surfaces (A) and (B) are inclined surfaces that show staircase effect at all building orientations. Surface (C), a semi-cylindrical surface along Y axis and surface (E) represents cylindrical surface along Z axis are chosen because parts with curved surfaces are more prone to staircase effect which causes higher surface and geometric inaccuracy. Surface (D) is plane rectangular surface which shows geometrical inaccuracy as the inclination of part changes due to staircase effect when build at different orientations. Geometric accuracy is measured by calculating the percentage error in dimensions of fabricated FDM model as compared to actual dimensions of CAD model. Dimensions are measured twice and the average values are reported for analysis.

Geometric Accuracy: Different dimensions of the component for the surfaces A to E of the FDM parts fabricated at different orientations (as shown in Fig. 4.10) are measured and compared with CAD dimensions. The percentage changes in dimensions are calculated for each sample built at different part orientations and are given in Table 4.1. Results in Table 4.1 and Table 4.2 show the change in dimensions to represent the loss in feature before and after chemical treatment of the components.

Table 4.1: Results of percentage error in specimens with and without chemical treatment

Surface A and Surface B (of triangular groove)								
Part orientation (degree)	From CAD data b_1 = 30 mm				From CAD data b_2 = 13.23 mm			
	Without chemical treatment		With chemical treatment		Without chemical treatment		With chemical treatment	
	b_1 (mm)	Error (%)	b_1 (mm)	Error (%)	b_2 (mm)	Error (%)	b_2 (mm)	Error (%)
0	30.20	0.67	30.13	0.43	13.05	-1.36	12.95	-2.12
15	30.26	0.87	30.10	0.33	13.33	0.76	13.01	-1.66
30	29.76	-0.80	29.98	-0.07	13.16	-0.53	12.79	-3.33
45	29.91	-0.30	30.03	0.10	13.15	-0.60	12.75	-3.63
60	30.07	0.23	30.11	0.37	13.12	-0.83	12.88	-2.65
75	29.86	-0.47	30.18	0.60	13.03	-1.51	12.99	-1.81
90	29.78	-0.73	30.20	0.67	13.16	-0.53	12.69	-4.08

Surface C (of semi-cylindrical groove)								
Part orientation (degree)	From CAD data d_2 = 7.5 mm				From CAD data h_2 = 10 mm			
	Without chemical treatment		With chemical treatment		Without chemical treatment		With chemical treatment	
	d_2 (mm)	Error (%)	d_2 (mm)	Error (%)	h_2 (mm)	Error (%)	h_2 (mm)	Error (%)
0	7.51	0.13	7.54	0.53	10.09	0.90	10.18	1.80
15	7.48	-0.27	7.55	0.67	10.10	1.00	10.13	1.30
30	7.53	0.40	7.54	0.53	10.27	2.70	10.14	1.40
45	7.39	-1.47	7.43	-0.93	10.28	2.80	10.13	1.30
60	7.42	-1.07	7.57	0.93	10.23	2.30	10.07	0.70
75	7.43	-0.93	7.47	-0.40	10.12	1.20	10.11	1.10
90	7.47	-0.40	7.48	-0.27	10.06	0.60	10.12	1.20

Surface D (rectangular flat surface)								
Part orientation (degree)	From CAD data l_1 = 45 mm				From CAD data l_2 = 25 mm			
	Without chemical treatment		With chemical treatment		Without chemical treatment		With chemical treatment	
	l_1 (mm)	Error (%)	l_1 (mm)	Error (%)	l_2 (mm)	Error (%)	l_2 (mm)	Error (%)
0	45.17	0.38	45.02	0.04	25.12	0.48	25.1	0.40
15	45.21	0.47	45.04	0.09	25.14	0.56	25.15	0.60
30	45.23	0.51	45.04	0.09	25.21	0.84	25.17	0.68
45	45.26	0.58	45.08	0.18	25.31	1.24	25.2	0.80
60	45.25	0.56	45.12	0.27	25.23	0.92	25.22	0.88
75	45.22	0.49	45.14	0.31	25.2	0.80	25.19	0.76
90	45.16	0.36	45.02	0.04	25.15	0.60	25.17	0.68

Surface E (cylindrical surface)								
Part orientation (degree)	From CAD Data d_1 = 10 mm				From CAD Data h_1 = 5 mm			
	Without chemical treatment		With chemical treatment		Without chemical treatment		With chemical treatment	
	d_1 (mm)	Error (%)	d_1 (mm)	Error (%)	h_1 (mm)	Error (%)	h_1 (mm)	Error (%)
0	9.79	-2.1	9.93	-0.7	5.19	3.8	5.06	1.2
15	9.71	-2.9	9.81	-1.9	5.24	4.8	5.1	2.0
30	9.77	-2.3	9.87	-1.3	5.2	4.0	5.09	1.8
45	9.63	-3.7	9.83	-1.7	5.16	3.2	5.05	1.0
60	9.67	-3.3	9.79	-2.1	5.16	3.2	5.03	0.6
75	9.71	-2.9	9.9	-1.0	5.15	3.0	5.06	1.2
90	9.81	-1.9	9.93	-0.7	5.18	3.6	5.07	1.4

For surfaces A, B (flat surfaces of the triangular groove) the dimensional deviation in parts without treatment is less than 1% for the width of the triangular slot (b_1) and 1.5% in depth of grove (b_2). The amount of error in width gets marginally reduced and remains almost in similar range after chemical treatment however the error in dimension b_2 increases to a maximum of 4%. The reason for this could be that the after the treatment sharp corner at the root of the groove gets rounded and some changes in dimension is observed. For surface C (semi-cylindrical surface) the maximum dimensional deviation is observed in 45° orientation whereas the minimum deviation in dimensions measured at 0° orientation. A small amount of decrease in error is noticed after the treatment of the surface. Surface D and E exhibits continuous increase in geometric inaccuracy with part orientation giving maximum at 45° orientation due to increase in staircase effect and 0° part orientation exhibit minimum dimensional inaccuracy due to no staircase effect. Similar trend in dimensional deviation is also observed after chemical treatment however error is reduced. Thus, it is majorly noted

that percentage change in dimensions after the chemical treatment remains almost in similar range however, in many cases error is reduced. Also, the surface of the FDM parts should be orientated either parallel or perpendicular direction with respect to axis of a part for achieving lowest geometric inaccuracy. However, for flat surfaces which are at angle in base component, a separate orientation angle based on the initial tilt of the surface may give minimum error. This variation in dimensions is due to staircase effect and is of the order of 1-2% in many cases.

Chemical treatment of the specimen also causes the sharp corners to get round off and represents some loss in feature. Taking the corner radius (of built part without chemical treatment) is same as that of the radius of deposited filament layer (0.089 mm), the feature loss is calculated after chemical treatment and shown in Table 4.2. From Table 4.2 it can be seen that for surface (A) and (B) maximum loss in feature occurs for 45° part orientation and for surface (C) and surface (D) maximum loss in feature occur for 15° and 90° part orientation. The corner radius values after treatment are in the order of less than a millimeter for most of the cases and reaches to maximum 1.6 mm.

Table 4.2: Results of loss in features of specimens after chemical treatment

Triangular surface (A and B)			
Without chemical treatment $r_1 = r_2 = r_3 = 0.089$ mm			
Part orientation (degree)	With chemical treatment		
	r_1 (mm)	r_2 (mm)	r_3 (mm)
0	0.497	1.228	0.469
15	0.373	1.148	0.535
30	0.396	0.960	0.521
45	0.663	1.640	0.667
60	0.543	1.270	0.542
75	0.403	0.980	0.471
90	0.597	1.050	0.635

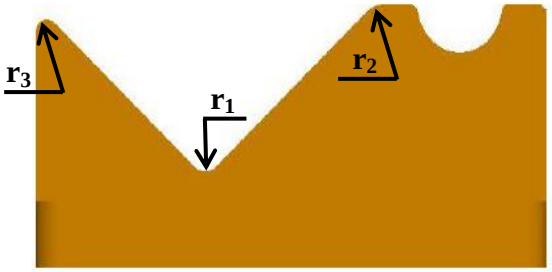

Semi cylindrical surface (C)			
Without chemical treatment $r_1 = r_2 = r_3 = 0.089$ mm			
Part orientation (degree)	With chemical treatment		
	r_1 (mm)	r_2 (mm)	r_3 (mm)
0	0.900	0.376	0.760
15	0.616	0.868	0.657
30	0.631	0.592	0.624
45	0.550	0.662	0.584
60	0.501	0.696	0.873
75	0.469	0.669	0.665
90	0.609	0.707	0.819

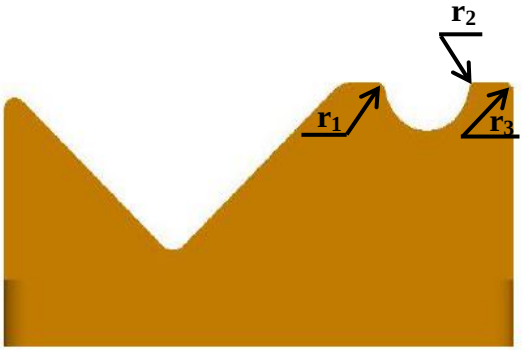

Rectangle surface (D)		
Without chemical treatment $r_1 = r_2 = 0.089$ mm		
Part orientation (degree)	With chemical treatment	
	r_1 (mm)	r_2 (mm)
0	0.698	1.030
15	1.007	0.924
30	0.965	1.123
45	1.023	1.071
60	0.901	0.954
75	0.755	1.039
90	1.623	1.132

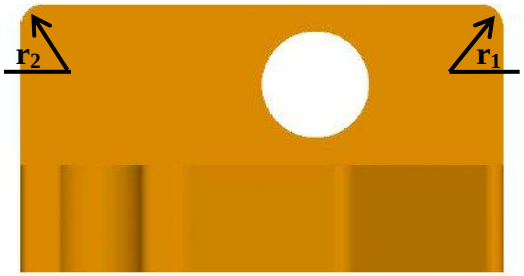

4.3.2 Part with Primitive and Freeform Surfaces

Parts are built at the three different part orientations about X, Y and Z axis and geometrical accuracy are measured for different primitive and freeform surfaces of FDM model.

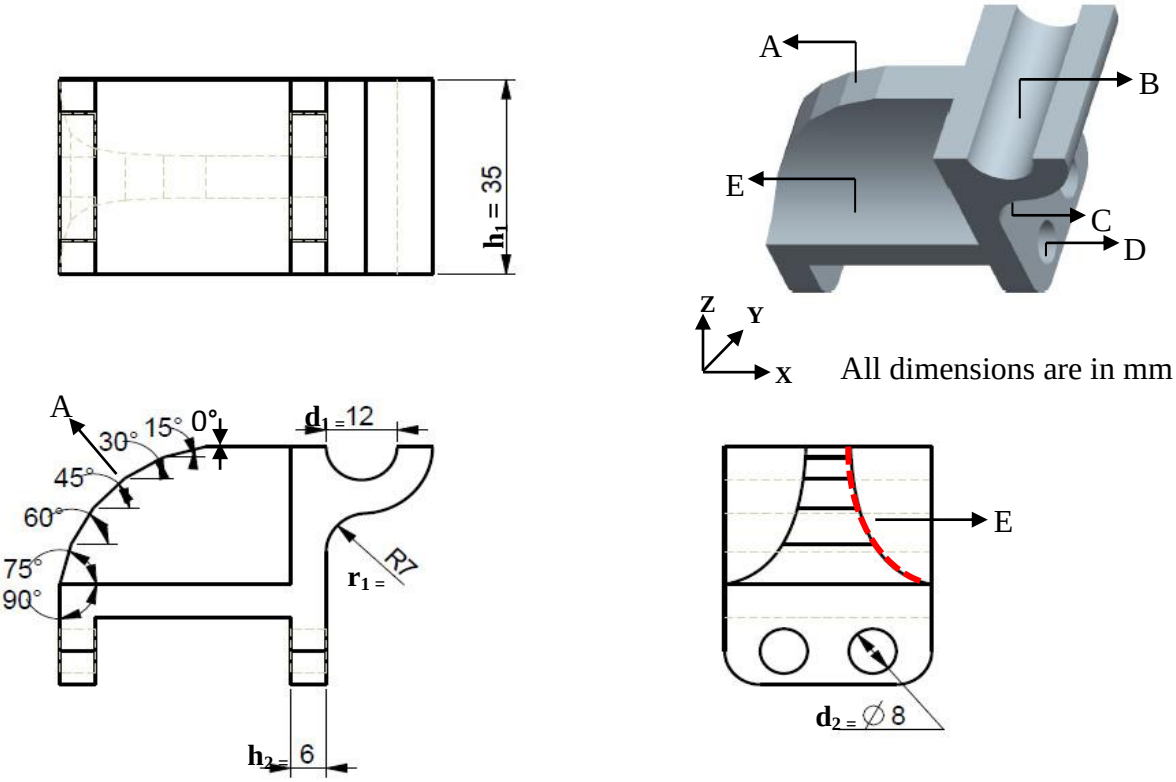

Figure 4.11: Part model with primitive and freeform surfaces

Figure 4.11 shows the detailed geometry and dimensions of individual features of FDM model. The primitive surface (A) is inclined surface with continuous slope variations at steps (change in angles) that show staircase effect without orientating the part during building

about a particular axis (X, Y and Z axis). Surface (B) which is a semi-cylindrical surface along Y axis, surface (C) represents curved surface along Y axis, surface (D) represents cylindrical surface along X axis and surface (E) is freeform surface (a freeform geometry suggests a complex, unsymmetrical geometry, especially one without cylindrical or quadrate features) are chosen to study the staircase effect which causes higher geometric inaccuracy. Geometrical inaccuracy is measured by calculating the percentage error in dimensions of fabricated FDM model as compared to actual dimensions of CAD model. Dimensions are measured twice and the average values are reported for analysis.

Geometric Accuracy: Different dimensions of the component for the surfaces A to E of the FDM parts fabricated at different orientations (as shown in Fig. 4.11) are measured and compared with CAD dimensions. The percentage deviations in dimensions are calculated for each sample built at different part orientation and are given in Table 4.3. Results in Table 4.3 and Table 4.4 show the change in dimensions to represent the loss in feature with and without chemical treatment of the components.

Table 4.3: Results of error in surface (A) dimensions with and without chemical treatment

Slope with different angles		Without chemical treatment			With chemical treatment		
Part orientation	Angle	Trial 1	Trial 2	Average	Trail 1	Trail 2	Average
X	0	0.154	0.27	0.212	0.01	0.242	0.126
X	15	14.778	14.653	14.716	14.647	14.619	14.633
X	30	30.562	30.662	30.612	30.386	30.108	30.247
X	45	45.583	44.869	45.226	45.176	45.253	45.215
X	60	59.745	59.881	59.813	59.723	59.798	59.761
X	75	74.983	75.166	75.075	74.95	74.816	**74.883**
X	90	89.959	89.92	**89.940**	89.761	89.96	89.861
Y	0	0.232	0.279	0.256	0.23	0.149	0.190
Y	15	15.918	15.157	15.538	15.461	15.364	15.413
Y	30	29.386	29.611	29.499	29.058	29.418	29.238
Y	45	44.124	44.423	44.274	43.493	43.978	43.736
Y	60	59.425	58.501	**58.963**	58.912	58.435	58.674
Y	75	74.84	74.48	74.660	74.41	74.495	74.453
Y	90	89.583	89.847	89.715	89.225	89.902	89.564
Z	0	0.319	0.302	0.311	0.305	0.311	0.308
Z	15	15.88	14.778	15.329	15.048	15.551	15.300
Z	30	30.766	30.319	30.543	30.284	30.05	30.167
Z	45	44.064	44.359	44.212	43.692	43.404	**43.548**
Z	60	59.492	59.356	59.424	59.75	59.229	59.490
Z	75	74.22	74.821	74.521	73.39	73.835	73.613
Z	90	89.792	89.827	89.810	89.687	89.838	89.763

Surface B (semi-cylindrical surface)								
Part orientation	From CAD data d_1 = 12 mm				From CAD data h_1 = 35 mm			
	Without chemical treatment		With chemical treatment		Without chemical treatment		With chemical treatment	
	d_1 (mm)	Error (%)	d_1 (mm)	Error (%)	h_1 (mm)	Error (%)	h_1 (mm)	Error (%)
X	11.886	-0.950	12.041	0.342	34.932	-0.194	35.142	0.406
Y	11.985	-0.125	12.247	2.058	34.859	-0.403	35.265	0.757
Z	12.314	2.617	12.501	4.175	34.389	-1.746	35.142	0.406

Surface C (curved surface)								
Part orientation	From CAD data r_1 = 7 mm				From CAD data h_1 = 35 mm			
	Without chemical treatment		With chemical treatment		Without chemical treatment		With chemical treatment	
	r_1 (mm)	Error (%)	r_1 (mm)	Error (%)	h_1 (mm)	Error (%)	h_1 (mm)	Error (%)
X	7.216	3.086	7.275	3.936	34.932	-0.194	35.142	0.406
Y	7.104	1.486	7.131	1.871	34.859	-0.403	35.265	0.757
Z	7.047	0.679	7.057	0.814	34.389	-1.746	35.142	0.406

Surface D (cylindrical surface)								
Part orientation	From CAD data d_2 = 8 mm				From CAD data h_2 = 6 mm			
	Without chemical treatment		With chemical treatment		Without chemical treatment		With chemical treatment	
	d_2 (mm)	Error (%)	d_2 (mm)	Error (%)	h_2 (mm)	Error (%)	h_2 (mm)	Error (%)
X	7.687	-3.913	7.965	-0.438	6.242	4.033	6.141	2.350
Y	7.523	-5.963	7.704	-3.700	6.169	2.817	5.969	-0.517
Z	7.687	-3.913	7.954	-0.575	6.321	5.350	6.014	0.233

For surfaces A (inclined surface with slope variation in steps) the maximum angle deviation for part surface built at different part orientation (along X, Y and Z axis) is less than 1.1°. The amount of deviation in angles gets marginally reduced after the chemical treatment as compared to slope angle before chemical treatment. The reason for this could be that after the chemical treatment the ABS plastic material get soften and slide past to each other thus filling the air gap (voids and crater) between successive layers thus reduces the staircase effect as a result the slope angle with respect to horizontal axis gets reduced. From Table 4.3 it can also be seen that before the chemical treatment the specimen built along Y axis with slope angle 60° shows maximum deviation in angle i.e. 1.037° due to staircase effect

(inclined surface) whereas specimen built along X with slope angle 90° shows minimum deviation in angle of 0.06° due to no staircase effect (flat surface). Similar, trend is observed after the chemical treatment of the component giving maximum deviation in slope angle of 1.452° for specimen built along Z axis having 45° slope angle (inclined surface) and minimum deviation in angle of 0.117° is observed for specimen built along X axis having 75° slope angle. For surface B (semi-cylindrical surface) and surface C (curved surface) the maximum dimensional deviation is observed in Z orientation whereas the minimum deviation in dimensions measured at Y orientation. A small amount of increase in error is noticed after the treatment of the surface. For surface D (cylindrical surface) the maximum dimensional deviation is observed for part built in Y orientation whereas minimum dimensional deviation is observed for part built in X orientation. After the chemical treatment small amount of decrease in error is noticed giving maximum deviation in Y orientation and minimum deviation in Z orientation. This variation in dimensions is due to staircase effect because after the chemical treatment staircase effect gets reduced which causes the change in dimensions.

For freeform surface (surface E) the dimensional deviation from CAD data shows different behavior as compared to regular flat or cylindrical surfaces. Figure 4.12 shows the amount of deviation in dimensions of freeform surface before and after the chemical treatment built at different part orientation (X, Y and Z axis). It can be seen that for part orientation along X axis dimension deviations from CAD data are moderately increases before the chemical treatment whereas after the chemical treatment a small amount of increase in error is noticed which does not remain constant throughout the slope of freeform surface i.e. dimensional deviation first increases than start decreases from CAD data as shown in Fig. 4.12(b). Dimensional deviation of 0.448 mm before chemical treatment is changed to 0.893 mm after the chemical treatment for X orientation part. For freeform surface built along Y orientation dimensional deviation is continuously increases form CAD data before chemical treatment. The amount of error in slope gets moderately increased and shows almost similar trend after the chemical treatment. Dimension deviation of 0.571 mm before chemical treatment is changes to 0.878 mm after the chemical treatment for Y orientation part. For part built along Z orientation dimensional error from CAD data is minimum before chemical treatment. Similar trend in slope variation is also observed after chemical treatment however error is reduced. Dimension deviation of 0.454 mm before chemical treatment is changes to 0.280 mm after the chemical treatment.

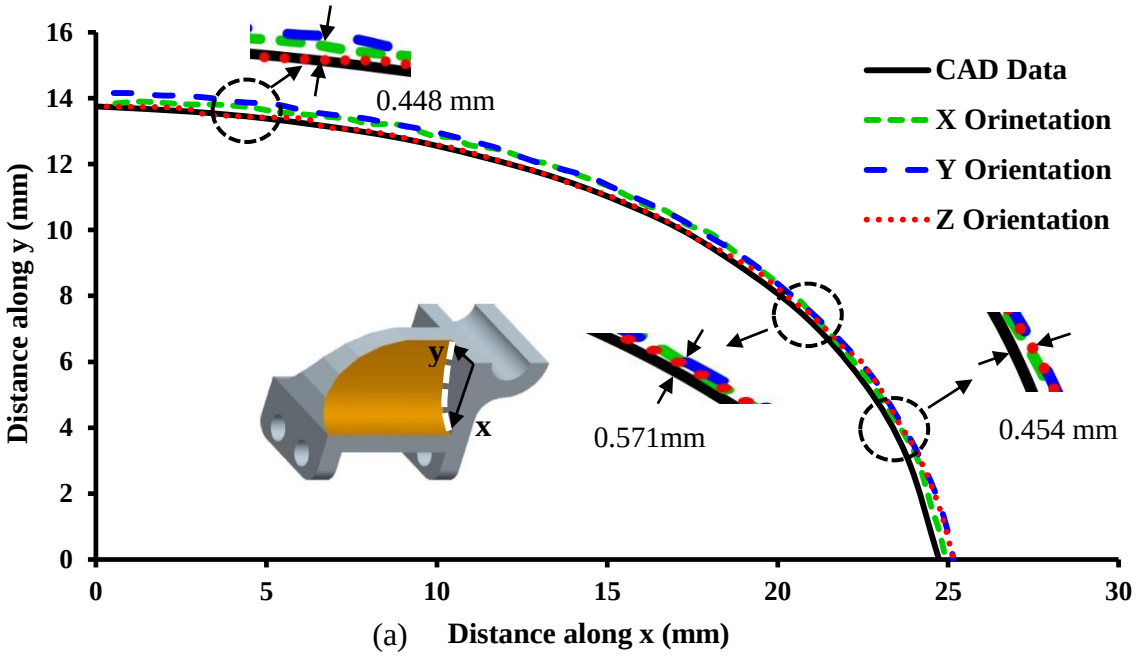

(a)

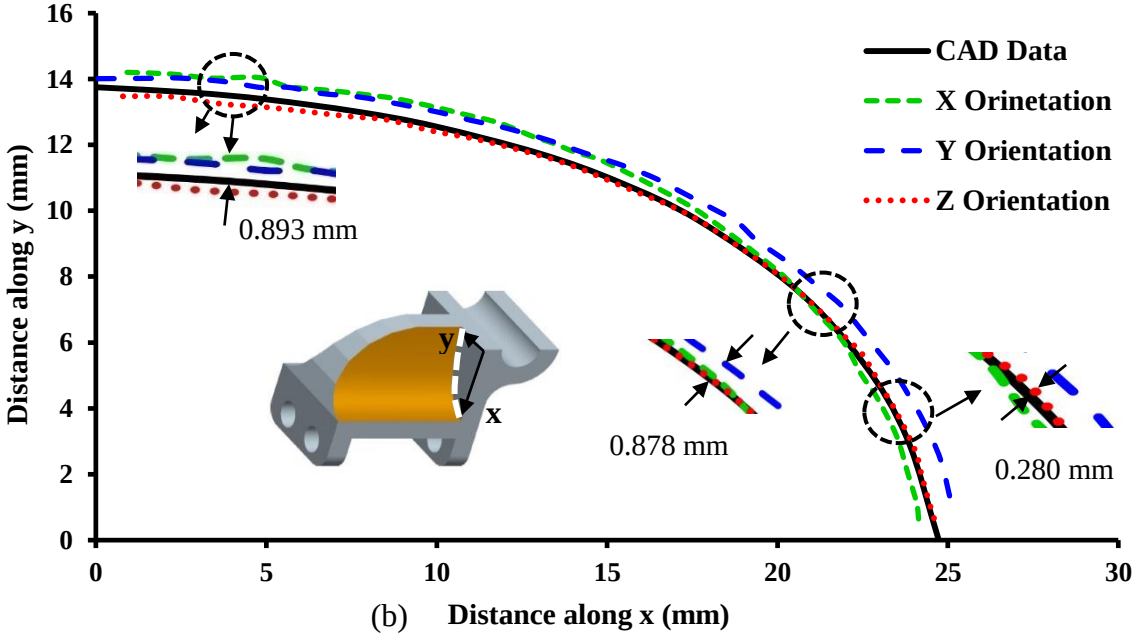

(b)

Figure 4.12: Geometric accuracy measurement for freeform surface (a) without chemical treatment and (b) with chemical treatment

Chemical treatment of the specimen also causes rounding off the sharp corners and leads to some loss in feature. Taking the corner radius is same as that of the radius of deposited filament layer for built parts without treatment (0.089 mm), the feature loss is calculated after chemical treatment and shown in Table 4.4. From Table 4.4 it can be seen that for surface (B) maximum loss in feature occur for X orientation part. The corner radius

values after treatment are in the order of one millimeter for every orientation and reaches to maximum of 1.3 mm.

Table 4.4: Results of lost in features of specimens after chemical treatment

Semi cylinder surface B			
Without chemical treatment $r_1 = r_2 = r_3 = 0.089$ mm			
Part orientation (degree)	With chemical treatment		
	r_1 (mm)	r_2 (mm)	r_3 (mm)
X	1.318	1.217	0.928
Y	1.103	1.37	0.793
Z	1.091	0.998	0.671

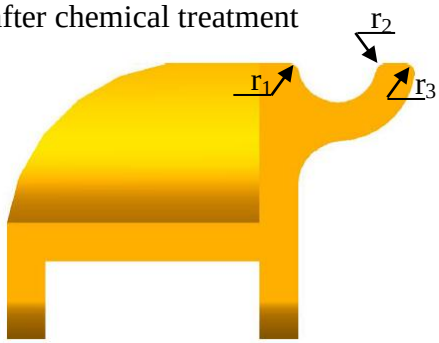

4.3.3 Part with Doubly Curved Surfaces

Parts are built at the three different part orientations about X, Y and Z axis and geometrical accuracy are measured for longitudinal and transverse curves (doubly curves) of FDM model. Figure 4.13 shows the schematic detailed geometry of FDM model.

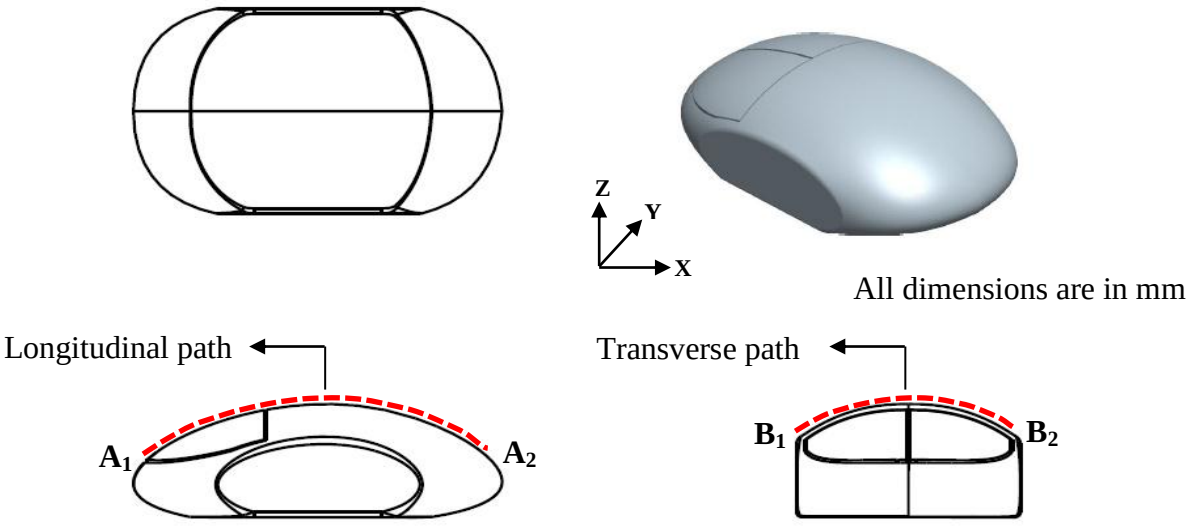

Figure 4.13: Part model with doubly curved surfaces

The doubly curved freeform surface with longitudinal curve A_1-A_2 and transverse curve B_1-B_2 is chosen as the next part for analyzing geometric deviation before and after post-built chemical treatment. Geometric accuracy is measured by plotting the curves (A_1-A_2 and B_1-B_2) of fabricated FDM model and compared to the curve of CAD model and

visualizing the dimensional deviation between two curves for both with and without chemical treatment.

Geometric Accuracy: The geometric accuracy of both the longitudinal curve A_1-A_2 and transverse curve B_1-B_2 of the component fabricated at X, Y and Z orientations before and after the chemical treatment are measured and compared with CAD dimensions as shown in Fig. 4.14 and Fig. 4.15.

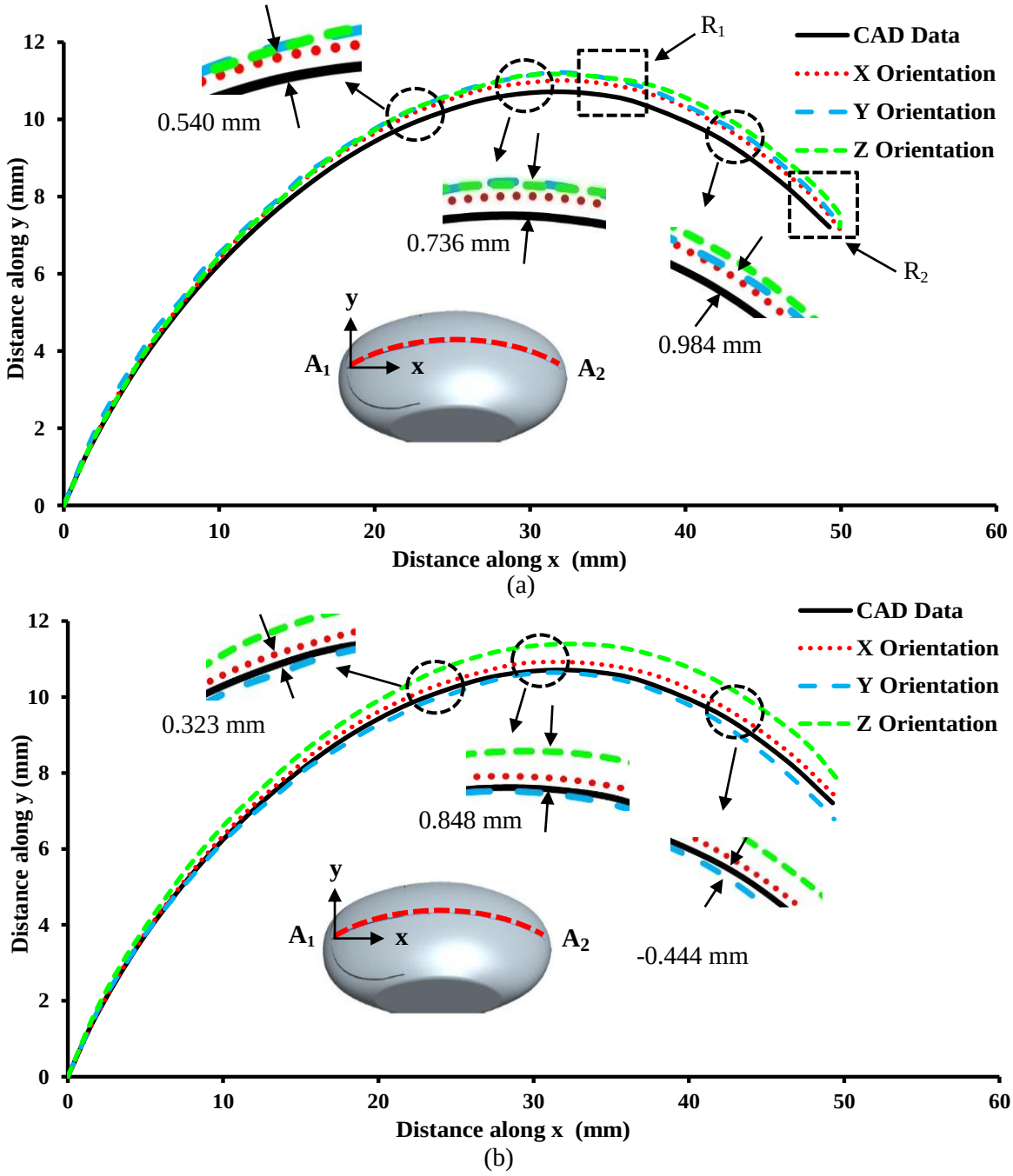

Figure 4.14: Geometric accuracy measurement for A_1-A_2 longitudinal curve: (a) without chemical treatment, (b) with chemical treatment

From Fig. 4.14 it can be seen that for longitudinal curve A_1-A_2 the dimensional deviation from CAD data are continuously increasing as the slope of curve A_1-A_2 increases due to increase in staircase effect. The dimensional deviation from CAD data is more where the slope of the curve changes rapidly i.e. at region R_1 where dimensional error for all the three orientations is maximum before chemical treatment (refer Fig 4.14(a)). It is also observed that the dimensional error start decreasing gradually as the slope of curve changes in reverse direction i.e. from region R_1 to R_2. It can be seen that for region R_2 dimensional errors is minimum for all the three orientation as compared to dimensional error at region R_1. After the chemical treatment of the specimen similar trend in dimensional error is also observed as shown in Fig. 4.14(b). It can be seen that the maximum dimensional error is observed for part built in Y and Z orientation whereas for X orientation dimensional error is moderately decreased after treatment where dimensional error of 0.540 mm decreases to 0.323 mm. For Y orientation maximum deviation of 0.984 mm changes to -0.444 mm (negative sign indicate slope is below CAD data slope) after chemical treatment whereas for Z orientation the dimensional error of 0.736 mm increase to 0.848 mm after treatment.

For transverse curve B_1-B_2 the dimensional error before and after the chemical treatment is shown in Fig. 4.15. It can be seen that dimensional error for X orientation is continuously increases as the slope of curve increases and reaches the maximum deviation at region R_1 and start decreasing afterward as the slope of curve decreases in reverse direction and reaches to minimum deviation at region R_2. This is mainly happening due to increase in staircase effect as the slope of curve increases and start decreasing as the slope of curve decreases in reverse direction. This trend in dimensional error is also observed after treatment but dimensional error is extensively increased as shown in Fig. 4.15(b) where dimensional deviation of 0.344 mm before treatment is changes to 0.683 mm after treatment. For Y and Z orientations dimensional deviation before chemical treatment is not much significant (less error) but dimensional error extensively increases after the chemical treatment as shown in Fig. 4.15(b) where minimum deviation of 0.164 mm for Y orientation is increases to -0.720 mm after the chemical treatment whereas for Z orientation 0.903 mm before treatment is changes to -0.383 mm after the chemical treatment. From Fig. 4.14 and Fig. 4.15 it can be seen that Y orientation is optimal orientation for fabrication of freeform parts because dimensional error for both longitudinal curve A_1-A_2 and transverse curve B_1-B_2 is minimum for both with and without chemical treatment.

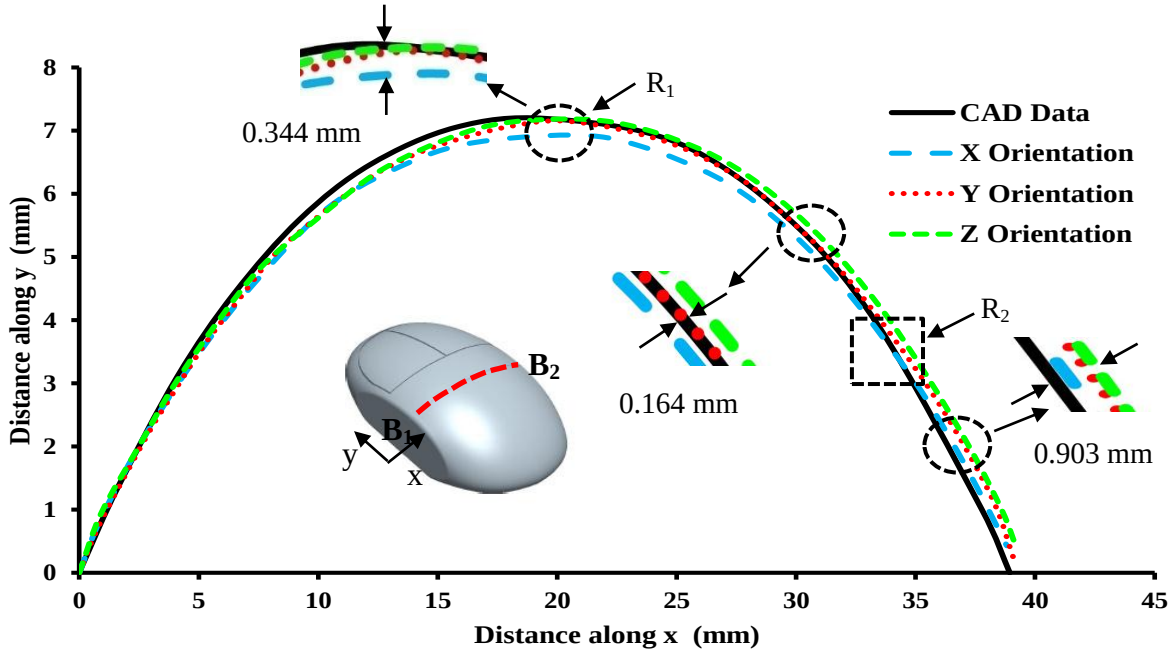

(a)

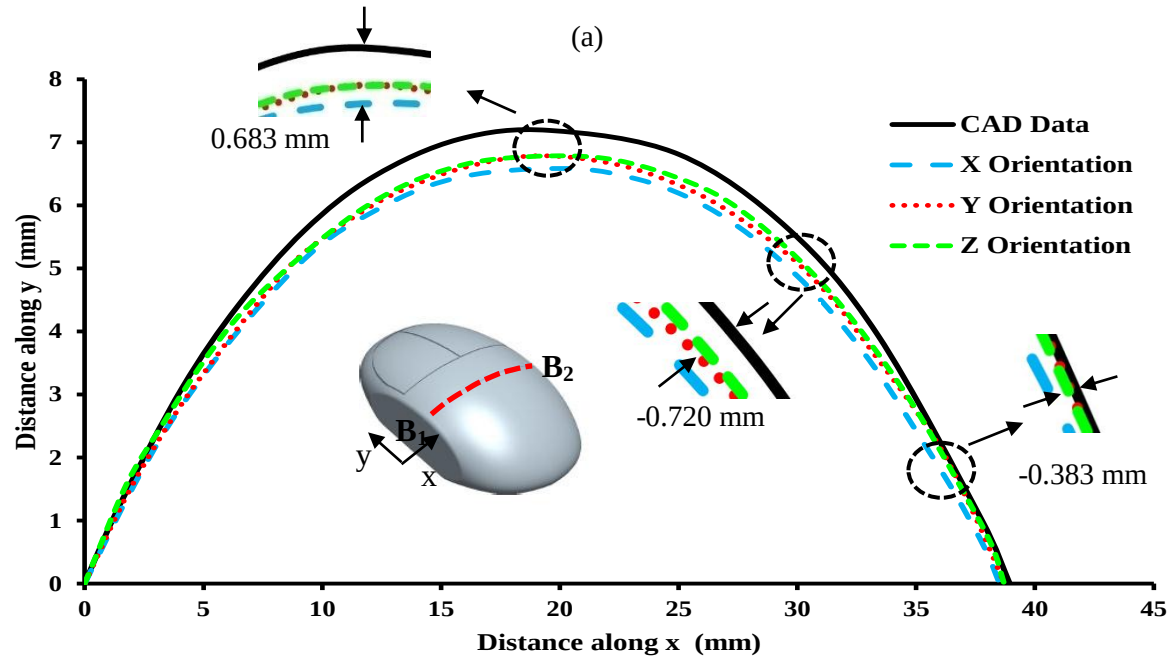

(b)

Figure 4.15: Geometric accuracy measurement for B_1-B_2 transverse curve: (a) without chemical treatment, (b) with chemical treatment

4.4 Surface Roughness Measurement

The surface roughness for all the components built at different part orientations and raster angles are measured and analyzed to study the effect of process parameters. Later, all the parts are chemically treated by exposing the parts to cold vapors of dimethylketone. Surface roughness is measured after the treatment and is compared with those obtained for the parts without post treatment. Roughness is measured twice on each surface of different part geometries with different primitive and freeform surfaces and average surface roughness (R_a) value are reported for analysis.

4.4.1 Roughness of Flat Surfaces

Surface roughness of all the component are measured in both along and across the length of the specimens twice (on flat surface) and average surface roughness (R_a) values are taken for each direction. Variation of R_a value for each test samples with and without the chemical treatment built at different part orientations and raster angles are represented by bar graphs as shown in Fig. 4.16. From Fig. 4.16 it can be seen that surface roughness measured along the length exhibit a much different behavior than surface roughness measured across the length.

Before the chemical treatment the specimens built with part orientation along the X axis provide the lowest surface roughness whereas orientations about Z axis exhibit much higher surface roughness when roughness are measured along the length of the specimen. A possible reason behind this phenomenon is that when a part is orientated along the Z axis number of layers increases each having rasters of smaller length, thus residual stresses increases due to increase in number of heating and cooling cycle which may have caused de-lamination, cracking or distortion of the specimen. Moreover due to small volume of each layer the servo motor has to change the direction in very short interval of time to remain synchronize in both the X and Y direction which causes the fluctuation in depositing the road in each layer. This leads to formation of void and air gap and increases the surface roughness of test specimens. The part built with orientation along the X axis exhibit higher surface roughness when measure across the length of the specimen. The best surface finish (R_a = 0.63 µm) is obtained when part is orientated along the Z axis and raster angle is 0° (Z-0) and surface roughness is measured across the length of the specimen whereas poor finish (R_a = 15.39 µm) is obtained when part is orientated along the Z axis and raster angle is 30° (Z-30) along the length of the specimen.

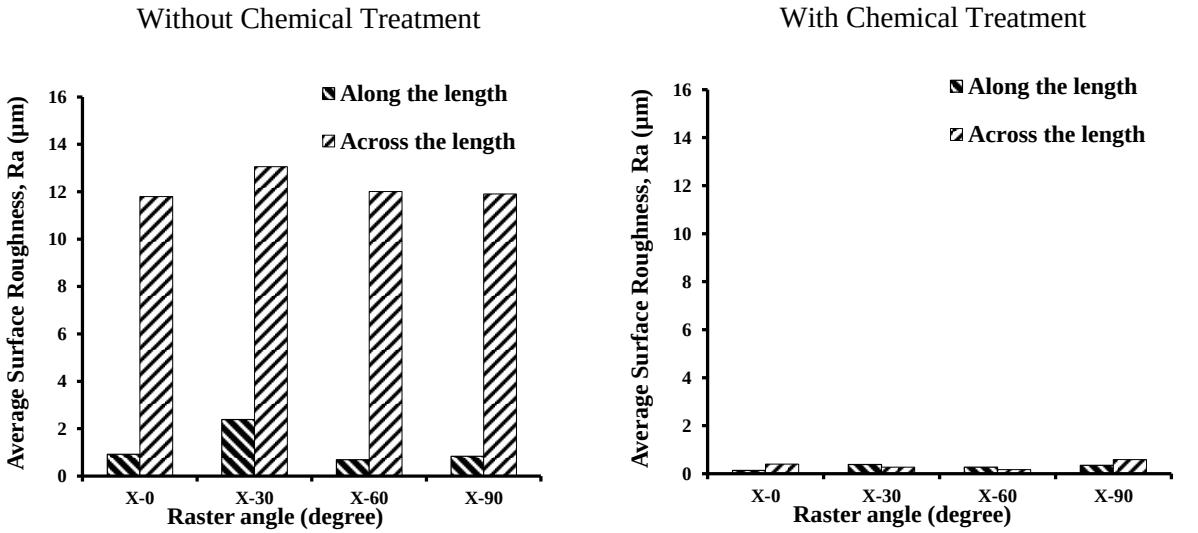

(a) X direction

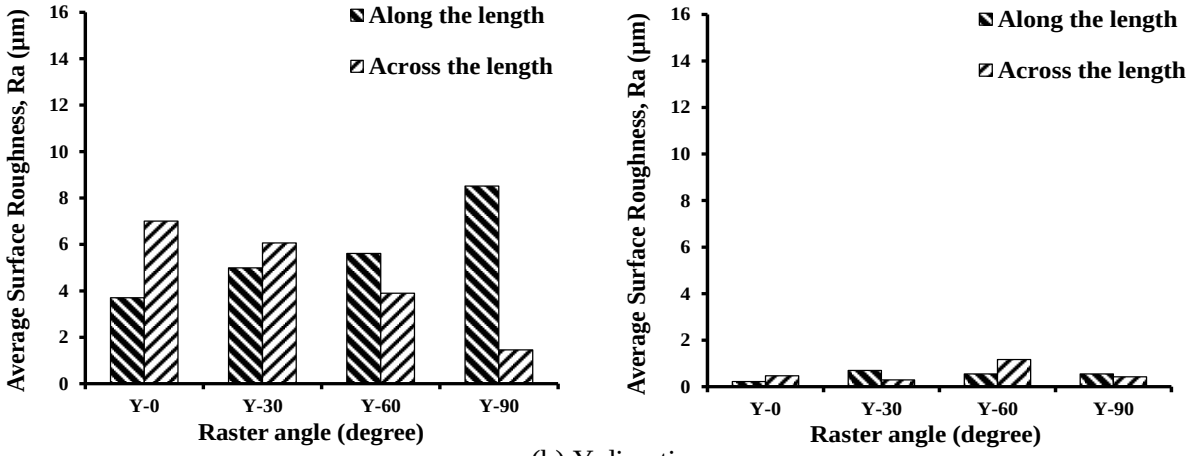

(b) Y direction

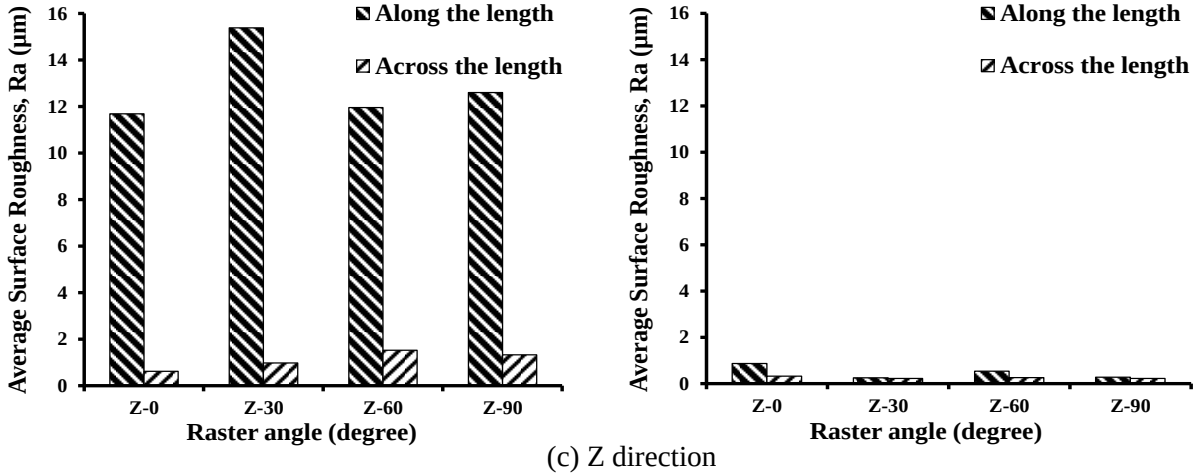

(c) Z direction

Figure 4.16: Surface roughness at flat surfaces of specimens built at different part orientations and raster angle with and without chemical treatment

The results indicate that while lower roughness measured along the length is achieved for part orientation along X axis, but the higher roughness is measured across the length direction and vice-versa for part orientation in Z axis. Moreover, a reasonably moderate surface roughness is noted for part orientation along Y axis with 30° and 60° raster orientation. However after the specimens are treated with cold vapor of acetone, a massive reduction in surface roughness values are observed as shown in Fig. 4.16. The maximum surface roughness of 13.05 µm for part built with along X axis with raster angle 30° is reduces to 0.270 µm after the chemical treatment when roughness is measured across the length of the specimen (refer Fig. 4.16(a)). Similarly the maximum surface roughness of 15.39 µm for part built along Z axis having raster angle 30° is reduced to 0.220 µm (refer Fig. 4.16(c)) after the chemical treatment when surface roughness is measured along the length of the specimen. The minimum surface roughness of 0.135 µm is obtained for specimen built along X axis and raster angle 0° (X-0) when roughness is measured along the length of the specimen.

Figure 4.16 demonstrates that a significant reduction in surface roughness is possible to achieve uniformly for all component built at different part orientations and raster angles after post-treatment with cold vapor of acetone. All the surfaces of component are consistently get exposed to the vapors for a sufficient duration and ensures a smooth surface all around the components. The process achieves a smooth, shiny surface finish due to softening of the outer layers because acetone breaks down the secondary bond between the ABS polymer chains to slide past to each other and reaches to more stable position. The surface tension in liquid like ABS plastic layers polished the surface textured especially the air gaps between successive layers. After the parts are taken out from the container, the acetone traces from the surface vaporize and the ABS plastic return back to its original hardness with well bonded continuous layers on its outer surface. The microscopic pictures of surfaces before and after chemical treatments are shown in Fig. 4.2 and Fig. 4.17. The distinct demarcation of layers present in parts before treatment gets eliminated after the chemical treatment. The treatment of parts helps in reducing the stair case effects of the parts after the treatment and helps in reducing the surface roughness.

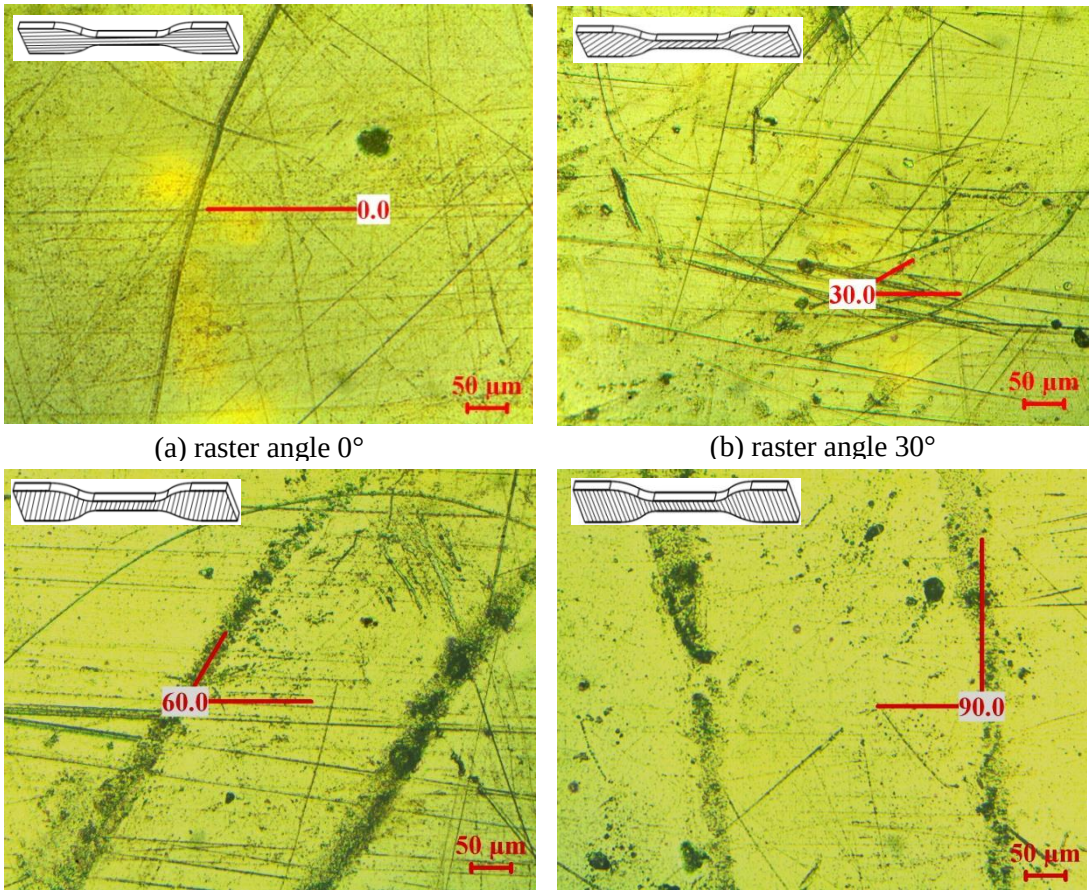

(a) raster angle 0° (b) raster angle 30°

(c) raster angle 60° (d) raster angle 90°

Figure 4.17: Optical microscopic images of specimens with flat surfaces built at four different raster angles after chemical treatment

4.4.2 Roughness of Primitive Surfaces

Surface roughness are measured for different primitive surfaces of FDM model (CAD model and geometric details shown in Fig. 4.10) and average surface roughness (R_a) values are shown in Fig. 4.18 for parts built at different orientations. For surfaces A, B (flat surfaces of the triangular groove) roughness is measured along and across the direction (X and Y axis respectively) and average values are reported. From Fig. 4.18(a) it can be seen that maximum surface roughness at surface (A) is obtained for 60° orientation whereas the minimum surface roughness for the same surface is achieved at 0° orientation. On the contrary, for surface B minimum surface roughness is obtained at 60° orientation and maximum is obtained at 0° orientation. The surfaces A and B being the two opposite surface of the triangle and parallel to Y axis (transverse) show the opposite behavior.

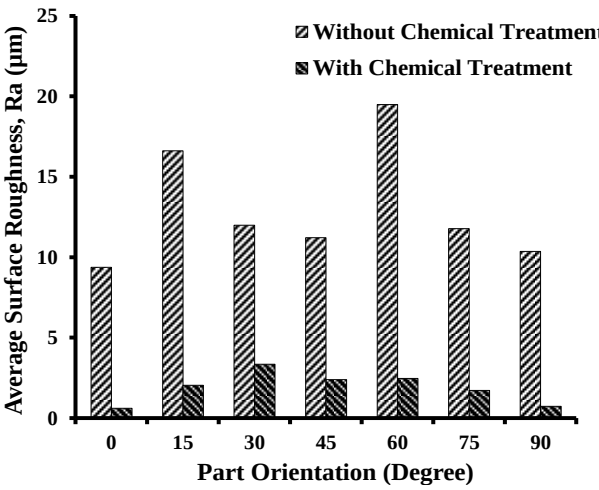

(a) Surface A

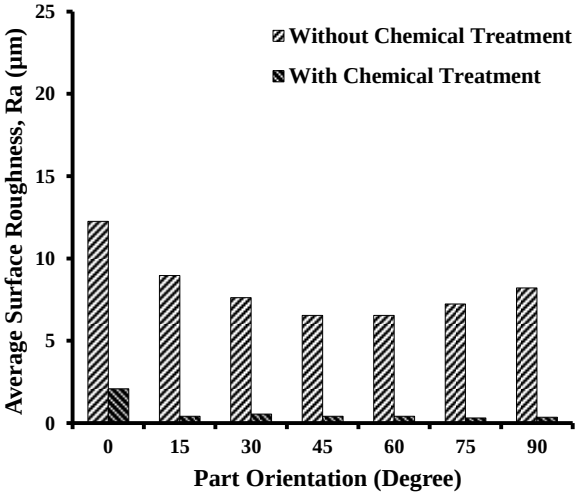

(b) Surface B

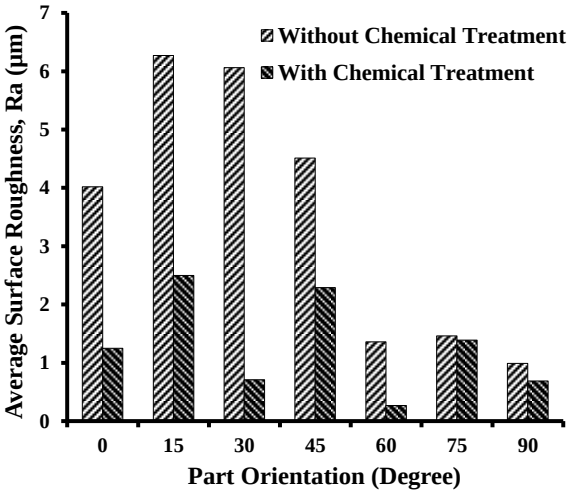

(c) Surface C

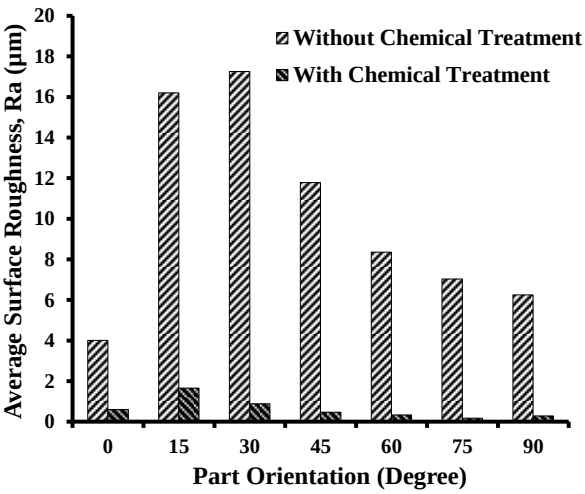

(d) Surface D

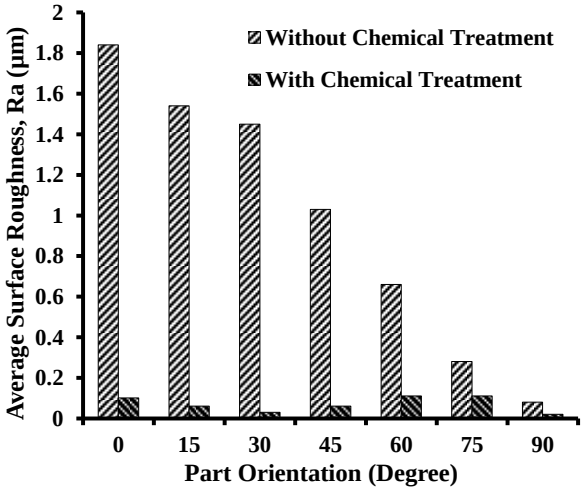

(e) Surface E

Figure 4.18: Surface roughness at primitive surfaces of specimen built at different part orientations with and without chemical treatment

It can be also seen from Fig. 4.18 that with cold vapor chemical treatment of the parts a significance reduction in surface roughness values are achieved. Although the difference between maximum and minimum surface roughness of the samples without treatment is very high, after treatment difference between maximum and minimum surface roughness for surface A or B is marginal. A minimum surface roughness of 0.62 µm and 0.31 µm is obtained for surfaces A and B, respectively after chemical treatment. For surface (C) which is in semi-cylindrical surface, surface roughness is measured only in a direction along the axis of the groove (Y axis) as on the curved surface (along X axis) roughness measurement was not possible. Variation of surface roughness for surface C (Fig. 4.18(c)) shows that roughness first increases giving maximum value at 15° part orientation and then start decreasing with minimum roughness measured at 90° orientation. Surface roughness of 0.99 µm before treatment is reduced to 0.69 µm for 90° orientation and 6.27 µm of maximum roughness before treatment is reduced to 2.5 µm for 15° orientation. Surface D, plane surface exhibits continuous increase in surface roughness with part orientation giving maximum at 30° orientation due to increase in staircase effect whereas 0° part orientation exhibit minimum surface roughness due to no staircase effect. In case of surface E which forms an inner surface of hollow cylinder (axis along Z axis) exhibit continuous decrease in surface roughness giving maximum at 0° orientation and minimum at 90° part orientation. From Fig. 4.18 it can be seen that specimen built with 90° part orientation exhibit optimal part deposition orientation for each primitive surface of FDM parts giving good quality of surface finish. After chemical treatment of the components, a minimum roughness of 0.29 µm is achieved for surface D (for 90° orientation) and 0.02 µm for surface E (for 90° orientation). Figure 4.18 demonstrates that a significant reduction in surface roughness is possible to achieve uniformly for all surfaces at different orientations after post-treatment by cold vapor of acetone. All the surfaces (internal or external) of a part are consistently get exposed to the vapors for a sufficient duration and ensures a smooth surface all around the components.

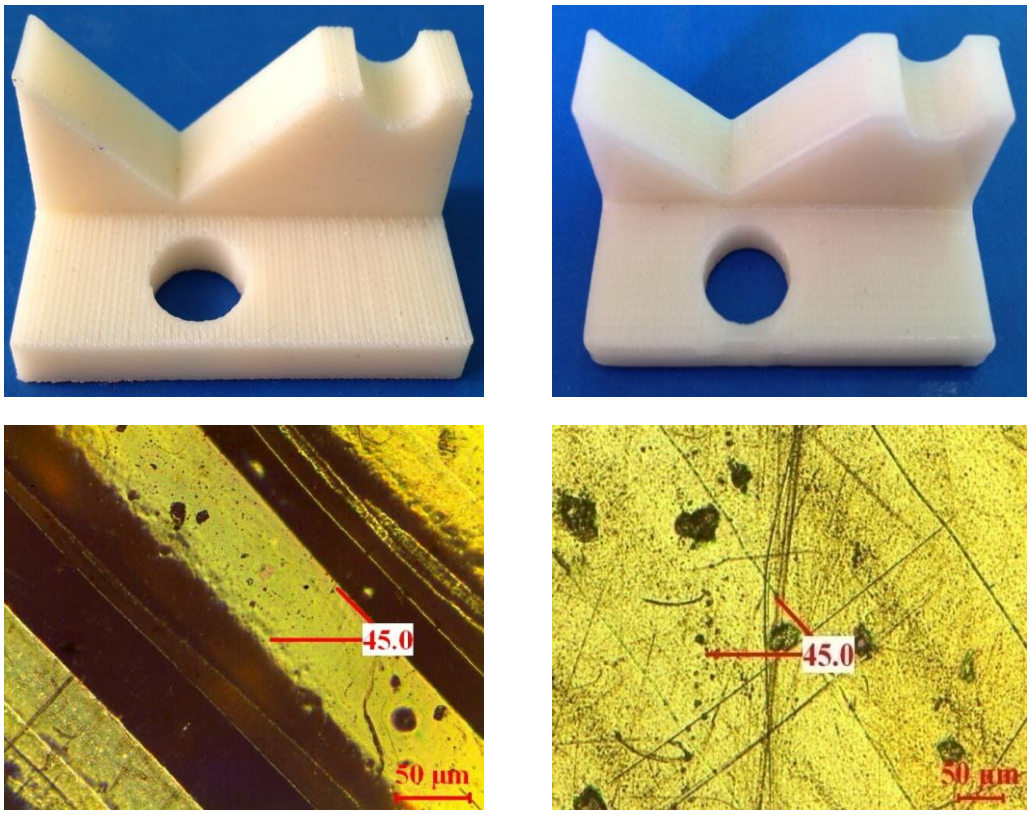

(a) (b)

Figure 4.19: Specimen appearance and optical microscopic images of build specimens (a) without chemical treatment and (b) with chemical treatment

The cold vapor treatment helps to achieve a smooth, shiny surface finish due to softening of the outer layers because acetone breaks down the secondary bond between the ABS polymer chains to slide past to each other and peaks of deposited layers are reduced. The surface tension in liquid like ABS plastic layers polished the surface textured especially the air gaps between successive layers. After the parts are taken out from the container, the acetone traces from the surface vaporize and the ABS plastic return back to its original hardness with well bonded continuous layers on its outer surface. The appearance and microscopic pictures of surfaces before and after chemical treatments are shown in Fig. 4.19. The distinct demarcation of layers present in parts before treatment gets eliminated after the chemical treatment. The treatment of parts helps in reducing the stair case effects of the parts after the treatment and helps in reducing the surface roughness. Stair case effects of the parts before and after the treatment for all samples are shown in Fig. 4.20.

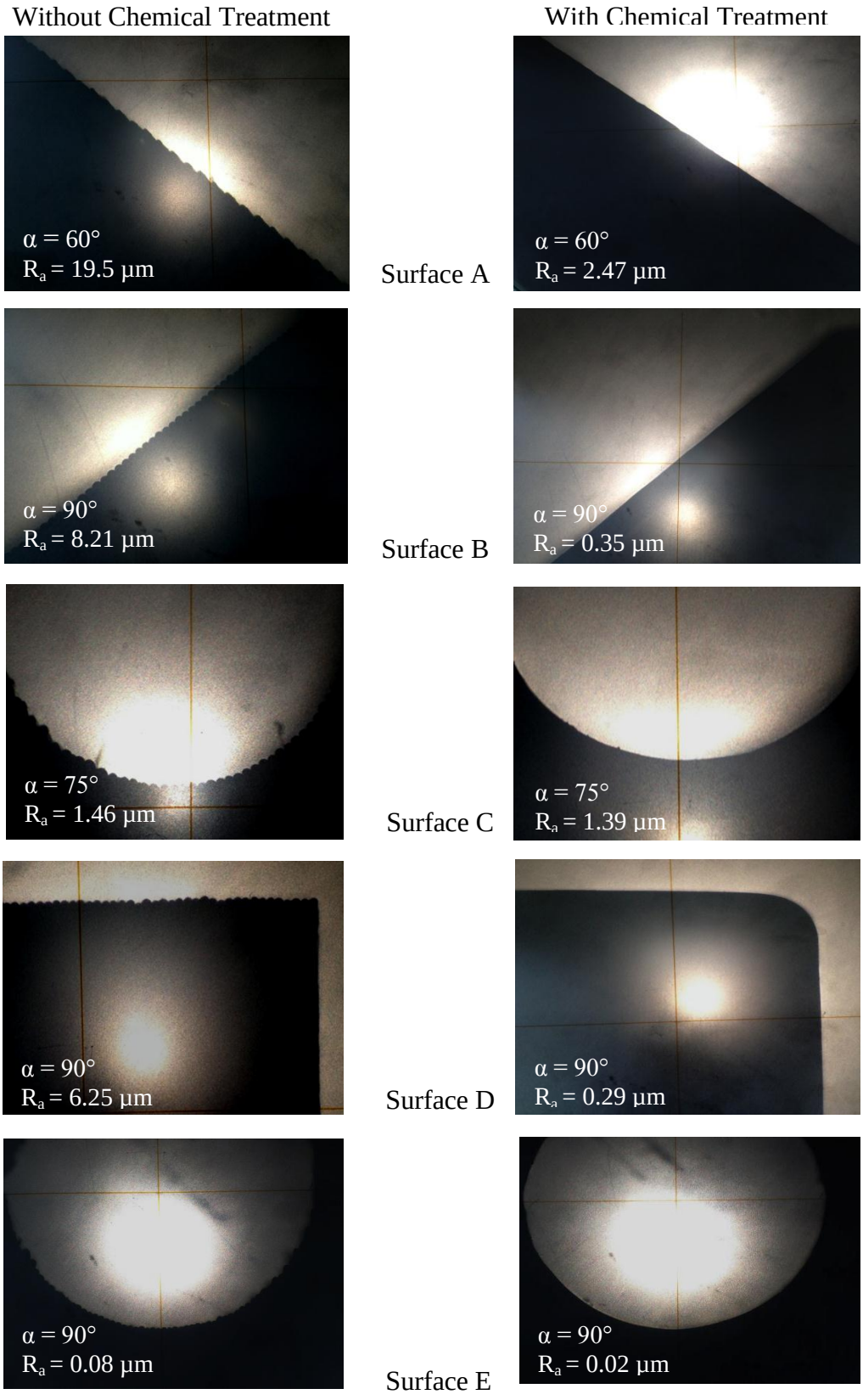

Figure 4.20: Staircase effect at primitive surfaces of specimen built at different part orientations with and without chemical treatment

4.4.3 Roughness of Primitive and Freeform Surfaces

Surface roughness is measured for part with primitive and freeform surfaces and average surface roughness (R_a) value is shown in Table 4.5 and Fig. 4.21 for part built at three different part orientation (along X, Y and Z axis).

Table 4.5: Results of surface roughness for specimen with and without chemical treatment

Surface A (Slope with different angles)		Without chemical treatment			With chemical treatment		
		R_a (micron)			R_a (micron)		
Part orientation	Angle	Trial 1	Trial 2	Average	Trial 1	Trial 2	Average
X	0	0.89	0.96	0.93	0.15	0.11	**0.13**
X	15	0.63	1.16	**0.90**	0.25	0.14	0.20
X	30	0.89	1.21	1.05	0.28	0.2	0.24
X	45	1.13	1.3	1.22	0.17	0.12	0.15
X	60	2.1	1.74	1.92	0.43	0.38	0.41
X	75	1.26	1.56	1.41	0.23	0.2	0.22
X	90	1.78	1.79	1.79	0.2	0.22	0.21
Y	0	4.86	3.68	4.27	0.62	0.29	0.46
Y	15	33.05	38.2	**35.63**	4.22	3.85	**4.04**
Y	30	27.76	25.47	26.62	1.85	1.29	1.57
Y	45	15.87	16.67	16.27	0.68	0.7	0.69
Y	60	14.7	13.2	13.95	1.25	0.39	0.82
Y	75	13.37	12.21	12.79	0.55	0.29	0.42
Y	90	12.82	12.67	12.75	0.37	0.14	0.26
Z	0	12.18	12.89	12.54	0.53	0.31	0.42
Z	15	13.16	11.86	12.51	0.28	0.52	0.40
Z	30	14.88	15.8	15.34	0.53	0.4	0.47
Z	45	18.11	17.78	17.95	0.37	0.4	0.39
Z	60	28.12	28.94	28.53	3.23	1.57	2.40
Z	75	19.65	17.95	18.80	1.9	2.45	2.18
Z	90	12.13	12.65	12.39	0.78	0.79	0.79

For surface A (inclined surface with continuous slope variation in steps) surface roughness is measured along the length and average value is reported as shown in Table 4.5. It can be seen from Table 4.5 that maximum surface roughness for surface A is obtained for part built along Y orientation with slope angle 15° whereas minimum surface roughness is obtained for part built along X orientation with slope angle 15°. However even though the maximum surface roughness is obtained for part built along Y orientation but orientation about Z axis gives relatively higher R_a value for all slope angles as shown in Table 4.5. A possible reason behind this phenomenon is that when part is orientation about Z axis

orientation of layers are in opposite direction to the direction in which surface roughness is measured as result we obtained more surface roughness for each surface with different slope angle. Therefore, for Z orientation part maximum surface roughness 28.92 µm is obtained for surface with 60° slope angle due to inclined surface is more prone to staircase effect whereas minimum surface roughness is 12.39 µm is obtained for surface with 90° slope angle due to no staircase effect. It can also be seen that after the chemical treatment of the parts a massive reduction is R_a value is achieved. The maximum surface roughness of 35.63 µm before treatment is reduced to 4.04 µm for Y orientation with slope angle 15° angle 0.90 µm minimum roughness before treatment is reduced to 0.20 µm for X orientation with slope angle 15°. The minimum surface roughness of 0.13 µm is possible after the chemical treatment for X orientation part with slope angle 0°.

For semi- cylindrical surface (surface B), roughness is measured along the axis of the groove i.e. along Y direction. Variation of surface roughness for surface B is shown in Fig. 4.21 which shows that part built along X orientation gives maximum R_a value whereas Z orientation gives minimum surface roughness. Surface roughness of 14.58 µm before chemical treatment is reduced to 0.58 µm for X orientation and 1.03 µm of roughness before chemical treatment is reduced to 0.29 µm for Z orientation. Surface C, is a curved surface, also exhibits similar trend as surface B as shown in Fig. 4.21(b) because here also surface roughness is measured along the length of groove (Y direction). In case of surface D which forms an inner surface of hollow cylinder surface roughness is measured along the length of groove i.e. X direction exhibits opposite trend as surface roughness measured for surface B and surface C. The maximum surface roughness is obtained for Z orientation whereas X orientation exhibit minimum surface roughness (refer Fig. 4.21(c)). For surface E which is a freeform surface exhibit minimum surface roughness for Y orientation whereas maximum surface roughness is obtained for Z orientation. From Fig. 4.21 it can also be seen that specimen built along Y orientation exhibit optimal part built orientation for almost each primitive surface giving good quality of surface finish. After chemical treatment of the samples, a minimum surface roughness of 0.36 µm is achieved for surface C along X orientation and 0.32 µm for surface D along X orientation.

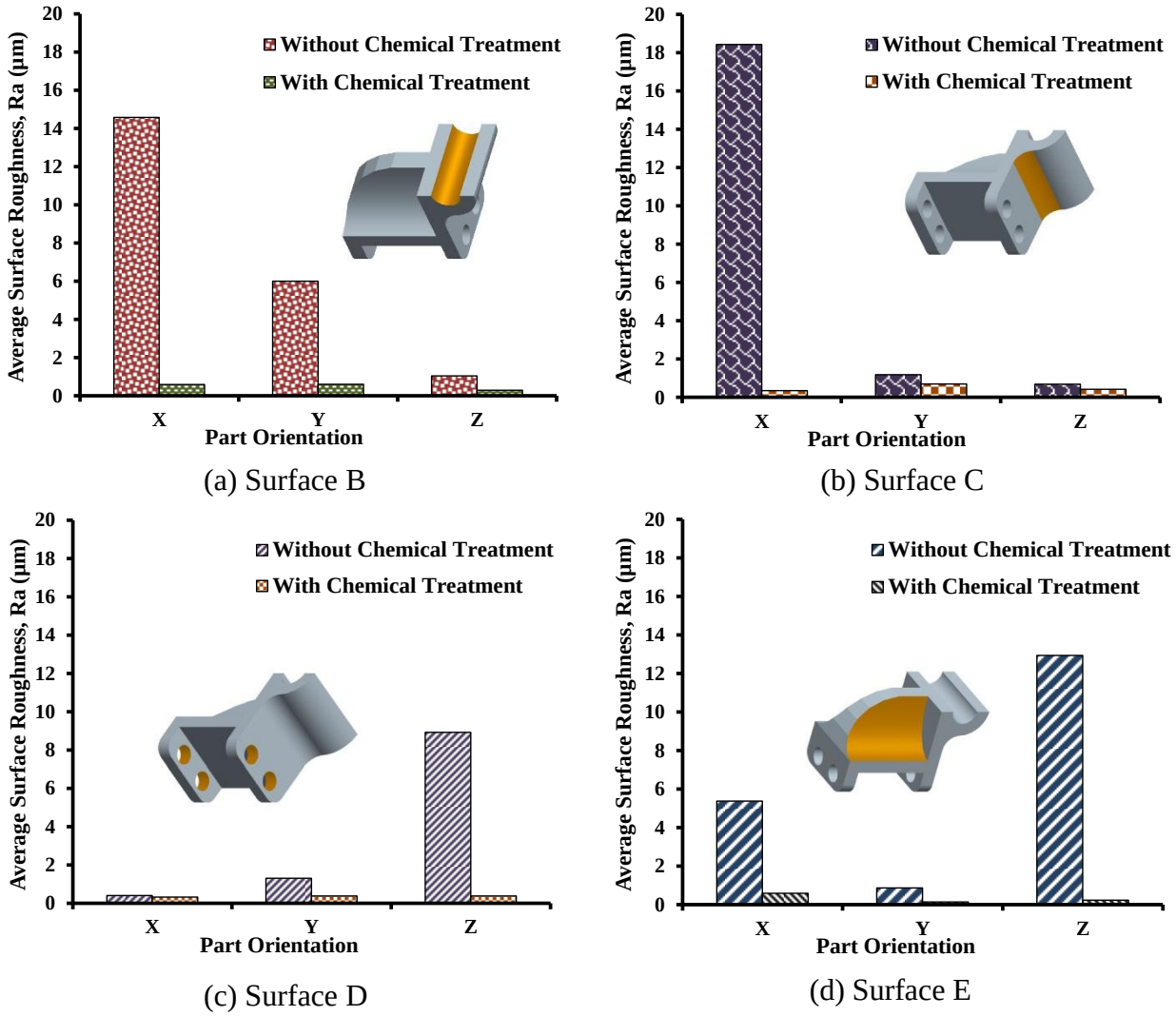

Figure 4.21: Surface roughness at primitive and freeform surfaces of specimens built at different part orientations with and without chemical treatment

Figure 4.21 demonstrates that a significant reduction in surface roughness is possible for all surfaces at different orientations after post-treatment by cold vapor of acetone. All the surfaces (internal or external) of a part are consistently get exposed to the vapors for a sufficient duration and ensures a smooth surface all around the components. The appearances of surfaces before and after the chemical treatment are shown in Fig. 4.22. The treatment of parts helps in reducing the stair case effects of the parts after the treatment and helps in reducing the surface roughness. Stair case effects of the parts before and after the treatment for all samples are shown in Fig. 4.23.

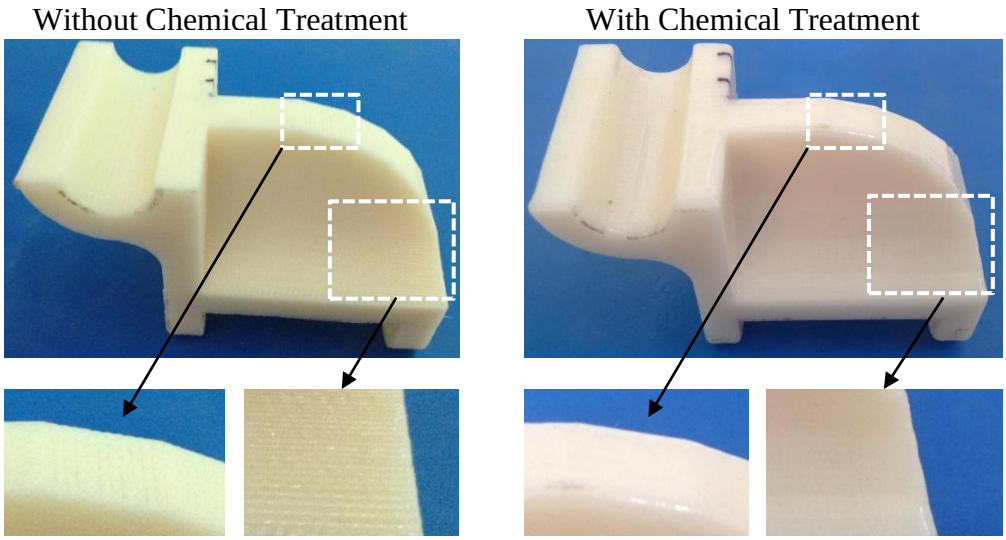

Figure 4.22: Appearance of primitive and freeform surfaces of build specimen with and without chemical treatment

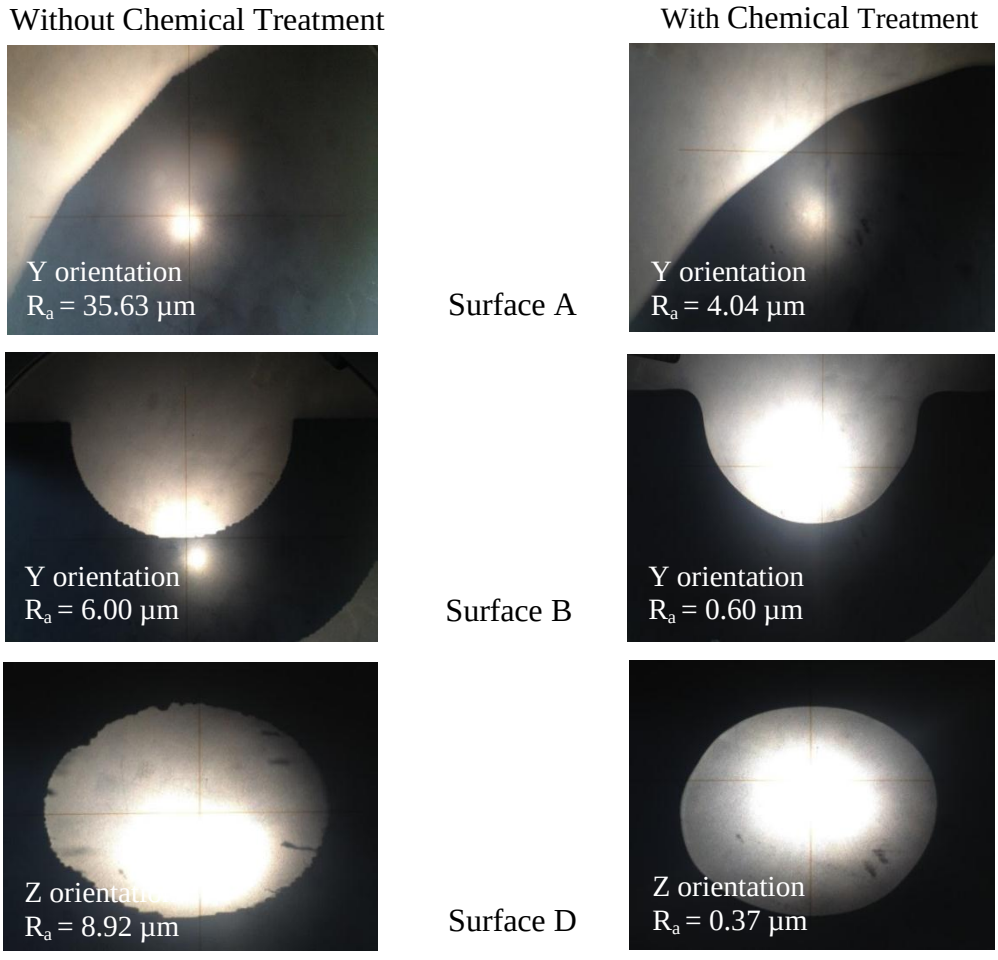

Figure 4.23: Staircase effect at primitive and freeform surfaces of specimens built at different part orientations with and without chemical treatment

4.4.4 Roughness of Doubly Curved Surfaces

Surface roughness is measured for doubly curves surfaces (longitudinal curve A_1-A_2 and transverse cure B_1-B_2) of FDM model and average surface roughness (R_a) values are shown in Fig. 4.24 for parts built at different orientations (along X, Y and Z axis). For longitudinal curve A_1-A_2 it can be seen that for part built along X orientation gives minimum roughness value whereas Z orientation exhibits maximum surface roughness due to increase in staircase effect. On the other hand for transverse curve B_1-B_2 exhibit opposite trend as surface roughness measured for longitudinal curve giving minimum surface roughness for Z orientation whereas X orientation exhibit maximum surface roughness. From Fig. 4.24 it can also be seen that with cold vapor treatment surface roughness reduced significantly. The maximum surface roughness of 12.09 µm before treatment is reduced to 0.48µm for Z orientation along longitudinal path and 1.17 µm minimum roughness is reduced to 0.34 µm for X orientation part. For transverse curve the maximum roughness of 12.40 µm before chemical treatment is reduced to 0.64 µm for X orientation.

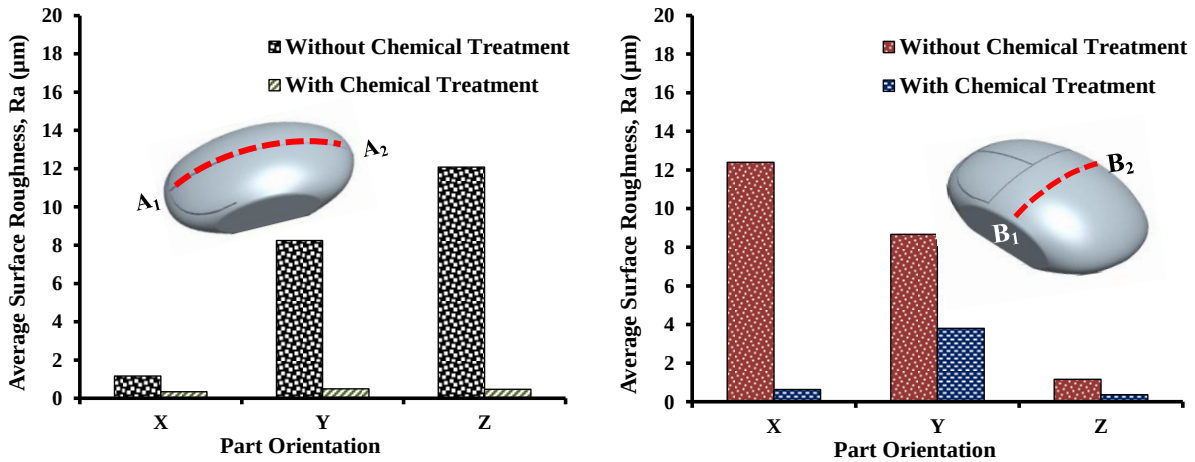

Figure 4.24: Surface roughness measurement for surface A: (a) longitudinal curve A_1-A_2 and (b) transverse curve B_1-B_2

Figure 4.24 demonstrates that a significant reduction in surface roughness is possible to achieve uniformly for all surfaces at different orientations after chemical treatment process. All the surfaces of a part are consistently get exposed to the vapors for a sufficient duration and ensures a smooth surface all around the components. The process achieves a smooth, shiny surface finish due to softening of the outer layers because acetone breaks down the secondary bond between the ABS polymer chains to slide past to each other and reaches to more stable position. The surface tension in liquid like ABS plastic layers polished the surface textured especially the air gaps between successive layers. After the parts are taken

out from the container, the acetone traces from the surface vaporize and the ABS plastic return back to its original hardness with well bonded continuous layers on its outer surface. The appearance of doubly curved surfaces before and after the chemical treatment is shown in Fig. 4.25. The treatment also reduces the staircase effect which helps in reducing the surface roughness. Figure 4.26 shows the staircase effect of the specimens with and without the chemical treatment for doubly curved surfaces.

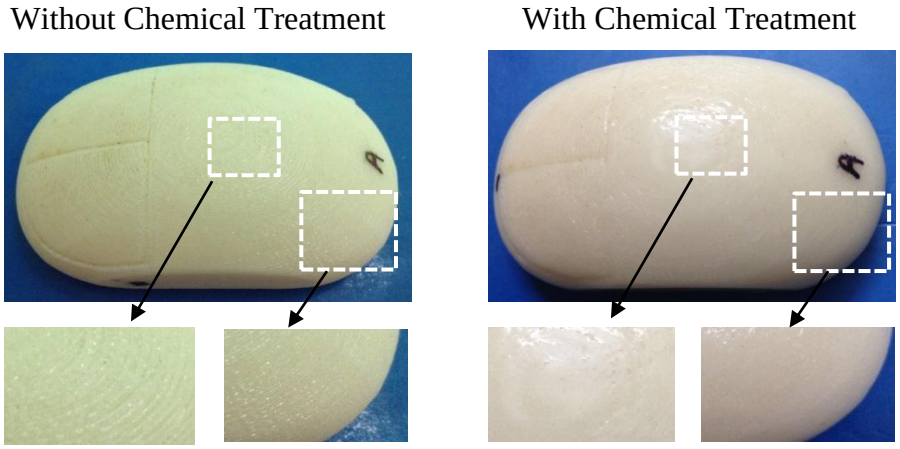

Figure 4.25: Appearance of doubly curved surfaces of build specimen with and without chemical treatment

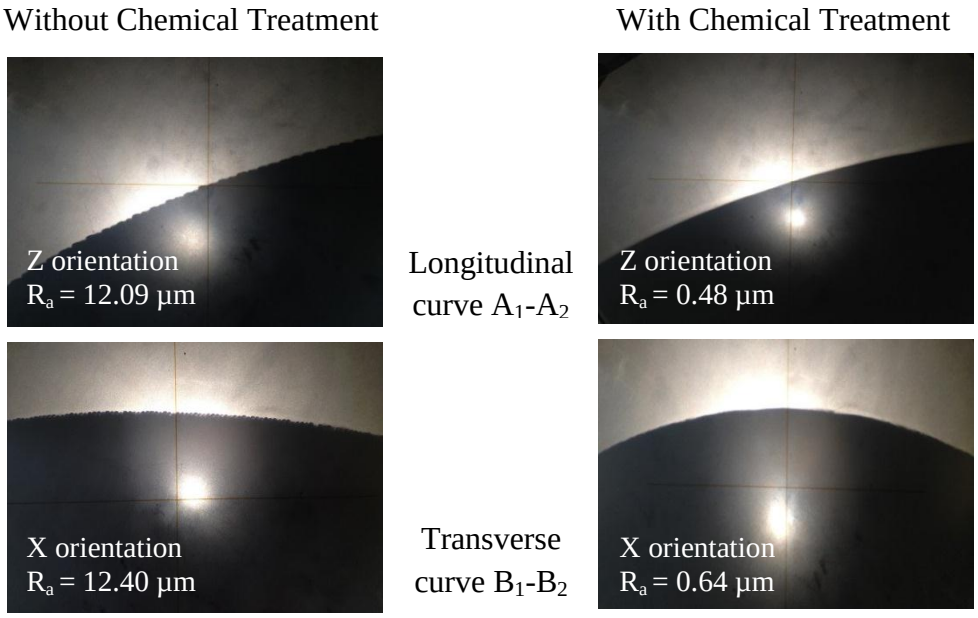

Figure 4.26: Staircase effect at doubly curved surfaces of built specimens built at different part orientations with and without treatment

4.5 Build Cost

For FDM parts, build time, model and support material consumption together represents the build cost. Figure 4.27(a) represents the comparison of build time, model and support material consumption at different part orientations for building tensile specimen whereas for flexural specimen the same is shown in Fig. 4.27(b). From Fig. 4.27, it can be observed that part orientation is more significant that influences build time than the raster angles of the specimen. The building height of the specimen is directly related to the part orientations and thus significantly influences the build time. In addition to the height of the specimen, the build time also depend upon the amount of support material and model material to be deposited in completing the specimen and also ideal time spent in moving the table in Z direction after completion of each layer.

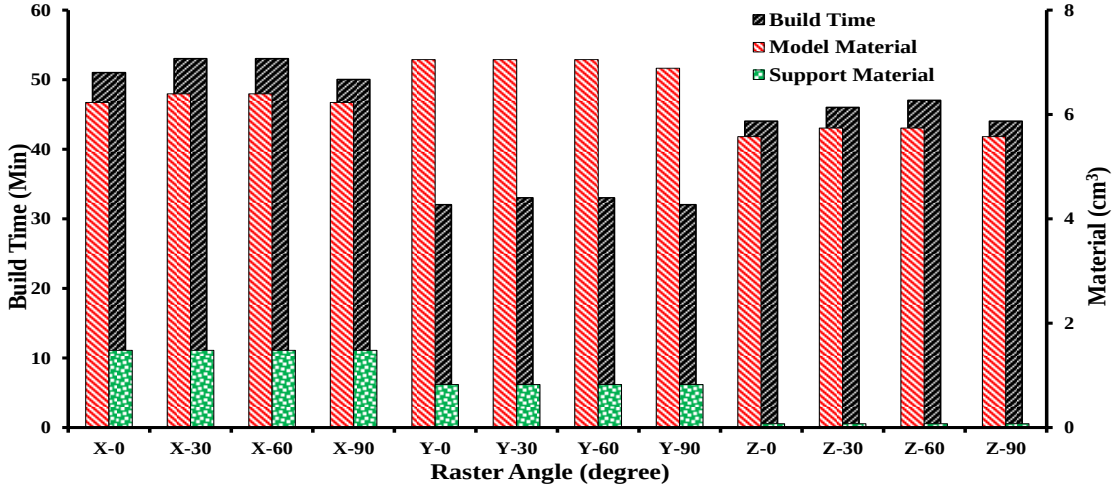

(a)

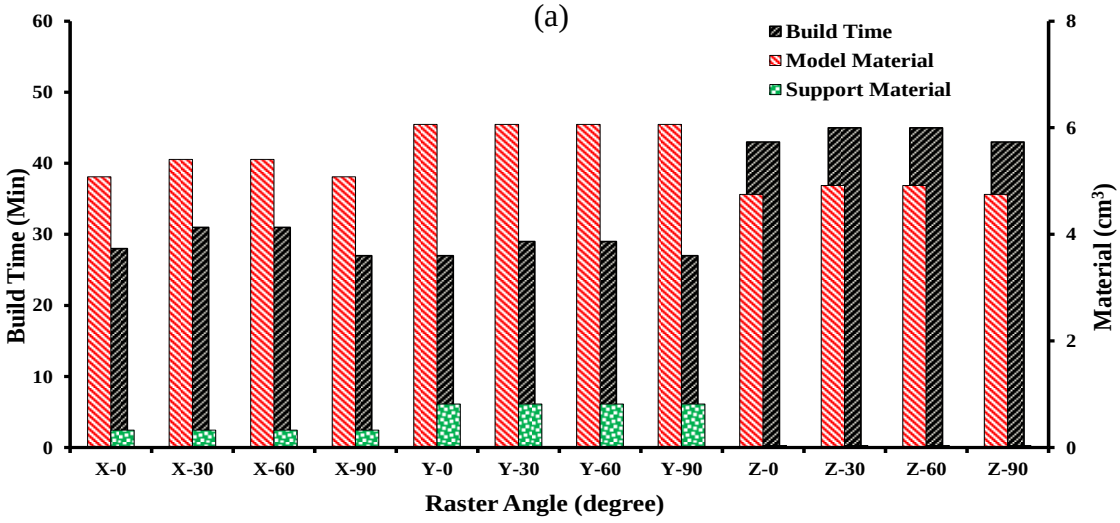

(b)

Figure 4.27: Build cost data for specimen built at different part orientations and raster angles for: (a) tensile specimens and (b) flexural specimens

Most commonly FDM parts are built on specific base plate and first few layers of model material is deposited to strengthen the base of component to be fabricated followed by deposition of support material to facilitate removal of actual component from base plate. Then the actual layers (model material) of the component are deposited for building the component. Thus, amount of support material required depends upon the total area of contact between specimen and base plate, along with overhung portion of component (geometry dependent support needed). Reducing the contact area decreases the amount of support material required which further reduces the amount of build time and cost of removing the support material. Figure 4.27 clearly indicates that minimum support material is consumed for both tensile and flexural specimen for part orientation about Z axis due to minimum contact area between specimen and base plate however, such parts give minimum tensile and flexural strength. Amount of model material required depends on the volume of the specimen and area of contact of the specimen with the base plate as well as raster angle of the specimen. Since volume of the specimen remain constant in both tensile and flexural testing the variation in model material consumption for different part orientations and raster angles depends mainly upon area of contact of the specimen with base plate and raster angles. A little variation in model material consumption for different raster angles (for same part orientation) could be due to the pattern of raster filling and the voids at the corners (Fig. 4.28). The size of these voids and occurrence extensively depends upon the angle between the raster lines and perimeter (raster angle). Figure 4.28 depicts the incomplete filling of layers at locations where raster turns around near the component periphery. Some unfilled sections can also be seen between two successive deposited layers (Fig. 4.28(c), (d)).

From Fig. 4.3 and 4.27(a) the optimal tensile strength-build time-material consumption relation is obtain for part orientation along Y axis among this the specimen with raster angle 0° (Y-0) exhibited optimal tensile strength, minimum build time and acceptable model and support material consumption whereas from Fig. 4.7 and 4.24(b) the optimal flexural strength-build time-material consumption relation is obtain for part orientation along X axis for which the specimen with raster angle 0° (X-0) exhibit optimal flexural strength, minimum build time and acceptable model and support material consumption.

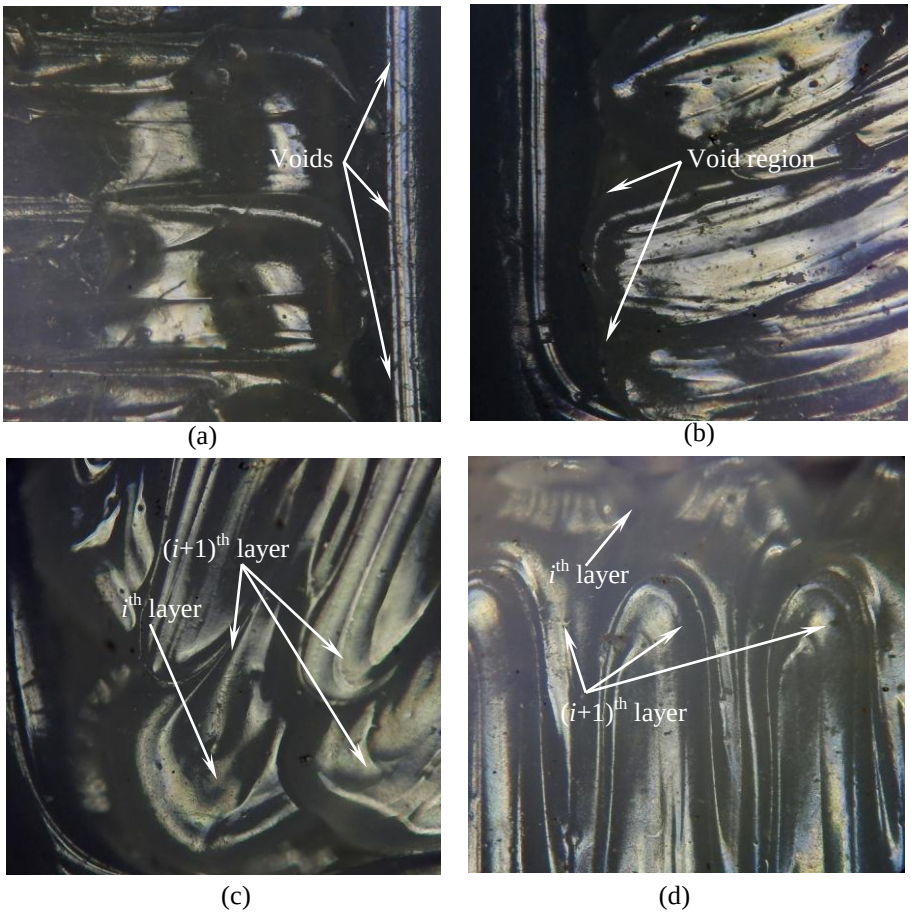

Figure 4.28: Optical microscope image of top surface of FDM specimen with flat surfaces showing perimeter voids for different raster angles: (a) Y-0, (b) Y-30, (c) Y-60 and (d) Y-90

4.5.1 Part with Primitive and Freeform Surfaces

For part with primitive and freeform surfaces the comparison of build time, model and support material consumption at different part orientations is shown in Fig. 4.29. From Fig. 4.29 it can be observed that building height of the specimen is directly related to the part orientations and thus significantly influences the build time. In addition to the height of the specimen, the build time also depend upon the amount of support material and model material to be deposited in completing the specimen and also ideal time spent in moving the table in Z direction after completion of each layer.

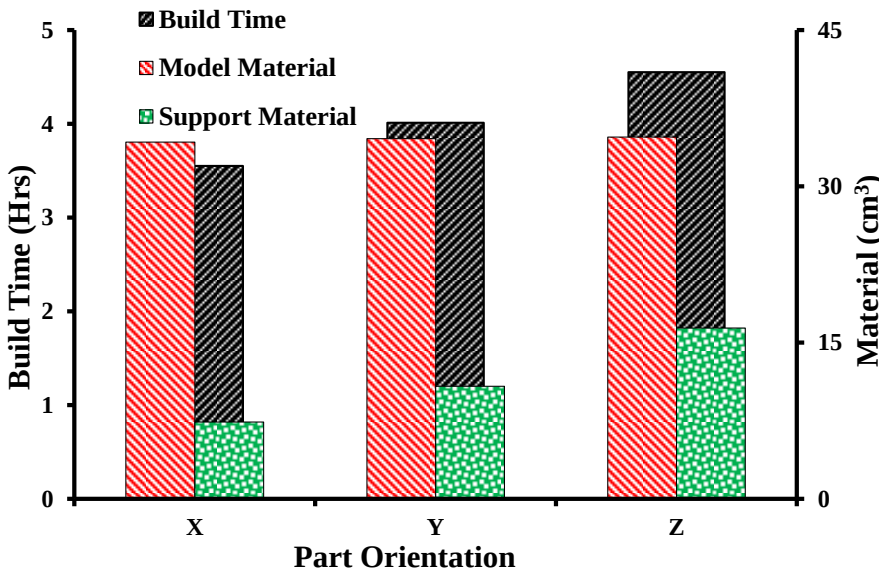

Figure 4.29: Build cost data for part with primitive and freeform surfaces built at different part orientations

Most commonly FDM parts are built on specific base plate and first few layers of model material is deposited to strengthen the base of component to be fabricated followed by deposition of support material to facilitate removal of actual component from base plate. Then the actual layers (model material) of the component are deposited for building the component. Thus, amount of support material required depends upon the total area of contact between specimen and base plate, along with overhung portion of component (geometry dependent support needed) as shown in Fig 4.30.

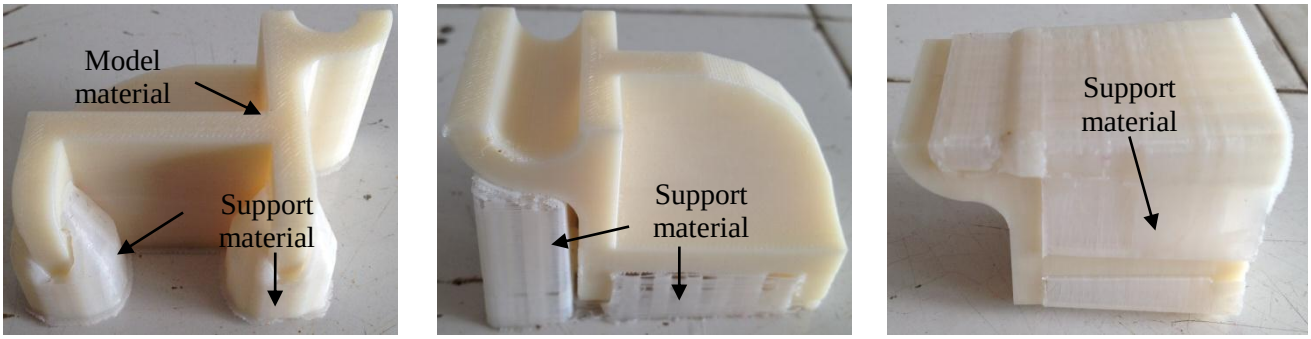

(a) (b) (c)

Figure 4.30: Support structure required for part with primitive and freeform surfaces built at different part orientations (a) X direction, (b) Y direction and (c) Z direction

Reducing the contact area decreases the amount of support material required which further reduces the amount of build time and cost of removing the support material. Figure

4.29 and Fig. 4.30 clearly indicates that minimum support material is consumed for part orientation about X axis due to minimum contact area between specimen and base plate. Amount of model material required depends on the volume of the specimen and area of contact of the specimen with the base plate. Since volume of the specimen remains constant the variation in model material consumption for different part orientations depends mainly upon area of contact of the specimen with base plate. Figure 4.29 and Fig. 4.30 clearly indicates that maximum model material is consumed for part orientation about *Z* axis due to maximum contact area between specimen and base plate.

4.5.2 Part with Doubly Curved Surfaces

For part with doubly curved surfaces the comparison of build time, model and support material consumption at different part orientations is shown in Fig. 4.31. From Fig. 4.31 it can be observed that building height of the specimen is directly related to the part orientations and thus significantly influences the build time. In addition to the height of the specimen, the build time also depend upon the amount of support material and model material to be deposited in completing the specimen and also ideal time spent in moving the table in Z direction after completion of each layer.

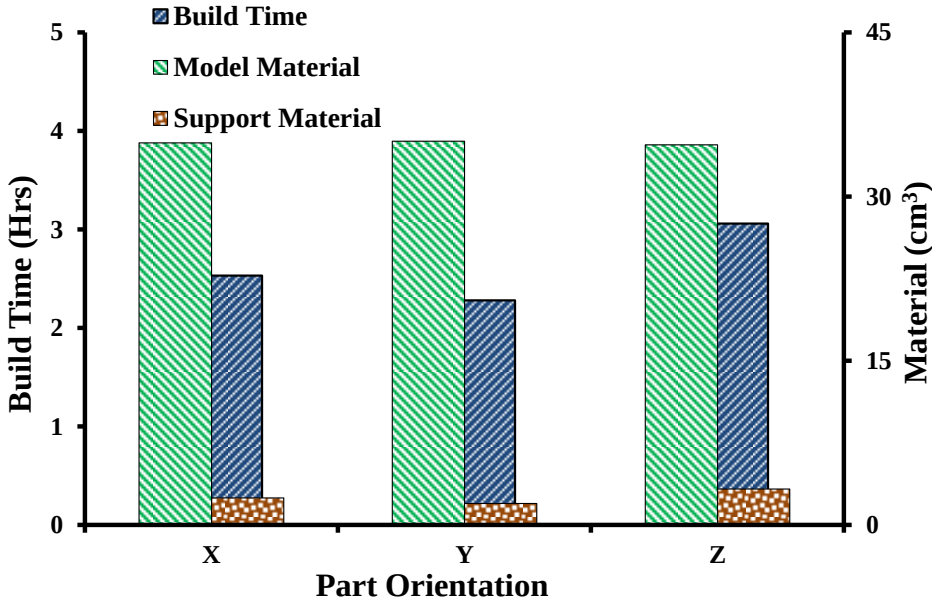

Figure 4.31: Build cost data for part with doubly curved surfaces built at different part orientations

Most commonly FDM parts are built on specific base plate and first few layers of model material is deposited to strengthen the base of component to be fabricated followed by deposition of support material to facilitate removal of actual component from base plate. Then the actual layers (model material) of the component are deposited for building the component. Thus, amount of support material required depends upon the total area of contact between specimen and base plate, along with overhung portion of component (geometry dependent support needed) as shown in Fig. 4.32.

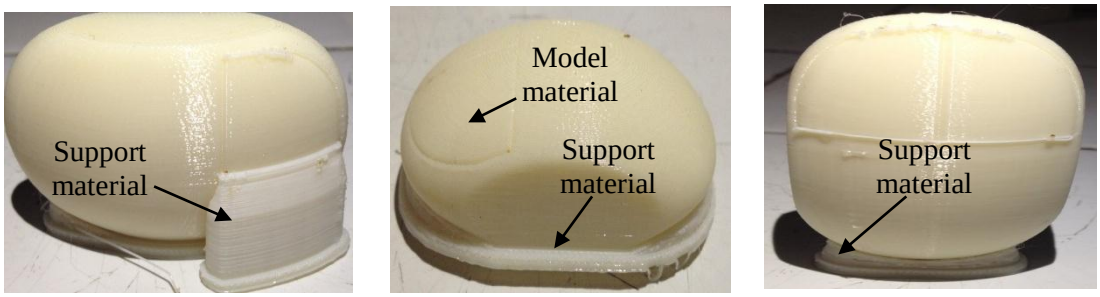

(a) (b) (c)

Figure 4.32: Support structure required for part with doubly curved surfaces built at different part orientations (a) X direction, (b) Y direction and (c) Z direction

Reducing the contact area decreases the amount of support material required which further reduces the amount of build time and cost of removing the support material. Figure 4.31 and Fig. 4.32 clearly indicates that minimum support material is consumed for part orientation about X axis due to minimum contact area between specimen and base plate. Amount of model material required depends on the volume of the specimen and area of contact of the specimen with the base plate. Since volume of the specimen remains constant the variation in model material consumption for different part orientations depends mainly upon area of contact of the specimen with base plate. Figure 4.31 and Fig. 4.32 clearly indicates that minimum model material is consumed for part orientation about Z axis due to minimum contact area between specimen and base plate.

4.6 Multi-response Optimization

In this experimental analysis, the effect of process parameters settings in FDM process studied. Experiments have been conducted considering part orientation and raster angle as process parameters for obtaining the responses like tensile strength, flexural strength, geometric accuracy, surface roughness and build time. In FDM process it is desired that fabricate part should have higher mechanical properties (tensile and flexural strength), improved geometrical and dimensional accuracy, surface finish and lower the build time. In order to optimize the FDM process parameters for the current experimental set, the multi response optimization using analytic hierarchy process commonly known as AHP has been considered.

4.6.1 Analytic Hierarchy Process

Analytic hierarchy process (AHP), is one of the powerful decision making methods used for solving several optimization problem related to several manufacturing processes because of its special advantages to handle both qualitative and quantitative attributes. This technique also helps in formulation of a complicated problem in a hierarchical structure having main target, criteria, sub-criteria and alternatives and the relation among these to favor insights into the decision-making process. The most important characteristics of AHP are combining the knowledge, experience foresights and individual opinions in a logical way. The AHP breaks down a decision making problems into several levels in such a way that they from a hierarchy with unidirectional hierarchical relationship between levels. The top level of the hierarchy is the main goal of the decision problem. The lower levels are the tangible and intangible criteria or subcriteria that contribute to the goal. The bottom level of the hierarchical structure is formed by alternatives to evaluate in terms of the criteria. AHP uses pairwise comparison to allocate weights to the elements of each level, measuring their relative importance with pairwise comparison table and finally global weights are calculated for assessment at the bottom level.

4.6.2 Steps involved in AHP

Basic steps that are generally involved in a standard AHP are:

- First of all decide the objective or goal of the problem.
- Identify the responses or criteria that will have direct or indirect impact on the process of decision making.

- The hierarchical structure is then constructed with the top level as the goal or the objective of the decision. The criteria and subcriteria are placed in the subsequent descending levels with the lowest level in the hierarchy is formed by alternatives as shown in Fig. 4.33.

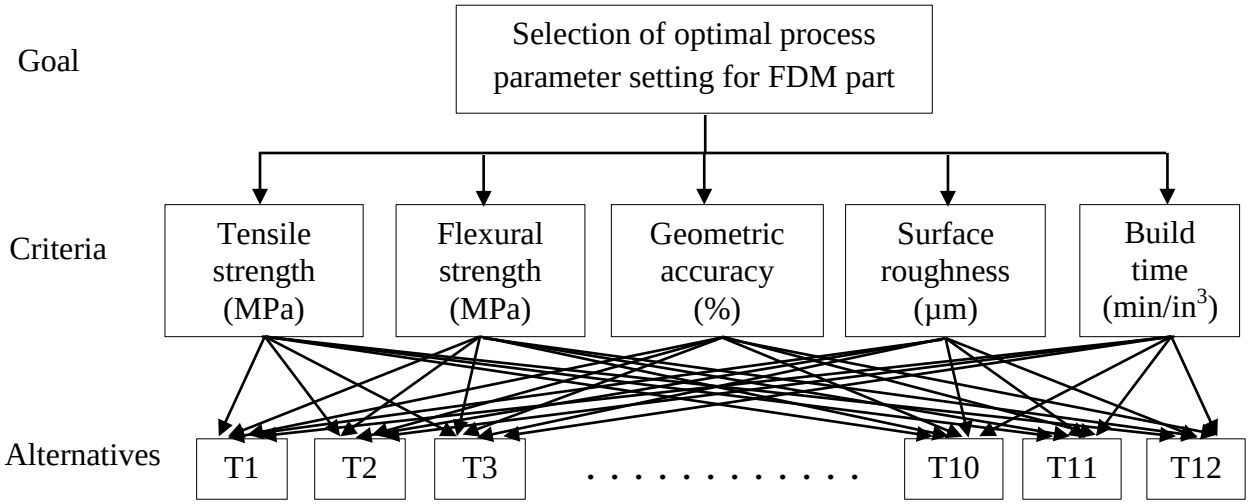

Figure 4.33: Hierarchy structure of the present analysis procedure

- After deciding the goal, criteria/ subcriteria and constructing the hierarchy structure, a pairwise comparison matrix is formed by comparing an element with other element of next higher level in order to find out the priority weight. For assigning rating for comparing one element with another, a scale for pairwise comparison is used as shown in Table 4.6. A typical pairwise comparison matrix [B] can be expressed as:

$$[B] = \begin{bmatrix} b_{11} & b_{12} & \dots\dots\dots & b_{1n} \\ b_{21} & b_{22} & \dots\dots\dots & b_{2n} \\ . & . & \dots\dots\dots & . \\ . & . & \dots\dots\dots & . \\ . & . & \dots\dots\dots & . \\ b_{n1} & b_{n2} & \dots\dots\dots & b_{nn} \end{bmatrix}$$

where, b_{kl} (for k, l =1, 2, 3,…, n) is the strength of preferences of the b_k over b_l corresponding to the criterion ($b_{kl} = b_k / b_l$), also $b_{lk} = 1/ b_{kl}$ and b_{kk} =1 for all values of k and l. Values of b_k and b_l were taken from the ratio scale for formation of pairwise comparison matrix. After all elements of the matrix were decided and calculated, consistency of the entries of the matrix was checked. B comparison matrix is said to be consistent if $b_{kl} \times b_{lm} = b_{km}$, for all values of k, l and m. For all consistent matrices $b_{kl} = b_k / b_l$, for all values of k and l.

Table 4.6: Scale for pairwise comparison [Bhattacharya *et al.*, 2011]

Rating	Preferential judgment
9	Extremely preferred
8	Between 7 and 9
7	Very strongly preferred
6	Between 5 and 7
5	Strongly preferred
4	Between 3 and 5
3	Moderately preferred
2	Between 1 and 3
1	Equally preferred

- To determine whether responses are consistent or not, we need to find out consistency ratio (CR) is found out which measures the degree of inconsistency in responses. The CR is defined by Eqn. 4.1 and must be 10 % or less (CR ≤ 0.1) for it to be acceptable [Chakraborty and Dey, 2006; Saaty, 1994]

$$CR = \frac{CI}{RI} \tag{4.1}$$

where, RI is random index which is generated by picking the values for order of matrix (*n*) as shown in Table 4.7.

Table 4.7: Random index (*RI*) for different matrix order (*n*) [Zeshui, 2004]

n	2	3	4	5	6	7	8	9	10	11	12
RI	0	0.52	0.89	1.12	1.26	1.36	1.41	1.46	1.49	1.52	1.54

CI is consistency index for a pairwise matrix and can be calculated by using Eqn. 4.2

$$CI = \frac{\lambda_m - n}{n - 1} \tag{4.2}$$

Where, λ_m is maximum eigen value and must be $\lambda_m \geq n$ where *n* being order of matrix.

- After the λ_m, CI and CR are satisfied than decision is taken based on normalized value, else the procedure is repeated till the value lie in desired range.
- Finally, the global weight is calculated by multiplying the priority weights of each alternative for different criteria with the criteria weight of pairwise comparison matrix. The maximum value of the global weight is generally considered the optimum

value and the corresponding alternative is selected for the optimal process parameter settings [Triantaphyllou and Mann, 1995].

4.6.3 Implementation of AHP

In the present work, FDM process parameters (part orientation and raster angle) are being optimized by using AHP method that will give maximum tensile and flexural strength, improved the geometric accuracy, surface quality and lower the build time. The experimental design layout is shown in Table 4.8, with trials T1 to T12 which are performed to predict the optimal process parameter settings. The trials T1 to T12 are performed at three different part orientations (along X, Y and Z axis) and at four different raster angles (0°, 30°, 60°, 90°) whereas the layer thickness (0.178 mm) and air gap is kept constant to measure the tensile strength, flexural strength, geometric accuracy, surface roughness and build time. Experimental results obtained after performing the trial T1 to T12 are given in Table 4.9 which shows that all the five responses varies significantly for each sample built at different part orientations and raster angles.

Table 4.8: Experimental design layout to predict optimum process parameter settings

Trial No.	Part Orientation	Raster Angle (Degree)	Layer Thickness (mm)	Air Gap (mm)
T1	X	0	0.178	0
T2	X	30	0.178	0
T3	X	60	0.178	0
T4	X	90	0.178	0
T5	Y	0	0.178	0
T6	Y	30	0.178	0
T7	Y	60	0.178	0
T8	Y	90	0.178	0
T9	Z	0	0.178	0
T10	Z	30	0.178	0
T11	Z	60	0.178	0
T12	Z	90	0.178	0

It can be noted from Table 4.9 that maximum tensile strength of 34.50 MPa is obtained with trial T3 whereas trial T2 gives maximum flexural strength of 58.5 MPa. Maximum geometric accuracy/ closeness are achieved with trial T4 and minimum surface roughness is achieved

for sample prepared with trial condition of T7. This clearly indicates that there is a need for optimization to select the best alternative for a desired goal.

Table 4.9: Results of tensile strength, flexural strength, geometric accuracy, surface roughness and average build time of FDM samples

Trial No.	Tensile strength (MPa)	Flexural strength (MPa)	Geometric accuracy (%)	Surface roughness (μm)	Average build time (min/cm3)
T1	32.60	55.20	99.47	6.35	6.99
T2	33.50	58.50	98.76	7.72	7.12
T3	34.50	56.10	98.74	6.34	7.12
T4	30.50	49.68	99.72	6.36	6.81
T5	35	51.96	99.30	5.74	4.50
T6	35.9	50.72	99.69	5.73	4.73
T7	35	50.48	99.08	4.82	4.73
T8	34.4	47.12	98.91	5.04	4.56
T9	18.50	23.40	98.86	6.16	8.43
T10	28.70	37.38	99.07	8.18	8.54
T11	27.60	39.24	99.10	6.74	8.64
T12	14.80	26.16	98.37	6.97	8.43

Choosing and comparing the two alternatives from experimental results rather than using subjective criteria as given in Table 4.6, eliminates the subjectivity and provide an objective evaluation. In order to use the experimental results for assigning the rating of one alternative to another for the pairwise comparison matrix, an approach as described by Bhattacharya *et al.* [2011] is implemented here in this work. The complete algorithm is implemented by using MATLAB software which is explained as step by step procedure as shown in Fig 4.34. A pairwise comparison matrix for criteria tensile strength, flexural strength, geometric accuracy, surface roughness and build time (5×5 matrix), is shown in Table 4.10. The tensile and flexural strength of the samples have been already provided in Section 4.2. Geometric accuracy of the samples is calculated by measuring five basic linear dimensions of the specimens. The error in dimensions is calculated by measuring the difference from the CAD dimensions of the geometry. From these deviations, the average errors in dimensions of build specimen are calculated and finally geometrical accuracy is calculated as (100-error) %. The criteria weight (relative importance of each criteria) is shown in the last column of Table 4.10 which is obtained after normalizing the eigen vectors corresponding to maximum eigen value (λ_m= 5.00). The pairwise comparison matrices of 12

alternatives (T1 to T12) are developed for tensile strength, flexural strength, geometric accuracy, surface roughness and build time using the experimental results (refer Table 4.9) to find out the optimum process parameters settings.

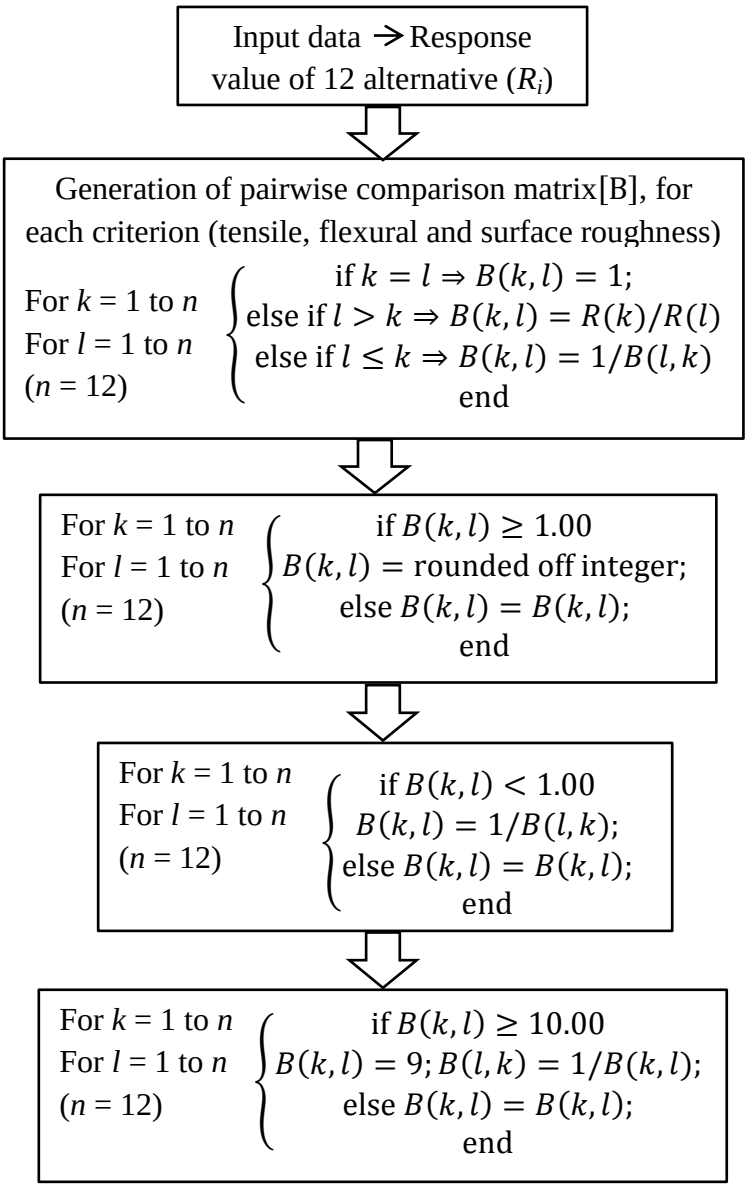

Figure 4.34: Step by step procedure used to convert the experimental results into pairwise comparison matrix [Bhattacharya *et al.*, 2011]

Table 4.10: Pairwise comparison matrix for different criteria

	Tensile strength	Flexural strength	Geometric accuracy	Surface roughness	Build time	Criteria weight
Tensile strength	1	8/9	8/5	8/6	8/3	0.26
Flexural strength	9/8	1	9/5	9/6	9/3	0.29
Geometric accuracy	5/8	5/9	1	5/6	5/3	0.16
Surface roughness	6/8	6/9	6/5	1	6/3	0.19
Build time	3/8	3/9	3/5	3/6	1	0.10
λ_m = 5.00				CR = 0		

Table 4.11: Pairwise comparison matrix between alternatives for tensile strength

	T1	T2	T3	T4	T5	T6	T7	T8	T9	T10	T11	T12	Priority weight
T1	1	1	1	1	1	1	1	1	2	1	1	2	0.0910
T2	1	1	1	1	1	1	1	1	2	1	1	2	0.0910
T3	1	1	1	1	1	1	1	1	2	1	1	2	0.0910
T4	1	1	1	1	1	1	1	1	2	1	1	2	0.0910
T5	1	1	1	1	1	1	1	1	2	1	1	2	0.0910
T6	1	1	1	1	1	1	1	1	2	1	1	2	0.0910
T7	1	1	1	1	1	1	1	1	2	1	1	2	0.0910
T8	1	1	1	1	1	1	1	1	2	1	1	2	0.0910
T9	1/2	1/2	1/2	1/2	1/2	1/2	1/2	1/2	1	1/2	1	1	0.0491
T10	1	1	1	1	1	1	1	1	2	1	1	2	0.0910
T11	1	1	1	1	1	1	1	1	1	1	1	2	0.0869
T12	1/2	1/2	1/2	1/2	1/2	1/2	1/2	1/2	1	1/2	1/2	1	0.0455
λ_m = 12.0345						CR = 0.0020 < 0.1							

Table 4.12: Pairwise comparison matrix between alternatives for flexural strength

	T1	T2	T3	T4	T5	T6	T7	T8	T9	T10	T11	T12	Priority weight
T1	1	1	1	1	1	1	1	1	2	1	1	2	0.0903
T2	1	1	1	1	1	1	1	1	3	2	1	2	0.1004
T3	1	1	1	1	1	1	1	1	2	2	1	2	0.0968
T4	1	1	1	1	1	1	1	1	2	1	1	2	0.0903
T5	1	1	1	1	1	1	1	1	2	1	1	2	0.0903
T6	1	1	1	1	1	1	1	1	2	1	1	2	0.0903
T7	1	1	1	1	1	1	1	1	2	1	1	2	0.0903
T8	1	1	1	1	1	1	1	1	2	1	1	2	0.0903
T9	1/2	1/3	1/2	1/2	1/2	1/2	1/2	1/2	1	1/2	1/2	1	0.0438
T10	1	1/2	1/2	1	1	1	1	1	2	1	1	1	0.0782
T11	1	1	1	1	1	1	1	1	2	1	1	2	0.0903
T12	1/2	1/2	1/2	1/2	1/2	1/2	1/2	1/2	1	1	1/2	1	0.0484
λ_m = 12.0896						CR = 0.0052 < 0.1							

Table 4.13: Pairwise comparison matrix between alternatives for geometric accuracy

	T1	T2	T3	T4	T5	T6	T7	T8	T9	T10	T11	T12	Priority weight
T1	1	1/2	1/2	2	1	2	1/2	1/2	1/2	1/2	1/2	1/3	0.0508
T2	2	1	1	4	2	4	1	1	1	1	1	1	0.1055
T3	2	1	1	4	2	4	1	1	1	1	1	1	0.1055
T4	1/2	1/4	1/4	1	1/2	1	1/3	1/4	1/4	1/3	1/3	1/6	0.0273
T5	1	1/2	1/2	2	1	2	1	1/2	1/2	1	1	1/2	0.0639
T6	1/2	1/4	1/4	1	1/2	1	1/3	1/4	1/4	1/3	1/3	1/5	0.0276
T7	2	1	1	3	1	3	1	1	1	1	1	1/2	0.0900
T8	2	1	1	4	2	4	1	1	1	1	1	1	0.1055
T9	2	1	1	4	2	4	1	1	1	1	1	1	0.1055
T10	2	1	1	3	1	3	1	1	1	1	1	1/2	0.0900
T11	2	1	1	3	1	3	1	1	1	1	1	1/2	0.0900
T12	3	1	1	6	2	5	2	1	1	2	2	1	0.1387
λ_m= 12.1314							CR = 0.0077 < 0.1						

Table 4.14: Pairwise comparison matrix between alternatives for surface roughness

	T1	T2	T3	T4	T5	T6	T7	T8	T9	T10	T11	T12	Priority weight
T1	1	1	1	1	1	1	1	1	1	1	1	1	0.0826
T2	1	1	1	1	1	1	2	2	1	1	1	1	0.0949
T3	1	1	1	1	1	1	1	1	1	1	1	1	0.0826
T4	1	1	1	1	1	1	1	1	1	1	1	1	0.0826
T5	1	1	1	1	1	1	1	1	1	1	1	1	0.0826
T6	1	1	1	1	1	1	1	1	1	1	1	1	0.0826
T7	1	1/2	1	1	1	1	1	1	1	1/2	1	1	0.0747
T8	1	1/2	1	1	1	1	1	1	1	1/2	1	1	0.0747
T9	1	1	1	1	1	1	1	1	1	1	1	1	0.0826
T10	1	1	1	1	1	1	2	2	1	1	1	1	0.0949
T11	1	1	1	1	1	1	1	1	1	1	1	1	0.0826
T12	1	1	1	1	1	1	1	1	1	1	1	1	0.0826
λ_m= 12.1091							CR = 0.0064 < 0.1						

Table 4.15: Pairwise comparison matrix between alternatives for build time

	T1	T2	T3	T4	T5	T6	T7	T8	T9	T10	T11	T12	Priority weight
T1	1	1	1	1	2	1	1	2	1	1	1	1	0.0910
T2	1	1	1	1	2	2	2	2	1	1	1	1	0.1005
T3	1	1	1	1	2	2	2	2	1	1	1	1	0.1005
T4	1	1	1	1	2	1	1	1	1	1	1	1	0.0866
T5	1/2	1/2	1/2	1/2	1	1	1	1	1/2	1/2	1/2	1/2	0.0503
T6	1	1/2	1/2	1	1	1	1	1	1/2	1/2	1/2	1/2	0.0576
T7	1	1/2	1/2	1	1	1	1	1	1/2	1/2	1/2	1/2	0.0576
T8	1/2	1/2	1/2	1	1	1	1	1	1/2	1/2	1/2	1/2	0.0538
T9	1	1	1	1	2	2	2	2	1	1	1	1	0.1005
T10	1	1	1	1	2	2	2	2	1	1	1	1	0.1005
T11	1	1	1	1	2	2	2	2	1	1	1	1	0.1005
T12	1	1	1	1	2	2	2	2	1	1	1	1	0.1005
λ_m= 12.1293							CR = 0.0076 < 0.1						

The pairwise comparison matrix for each alternative (tensile, flexural, geometric accuracy, surface roughness and build time) is given in Table 4.11 to 4.15. The last column of these tables shows the priority weight of the alternative calculated for maximum eigen value (λ_m). The CR values are also calculated and are observed to be less than 0.1 thus depicting the consistency in the results. The priority weight for all the alternatives for each of the five criteria is assigned to five columns of a priority matrix [P] (a 12 × 5 matrix). A column matrix [C] which was named as criteria matrix (a 5 × 1 matrix) contained criteria weight of (tensile, flexural, geometric accuracy, surface roughness and build time) as obtained from Table 4.10. The global weight matrix [G], (a 12 × 1 matrix) is obtained by multiplying the priority matrix and criteria matrix and is given by

$$[P_{12\times5}] \times [C_{5\times1}] = [G_{12\times1}].$$

$$\begin{bmatrix} 0.0910 & 0.0903 & 0.0508 & 0.0826 & 0.0910 \\ 0.0910 & 0.1004 & 0.1055 & 0.0949 & 0.1005 \\ 0.0910 & 0.0968 & 0.1055 & 0.0826 & 0.1005 \\ 0.0910 & 0.0903 & 0.0273 & 0.0826 & 0.0866 \\ 0.0910 & 0.0903 & 0.0639 & 0.0826 & 0.0503 \\ 0.0910 & 0.0903 & 0.0276 & 0.0826 & 0.0576 \\ 0.0910 & 0.0903 & 0.0900 & 0.0747 & 0.0576 \\ 0.0910 & 0.0903 & 0.1055 & 0.0747 & 0.0538 \\ 0.0491 & 0.0438 & 0.1055 & 0.0826 & 0.1005 \\ 0.0910 & 0.0782 & 0.0900 & 0.0949 & 0.1005 \\ 0.0869 & 0.0903 & 0.0900 & 0.0826 & 0.1005 \\ 0.0455 & 0.0484 & 0.1387 & 0.0826 & 0.1005 \end{bmatrix} \times \begin{bmatrix} 0.26 \\ 0.29 \\ 0.16 \\ 0.19 \\ 0.10 \end{bmatrix} = \begin{bmatrix} 0.0827 \\ 0.0977 \\ 0.0943 \\ 0.0785 \\ 0.0809 \\ 0.0757 \\ 0.0842 \\ 0.0864 \\ 0.0681 \\ 0.0888 \\ 0.0889 \\ 0.0739 \end{bmatrix}$$

The maximum global weight obtained from matrix [G] was calculated to be 0.0977 (refer Table 4.16) which corresponds to T2 alternative i.e. when part is fabricated in X orientation with raster angle 30° (X-30). The second highest global weight which is 0.0943 corresponds to T3 alternative i.e. when part is fabricated in X orientation with 60° raster angle (X-60). From alternative T2 and T3 it can be seen that for T2 alternative the higher mechanical strength is obtained as compared to T3 alternative (1.6 % higher mechanical strength) but T3 alternative gives good surface quality as compared to T2 alternative. Surface finish in T3 alternative is improved by 18 % as compared to T2 alternative whereas the geometric accuracy and average build time for both the cases are almost same. Therefore, if the requirement is the mechanical strength and surface roughness has relatively low importance (in case of functional parts) than the T2 alternative as optimal process parameters settings for fabrications of FDM parts. However, if a little preference is given to surface quality (in case of aesthetic parts) and mechanical properties are not much important than we can consider T2 alternative as optimal process parameters settings for fabrication of parts. Thus trial T2 or T3 can be selected as the optimal solution that will globally optimize all the four responses for fabrication a functional part.

Table 4.16: Global weight calculation between alternatives of FDM specimen

Trial No.	Tensile strength priority weight	Flexural strength priority weight	Geometric accuracy priority weight	Surface roughness priority weight	Build time priority weight	Global weight
T1	0.0910	0.0903	0.0508	0.0826	0.0910	0.0827
T2	0.0910	0.1004	0.1055	0.0949	0.1005	0.0977
T3	0.0910	0.0968	0.1055	0.0826	0.1005	0.0943
T4	0.0910	0.0903	0.0273	0.0826	0.0866	0.0785
T5	0.0910	0.0903	0.0639	0.0826	0.0503	0.0809
T6	0.0910	0.0903	0.0276	0.0826	0.0576	0.0757
T7	0.0910	0.0903	0.0900	0.0747	0.0576	0.0842
T8	0.0910	0.0903	0.1005	0.0747	0.0538	0.0864
T9	0.0491	0.0438	0.1005	0.0826	0.1005	0.0681
T10	0.0910	0.0782	0.0900	0.0949	0.1005	0.0888
T11	0.0869	0.0903	0.0900	0.0826	0.1005	0.0889
T12	0.0455	0.0484	0.1387	0.0826	0.1005	0.0739

Chapter 5

Conclusions and Scope for Future Work

5.1 Conclusions

In the present work, the effect of part orientation and raster angles on tensile strength, flexural strength, geometric accuracy, surface roughness and build cost of FDM specimens are investigated experimentally. Also, parts are chemically treated with cold vapors of dimethylketone and response variables are measured after the treatment to compare with those obtained for the parts without chemical treatment. An optimal set of process variables which gives optimum performance is identified using a modified approach of AHP process. The important conclusions drawn from the present study are summarized below.

- Mechanical properties results indicate that part orientation is more significant factor than raster angle that influences the tensile and flexural strength of the FDM specimens.
- Higher mechanical strengths are obtained when parts are built with part orientation along X axis and a similar range of strength is also obtained with Y orientation. However, inferior strength for part orientation along Z axis due to very weak bonding between the rasters. Similar trend in mechanical strength is also observed after the chemical treatment but tensile and flexural strengths are decreased by 37 % and 23 % (maximum) after chemical treatment.
- Surface roughness results for flat surfaces indicate that smoothest surface is obtained for specimen built with orientation along Z axis when roughness is measured across the length. Fabricated parts with orientation along X axis gives better finish along the length of the specimen. There is not much difference between surface roughness when measured in either direction for specimen built with orientation along Y axis.
- Surface roughness results for part with primitive surfaces indicate that a reasonable low surface finish is obtained for part built at 90° part orientation for each primitive surface of FDM model. For parts with doubly curve/ freeform surfaces the reasonably good surface finish is obtained when specimen is built along Y orientation as compared to other orientations.

- Post-build treatment with cold vapors of acetone yielded a dramatic improvement in surface finish due to reduction/elimination in staircase effect present on surfaces and as low as 0.02 µm surface roughness is possible to achieve.
- Geometric accuracy results indicate that to obtain minimum dimensional deviation of parts, surfaces of the FDM part should be orientated either parallel or in perpendicular direction with respect to the axis of a part.
- Chemical treatment causes variation in geometric accuracy of FDM specimens as compared to specimens without any chemical treatment due to reduction in staircase effect after treatment. In many cases dimensional deviation is reduced after chemical treatment.
- Chemical treatment with cold vapor could as one excellent alternative for FDM parts to improve surface quality without much sacrifice in mechanical strength and dimensional or feature geometry loss.
- Build cost results indicate that lowest model and support material consumption is obtained at Z orientation but built time is more and mechanical strength is the worst. Model and support material consumption as well as built time is significantly lower for part orientation about Y as compared to X.
- Build cost results for part with primitive and freeform surfaces indicate that lowest model and support material consumption and build time is obtained for part built along Z orientation as compared to other two orientations. Build cost results also indicate that support material consumption and the built time depend of the geometric complexity of the parts.
- For selecting the optimum orientation to achieve higher mechanical strength at lower surface roughness and build cost part orientation along X with raster at 30° (X-30) can be selected. Part along Y axis with raster at 60° could also be chosen which results in much improved surface finish as compared to X-30 with small sacrifice in mechanical strength.
- Analytic hierarchy process results indicate that optimum solution is achieved when part built along X orientation with raster angle 30° (X-30) which optimized all five response variable i.e. maximum tensile and flexural strength, improved geometric accuracy and surface quality and lower the build time.

5.2 Scope for Future Work

The present work also leaves scope for future investigators to explore many aspects of FDM and other RP processes. Some recommendations for future research are:

- The effect of process parameters such as part orientation and raster angle on wear nature of FDM parts can be studied.
- The effect of part orientation, raster angle and chemical treatment on impact and compressive strength of FDM parts can be studied.
- The effect of other dimethylketone solution such as ethylene on surface quality and geometric accuracy may be explored in terms of solution concentration and process time.
- The study of part distortions and mechanical behavior in FDM process using finite element analysis can be carried out.
- The work may be extended to study the effect of chemical treatment on geometric accuracy and surface finish of curved surfaces (closed curved geometry or open curved geometry).

References

Agarwala, M.K.; Jamalabad, V.R.; Langrana, N.A.; Safari, A.; Whalen, P.J.; Danforth, S.C. (1996) Structural quality of part processed by fused deposition. *Rapid Prototyping Journals*, 2(4): 4–19.

Ahn, D.; Kweon, J.H.; Kwon, S.; Song, J.; Lee, S. (2009) Representation of surface roughness in fused deposition modelling. *Journal of Materials processing Technology*, 209: 5539–5600.

Ahn, S.H.; Montero, M.; Odell, D.; Roundy, S; Wright, P.K. (2002) Anisotropic material properties of fused deposition modelling ABS. *Rapid Prototyping Journal*, 8(4): 248–257.

Alexander, P.; Allen, S.; Dutta, D. (1998) Part orientation and build cost determination in layered manufacturing. *Computer-Aided Design*, 30(5): 343–356.

Ali, F.; Chowdary, B.V.; Maharaj, J. (2014) Influence of some process parameters on build time, material consumption, and surface roughness of FDM processed parts: Inferences based on the taguchi design of experiments. In *Proceedings of the IAJC/ISAM Joint International Conference*, Orlando, Florida, USA, September 25-27.

Anitha, R.; Arunachalam, S.; Radhakrishnan, P. (2001) Critical parameters influencing the quality of prototypes in fused deposition modelling. *Journal of Material Process Technologies*, 118: 385–388.

ASTM D638-02. (2002) Standard test method for tensile properties of plastics. *ASTM International, West Conshohocken, PA, USA.*

ASTM D790-02. (2002) Standard test methods for flexural properties of unreinforced and reinforced plastics and electrical insulating materials. *ASTM International, West Conshohocken, PA, USA.*

Bakar, N.S.A.; Alkahari, M.R.; Boejang, H. (20100 Analysis on fused deposition modelling performance. *Journals of Zheijiang University-Science A*, 11(12):972–977.

Bandyopadhyay, A.; Balla, V.K.; Sheldon, A.; Bernard; Bose, S. (2011) Micro layered manufacturing. *Micro-Manufacturing Design and Manufacturing of Micro-Products*. DOI: 10.1002/9781118010570.ch5.

Bellehumeur, C.T.; Sun, Q.; Rizvi, G.M.; Gu, P. (2008) Effect of processing conditions on the bonding quality of FDM polymer filaments. *Rapid Prototyping Journal*, 14(2): 72–80.

Bellini, A.; Guceri, S. (2003) Mechanical characterization of parts fabricated using fused deposition modeling. *Rapid Prototyping Journals*, 9(4): 252–264.

Bellini, A.; Guceri, S. (2003) Mechanical characterization of parts fabricated using fused deposition modeling. *Rapid Prototyping Journal*, 9(4): 252–264.

Bharath, V.; Dharma, P.N.; Henderson, M. (2000) Sensitivity of RP surface finish to process parameter variation. *Solid Freeform Fabrication Proceedings*, 251–258.

Bhattacharya, A.; Batish, A.; Singh, G. (2012) Optimization of powder mixed electric discharge machining using dummy treated experimental design with analytic hierarchy process. *Proceedings of Institution of Mechanical Engineers Part B Journal of Engineering Manufacturing*, 226(1): 103–116.

Boschetto, A.; Giordano, V.; Veniali, F. (2013a) Surface roughness prediction in fused deposition modelling by neural networks. *The International Journal of Advanced Manufacturing Technology*, 67: 2727 –2742.

Boschetto, A.; Giordano, V.; Veniali, F. (2013b) 3D roughness profile model in fused deposition modelling. *Rapid Prototyping journal*, 19(4): 240–252.

Byun, H.S.; Lee, K.H. (2005) Determination of the optimal part orientation in layered manufacturing using a genetic algorithm. *International Journal of Production Research*, 43(13): 2709–2724.

Byun, H.S.; Lee, K.H. (2006) Determination of the optimal build direction for different rapid prototyping processes using multi-criterion decision making. *Robotics and Computer-Integrated Manufacturing*, 22: 69–80.

Campbell, R.I.; Martorelli, M.; Lee, H.S. (2002) Surface roughness visualisation for rapid prototyping models. *Computer-Aided Design*, 34: 717–725.

Chakraborty, S.; Dey, S. (2006) Design of an analytic hierarchy-process-based expert system for non-traditional machining process selection. *The International Advanced Manufacturing Technology*, 31: 490–500.

Cheah, C. M.; Fuh, J. Y. H.; Nee, A. Y. C.; Lu, L.; Choo, Y. S.; Miyazawa, T. (1997) Characteristics of photopolymeric material used in rapid prototypes part II. Mechanical properties at post-cured state. *Journal of Materials Processing Technology*, 67(1-3): 46–49.

Cheng, W.; Fuh, J.Y.H.; Nee, A.Y.C.; Wong, Y.S.; Loh, H.T.; Miyazawa, T. (1995) Multi-objective optimization of part-building orientation in stereolithography. *Rapid Prototyping Journal*, 1(4): 12–23.

Chockalingam, K.; Jawahar, N.; Chandrasekar, U.; Ramanathan, K.N. (2008) Establishment of process model for part strength in stereolithography. *Journal of Materials Processing Technology*, 208: 348–365.

Chua, C.K.; Leong, K.F. (2000) Rapid prototyping: principles and applications in manufacturing. *World Scientific.*

Chua, C.K.; The, S.H.; Gay, R.K.L. (1999) Rapid prototyping and virtual manufacturing in product design and manufacturing. *International Journal of Advanced Manufacturing Technology*, 15: 597–603.

Dao, Q.; Frimodig, J.C.; Le, H.N.; Li, X.; Putnam, S.B.; Golda, K.; Foyos, J.; Noorani, R.; Fritz, B. (1999) Calculation of shrinkage compensation factors for rapid prototyping (FDM 1650). *Computer Applications in Engineering Education*, 7(3): 186–195.

Dolenc, A. and Makela, I. (1994) Slicing procedure for layered manufacturing technique, *Computer Aided Design*, 1(2): 4–12.

Dong, B.; Qi, G.; Gu, X.; Wei, X. (2008) Web service oriented manufacturing resource applications for networked product development. *Advanced Engineering Informatics*, 22: 282–295.

Durgun, I.; Ertan, R. (2014) Experimental investigation of FDM process for improvement of mechanical properties and production cost. *Rapid Prototyping Journal*, 20(3): 228–235.

Es-Said, O.S.; Foyos, J.; Noorani, R.; Mendelson, M.; Marloth, R. (2000) Effect of layer orientation on mechanical properties of rapid prototyped samples. *Materials and Manufacturing Processes, 15* (1): 107–122.

Frank, D.; Fadel, G. (1995) Expert system-based selection of the preferred direction of build for rapid prototyping processes. *Journal of Intelligent Manufacturing,* 6: 339–345.

Galantucci, L.M.; Lavecchia, F.; Percoco, G. (2009) Experimental study aiming to enhance the surface finish of fused deposition modeled parts. *CIRP annals-Manufacturing Technology, 58*: 189–192.

Galantucci, L.M.; Lavecchia, F.; Percoco, G. (2010) Quantitative analysis of a chemical treatment to reduce roughness of parts fabricated using fused deposition modelling. *CIRP annals-Manufacturing Technology*, 59: 247–250.

Gurrala, P.K.; Regalla, S.P. (2014a) Part strength evolution with bonding between filaments in fused deposition modelling. *Virtual and Physical Prototyping*, 9(3): 141–149.

Gurrala, P.K.; Regalla, S.P. (2014b) Multi-objective optimization of strength and volumetric shrinkage of FDM parts. *Virtual and Physical Prototyping*, 9(2): 127–38.

Han, W.; Jafari, M.A.; Seyed, K. (2003) Process speeding up via deposition planning in fused deposition-based layered manufacturing processes. *Rapid Prototype Journal*, 9(4): 212–218.

Hayasi, M.; Asiabanpour, B. (2014) Close to CAD model curved-form adaptive slicing. *Rapid Prototyping Journal*, 20(2): 133–144.

Hope, R.L.; Roth, R.N.; Jacobs, P.A. (1997) Adaptive slicing with sloping layer surfaces. *Rapid Prototyping Journal*, 3(3): 89–98.

Hopkinson, N.; Hagur, R.J.M.; Dickens, P.H. (2006) Rapid manufacturing: an industrial revolution of the digital age. *England: John Wiley & Sons Inc.*

Hossain, M.S.; Jorge, R.; Espalin, D.; Perez, M.; Wicker, R. (2013) Improving tensile mechanical properties of FDM manufactured specimens via modifying build parameters. *W.M. Keck Center for 3D Innovation, The University of Texas.*

Hur, J.; Lee, K. (1998) The development of a CAD environment to determine the preferred build-up direction for layered manufacturing. *The International Journal of Advanced Manufacturing Technology*, 14(4): 247–254.

Jain, P.K.; Pandey, P.M.; Rao, P.V.M. (2008) Experimental investigations for improving part strength in selective laser sintering. *Virtual and Physical Prototyping*, 3(3): 177–188.

Jamieson R.; Hacker, H. (1995) Direct slicing of CAD models for rapid prototyping. *Rapid Prototyping Journal*, 1(2): 4–12.

Kai, C.C.; Fai, L.K. (2000) Rapid prototyping: principles and applications in manufacturing. *World Scientific, Singapore*.

Kattethota, G.; Henderson, M. (1998) A visual tool to improve layered manufacturing part quality. *Proceedings of the Solid Freeform Fabrication Symposium, Austin, TX, 327–334.*

Kim, G.D.; Oh, Y.T. (2008) A benchmark study on rapid prototyping processes and machines: Quantitative comparisons of mechanical properties, accuracy, roughness, speed, and material cost.0 *Proceedings of the Institution of Mechanical Engineers, Part B: Journal of Engineering Manufacture*, 222(2): 201-215.

Kulkarni, P.; Dutta, D. (1996) An accurate slicing procedure for layered manufacturing. *Computer-Aided Design*, 28(9): 683–697.

Lee, B.H.; Abdullah, J.; Khan, Z.A. (2005) Optimization of rapid prototyping parameters for production of flexible ABS object. *Journal of Materials Processing Technology*, 169: 54–61.

Lee, K.H.; Choi, K. (2000) Generating optimal slice data for layered manufacturing. *The International Journal of Manufacturing Technology*, 16: 277–284.

Perez, C.J.L. (2002) Analysis of the surface roughness and dimensional accuracy capability of fused deposition modelling processes. *International Journal of Production Research*, 40(12): 2865–2881.

Ma, W.; He, P. (1999) An adaptive slicing and selective hatching strategy for layered manufacturing. *Journal of Materials Processing Technology*, 89–90: 191–197.

Mani, K.; Kulkarni, P.; Dutta, D. (1999) Region-based adaptive slicing. *Computer-Aided Design*, 31: 317–333.

Marcincinova, N.; Ludmila; Marcincin, J.N. (2013) Rapid prototyping in developing process with CA systems application. *Applied Mechanics and Materials*, 464: 399–405.

Masood, S.H.; Rattanawong, W. (2002) A genetic part orientation system based on volumetric error in rapid prototyping. *The International Journal of Advanced Manufacturing Technology*, 19: 209–216.

Masood, S.H.; Rattanawong, W.; Iovenitti, P. (2000) Part build orientations based on volumetric error in fused deposition modelling. *The International Journal of Advanced Manufacturing Technology*, 16: 162–168.

McMains, S.A. (1995) Rapid prototyping of solid 3-dimensional parts. *Master's Project, University of California, Berkeley*.

Nagy, M.S.; Matylsi, G.Y. (2003) Analysis of STL file. *Mathematical and Computer Modelling*, 38: 945–960.

Nancharaiah, T.; Raju, D.R.; Raju, V.R. (2010) An experimental investigation on surface quality and dimensional accuracy of FDM components. *International Journal on Emerging Technologies*, 1 (2): 106–111.

Panda, S.K.; Padhee, S.; Sood, A.K.; Mahapatra, S.S. (2009) Optimization of fused deposition modelling (FDM) process parameters using bacterial foraging technique. *Intelligent Information Management*, 1: 89–97.

Pandey, P.M.; Reddy, N.V.; Dhande, S.G. (2003a) Slicing procedure in layered manufacturing: a review. *Rapid Prototyping Journal*, 9(5): 274–288.

Pandey, P.M.; Reddy, N.V.; Dhande, S.G. (2003b) Improvement of surface finish by staircase machining in fused deposition modelling. *Journal of Material Processing Technology*, 132: 323–331.

Pandey, P.M.; Thrimurthulu, K.; Reddy, N.V. (2004) Optimal part deposition orientation in FDM by using a multicriteria genetic algorithm. *International Journal of Production Research*, 42(19): 4069–4089.

Pandey, P.M.; Reddy, N.V.; Dhande, S.G. (2007) Part deposition orientation studies in layered manufacturing. *Journals of Material Processing Technology*, 185: 125–131.

Paul, R.; Anand, S. (2003) Optimal part orientation in rapid manufacturing process for achieving geometric tolerances. *Journal of Manufacturing Systems*, 30: 214–22.

Pennington, R.C.; Hoekstra, N.L.; Newcomer, J.L. (2005) Significant factors on the dimensional accuracy of fused deposition modeling. *Proceedings of the Institution of Mechanical Engineers, Part E: Journal of Process Mechanical Engineering*, 219(1): 89–92.

Percoco, G.; Lavecchia, F.; Galantucci, L.M. (2012) Compressive properties of FDM rapid prototypes treated with a low cost chemical finishing. *Journal of Applied Sciences, Engineering and Technology*, 4(19): 3838–3842.

Pham, D.T.; Dimov, S.S. (2001) Rapid manufacturing. *Springer-Verlag London Limited*.

Phatak, A.M.; Pande, S.S. (2012) Optimum part orientation in rapid prototyping using genetic algorithm. *Journal of Manufacturing Systems*, 31: 395–402.

Rattanawong, W.; Masood, S.H.; Iovenitti, P. (2001) A volumetric approach to part-build orientations in rapid prototyping. *Journal of Materials Processing Technology*, 119: 348–353.

Reddy, B.V.; Reddy, N.V.; Ghosh, A. (2007) Fused deposition modelling using direct extrusion. *Virtual and Physical Prototyping*, 2(1): 51–60.

Rodriguez, J.F.; Thomas, J.P.; Renaud, J.E. (2001) Mechanical behaviour of acrylonitrile butadiene styrene (ABS) fused deposition materials. Experimental investigation. *Rapid Prototyping Journal*, 7 (3): 148–158.

Rosochowski, A.; Matuszak, A. (2000) Rapid tooling – the state of the art. *Journal of Materials Processing Technology*, 106: 191–198.

Saaty, T.L. (1994) How to make a decision: analytic hierarchy process. *Interfaces*, 26(6): 19–43.

Sabourin, E.; Houser, S.A.; Bohn, J.H. (1996) Adaptive slicing using stepwise uniform refinement. *Rapid Prototyping Journal*, 2(4): 20–26.

Sabourin, E.; Houser, S.A.; Bohn, J.H. (1997) Accurate exterior, fast interior layered manufacturing. *Rapid Prototyping Journal*, 3(2): 44–52.

Schmidt, M.; Pohle, D.; Rechtenwald, T. (2007) Selective laser sintering of PEEK. *CIRP annals-Manufacturing Technology*, 56(1): 205–208.

Seth, A.; Dutta, D. (1994) On the computation of part orientation using support structures is layered manufacture. *Technical Report UM-MEAM-TR-94-15, The University of Michigan, Ann Arbor, MI.*

Shan, Z.; Yan, Y.; Zhang, R.; Lu, Q.; Guan, L. (2003) Rapid manufacture of metal tooling by rapid prototyping. *International Journal of Advanced Manufacturing Technology*, 21: 469–475.

Sood, A.K.; Ohdar, R.K.; Mahapatra, S.S. (2009) Improving dimensional accuracy of fused deposition modelling processed part using grey taguchi method. *Material and Design*, 30: 4243–4252.

Sood, A.K.; Ohdar, R.K.; Mahapatra, S.S. (2010) Parametric appraisal of fused deposition modelling processed process using grey taguchi method. *Proceedings of Institution of Mechanical Engineers Part B Journal of Engineering Manufacturing*, 224(1): 135–145.

Sood, A.K.; Equbal, A.; Toppo, V.; Ohdar, R.K.; Mahapatra, S.S. (2012a) An investigation on sliding wear of FDM built parts. *CIRP Journal of Manufacturing Science and Technology*, 5: 45–54.

Sood, A.K.; Ohdar, R.K.; Mahapatra, S.S. (2012b) Experimental investigation and empirical modelling of FDM process for compressive strength improvement. *Journal of Advanced Research*, 3: 81–90.

Sreeram, P.N.; Dutta, D. (1994) Determination of optimal orientation based on variable slice thickness in layered manufacturing. *Technical Report UM-MEAM-TR-94-14, The University of Michigan, Ann Arbor, MI.*

Tata, K.; Fadel, G.; Bagchi, A.; Aziz, N. (1998) Efficient slicing for layered manufacturing. *Rapid prototyping journal*, 4(4): 151–167.

Thrimurthulu, K.; Pandey, P.M.; Reddy, N.V. (2004) Optimum part deposition orientation in fused deposition modelling. *International Journal of Machine Tools & Manufacture*, 44: 58–594.

Tolio, T.; Ceglarek, D.; Elmaraghy, H.A.; Fischer, A.; Hu, S.J.; Laperrière, L.; Newman, S.T.; Vancza, J. (2010) SPECIES-Co-evolution of products, processes and production systems. *CIRP Annals-Manufacturing Technology*, 59: 672–693.

Triantaphyllou, E; Mann, S.H. (1995) Using the analytic hierarchy process for decision making in engineering applications: some challenges. *International Journal of Industrial Engineering: Applications and Practice*, 2(1): 35–44.

Tyberg, J.; Bohn, J.H. (1998) Local adaptive slicing. *Rapid prototyping Journal*, 4(3): 118–127.

Tymrak, B.M.; Kreiger, M.; Pearce, J.M. (2014) Mechanical properties of component fabricated with open-source 3-D printers under realistic environmental conditions. *Materials and Design*, 58: 242–246.

Wang, R.J.; Wang, L.; Zhao, L.; Liu, Z. (2007) Influence of process parameters on part shrinkage in SLS. *The International Journal of Advance Manufacturing Technology*, 33: 498–504.

Xu, F.; Loh, H.T.; Wong, Y.S. (1999) Considerations and selection of optimal orientation for different rapid prototyping systems. *Rapid prototyping Journal*, 5: 54–60.

Xu, F.; Wong, Y.S.; Loh, H.T. (2000) Toward generic models for comparative rapid prototyping and manufacturing. *Journal of Manufacturing Systems*, 19: 283–296.

Xu, F.; Wong, Y.S.; Loh, H.T.; Fuh, J.Y.H.; Miyazawa, T. (1997) Optimal orientation with variable slicing in stereolithography. *Rapid Prototyping Journal*, 3(3): 76–88.

Yan, Y.; Li, S.; Zhang, R.; Lin, F.; Wu, R.; Lu, Q.; Xiong, Z.; Wang, X. (2009) Rapid prototyping and manufacturing technology: principle, representative technics, applications, and development trends. *Tsinghua Science & Technology*, 14: 1–12.

Zeshui, X.U. (2004) A practical method for improving consistency of judgment matrix in the AHP. *Journal of Systems Science and Complexity*, 17(2): 169–175.

Zhao, Z.; Laperriere, L. (2000) Adaptive direct slicing of the solid model for rapid prototyping. *International Journal of Production Research*, 38(3): 89–98.

Zhou, J.; Herscovici, D.; Chen, C. C. (2000) Parametric process optimization to improve the accuracy of rapid prototyped stereolithography parts. *International Journal of Machine Tools and Manufacture*, 40: 363–379.

Zhou, M.Y.; Xi, J.T.; Yan, J.Q. (2004) Adaptive direct slicing with non-uniform cusp heights for rapid prototyping. *The International Advanced Manufacturing Technology*, 23: 20–27.

Publications

1. Ashu Garg, Anirban Bhattacharya, Ajay Batish, On surface finish and dimensional accuracy of FDM parts after cold vapor treatment. *Materials and Manufacturing Processes*, (2015) **Accepted**.
2. Ashu Garg, Anirban Bhattacharya, Ajay Batish, Failure investigation of FDM parts fabricated at different raster angles under tensile and flexural loading. *Proceedings of Institute of Mechanical Engineers Part B: Journal of Engineering Manufacture*, **Revision submitted**.
3. Ashu Garg, Anirban Bhattacharya, Ajay Batish, On part quality and building aspects of fused deposition modeling process. *Materials and Design*, **Manuscript submitted**.